1969

Magnetism and bonding in potassium trichlorocuprate (II)

George Joseph Maass
Iowa State University

MAGNETISM AND BONDING IN POTASSIUM TRICHLOROCUPRATE (II)

by

George Joseph Maass

A Dissertation Submitted to the
Graduate Faculty in Partial Fulfillment of
The Requirements for the Degree of
DOCTOR OF PHILOSOPHY

Major Subject: Physical Chemistry

Approved:

Signature was redacted for privacy.

In Charge of Major Work

Signature was redacted for privacy.

Head of Major Department

Signature was redacted for privacy.

Dean of Graduate College

Iowa State University
Of Science and Technology
Ames, Iowa

1969

TABLE OF CONTENTS

	Page
INTRODUCTION	1
LITERATURE REVIEW	5
APPARATUS	11
EXPERIMENTAL PROCEDURE	51
EXPERIMENTAL RESULTS	59
CALCULATIONS	80
CONCLUSIONS	111
BIBLIOGRAPHY	113
ACKNOWLEDGEMENTS	117
APPENDIX	118

LIST OF FIGURES

		Page
Figure 1.	Molecular orbital diagram for the $Cu_2Cl_6^{=}$ dimer	4
Figure 2.	Circuit diagram for the overall bridge assembly	21
Figure 3.	The external inductor	22
Figure 4.	Fine inductance assembly	23
Figure 5.	Fine inductor circuit	24
Figure 6.	The step inductor and supporting plexiglass frame	25
Figure 7.	Placement of individual coils in the step inductor primary	26
Figure 8.	Circuit diagram for step inductor primary	27
Figure 9.	Circuit diagram for step inductor secondary	28
Figure 10.	Mutual inductance bridge assembly	30
Figure 11.	Inside of bridge panel	31
Figure 12.	Cryostat	32
Figure 13.	Circuit for supplying heat to the sample chamber	33
Figure 14.	Pumping lines leading to top of cryostat	34
Figure 15.	Manostat assembly	35
Figure 16.	Manostat component	36
Figure 17.	Manostat component	37
Figure 18.	Manostat component	38
Figure 19.	Manostat component	39

		Page
Figure 20.	Manostat component	40
Figure 21.	Cryostat and related equipment	41
Figure 22.	Electron spin resonance spectrometer and magnet	44
Figure 23.	Device for aligning one of the dimers in the unit cell with the magnetic field	45
Figure 24.	Orientation of the $Cu_2Cl_6^{=}$ dimers with respect to the crystal axes	50b
Figure 25.	The center of the sample coil is 44 inches from a reference point at the top of the cryostat	54
Figure 26.	Reciprocal molar susceptibility vs. temperature for $KCuCl_3$ powder	61
Figure 27.	Experimental points and theoretical curves for susceptibility	62
Figure 28.	Reciprocal susceptibility vs. temperature for a $KCuCl_3$ single crystal with its a axis aligned parallel to the external field	65b
Figure 29.	Reciprocal susceptibility vs. temperature for a $KCuCl_3$ with its b axis aligned parallel to the external field	67
Figure 30.	Susceptibility for a $KCuCl_3$ crystal with its a and b axes aligned perpendicular to the external field	69
Figure 31.	Comparison of susceptibility curves for $KCuCl_3$ powder and single crystals in various orientations	70
Figure 32.	Susceptibility curve for the external field being parallel to the plane of the Cu-Cu vectors in the dimer	72

		Page
Figure 33.	Susceptibility curve for the external field being perpendicular to the plane of the Cu-Cu vectors in the dimer	74
Figure 34.	Susceptibility for the field parallel to the a axis at two different field intensities	76b
Figure 35.	First derivative of ESR absorption for $KCuCl_3$ powder	77
Figure 36.	First derivative of ESR absorption for a $KCuCl_3$ single crystal. 0^o means the external field is parallel to the x axis of one of the dimers in the crystal (see Figure 39 for axes). Note that the baseline has been shifted with each successive rotation	78b
Figure 37.	90^o refers to the field being perpendicular to both x and y axes in one of the dimers of the crystal	79
Figure 38.	Experimental and Ising susceptibility curves	91
Figure 39.	Coordinate system for the $Cu_2Cl_6^=$ dimer	92
Figure 40.	Atomic orbitals comprising the B_{1g}^* and B_{2u}^* molecular orbitals	93
Figure 41.	Energy level diagram for $KCuCl_3$	108

LIST OF TABLES

		Page
Table 1.	Comparison of step inductor units to fine inductor units	14
Table 2.	Purity of $KCuCl_3$	47
Table 3.	Atomic positions within the $Cu_2Cl_6^=$ dimer	49
Table 4.	Reciprocal molar susceptibility of $KCuCl_3$ powder. $\frac{1}{\chi_m} = \frac{56.32}{\Delta M}$	60
Table 5.	Reciprocal molar susceptibility of $KCuCl_3$ single crystal, sample #1, $\frac{1}{\chi_m} = \frac{11.79}{\Delta M}$, field parallel to a axis	63
Table 6.	Reciprocal molar susceptibility of $KCuCl_3$ single crystal, sample #2, $\frac{1}{\chi_m} = \frac{30.67}{\Delta M}$, field parallel to a axis	64
Table 7.	Reciprocal molar susceptibility of $KCuCl_3$ single crystal, sample #3, $\frac{1}{\chi_m} = \frac{20.30}{\Delta M}$, field parallel to b axis	66
Table 8.	Reciprocal molar susceptibility of $KCuCl_3$ single crystal, sample #4, $\frac{1}{\chi_m} = \frac{27.96}{\Delta M}$, field perpendicular to a and b axes	68
Table 9.	Reciprocal molar susceptibility of $KCuCl_3$ single crystal, sample #5, $\frac{1}{\chi_m} = \frac{14.36}{\Delta M}$, field parallel to plane of Cu-Cu vectors	71
Table 10.	Reciprocal molar susceptibility of $KCuCl_3$ single crystal, sample #6, $\frac{1}{\chi_m} = \frac{13.48}{\Delta M}$, field perpendicular to the plane of the Cu-Cu vectors	73

		Page
Table 11.	Reciprocal molar susceptibility of $KCuCl_3$ single crystal, sample #2, field dependence - oscillator 40 $\frac{1}{xm} = \frac{30.67}{\Delta \cdot M}$	75
Table 12.	Reciprocal susceptibility as a function of temperature for the singlet-triplet separation being 55k	82
Table 13.	1/xm as a function of T for the spin = 1 Ising model	84
Table 14.	Comparison of g values calculated from Susceptibility Data and from ESR Data	87
Table 15.	Molecular orbital coefficients for $\frac{e^2}{r_{ij}}$ and $\frac{e^2}{r_{i\alpha}}$ integrals	97
Table 16.	Evaluated integrals (in atomic units). A and B refer to copper d_{xy} orbitals	98
Table 17.	Evaluated integrals. A and B refer to copper $d_{x^2-y^2}$ orbitals	98
Table 18.	Evaluated integrals. A and B refer to a linear combination of d_{xz} and d_{yz} on the copper atoms	99
Table 19.	Values of integrals for $\alpha = 0.9$, $\beta = 0.6$	99

INTRODUCTION

The problem of describing the behavior of electrons in solids is one which can be solved in principle (Slater, 1965), but which is, without gross approximations, intractable for even the simplest systems. At one extreme, there are Van der Waals solids, such as solid neon, which might be described by weakly interacting orbitals, having the electrons substantially localized on the atoms. At the other extreme are the metallic conductors in which a localized description is clearly inappropriate. Even a non-localized description in terms of one electron states may not always be sufficient. Somewhere in this milieu lie systems, such as naphthalene, in which a non-localized picture of electrons within individual molecules seems to be satisfactory. Between this case and that of the simple metals lie systems such as the one studied in this work. These are the systems in which, one might guess from the crystal structure, both localized molecular interactions and delocalized "crystal" interactions exist. If the former are sufficiently stronger than the latter, then a description such that the intermolecular forces are negligible with respect to intramolecular forces would be valid. (Caveat lector that what one chooses to call a "molecule" in such systems is not always a clear cut decision).

Regardless of which treatment is used, symmetry may sometimes be used to simplify the problem. If a non-localized description is appropriate, it is the symmetry of the space group of the lattice that must be satisfied. To the extent that one may use a localized molecular description, it is the symmetry of the molecular point group that will be useful.

The system of interest in this work is $KCuCl_3$, potassium trichlorocuprate (II). In this system, consisting of $Cu_2Cl_6^{=}$ dimers, the fact that the distance between the dimers is large with respect to the Cu-Cl distances within the dimer gave rise to the idea that one might be able to describe the properties of this compound on the basis of a relatively simple model of discrete, noninteracting dimer species. In particular, this system would be expected, from localized symmetry considerations alone, to have a ground state which is either a spin triplet or a singlet not far from a triplet. (Willett et al., 1963) Both electron spin resonance and magnetic susceptibility measurements are powerful tools in determining the correctness of such a picture. The spin resonance measurements yield information concerning the orbital degeneracy of the state populated at the temperature of the measurement, the spin degeneracy of such a state, and the directional dependence of the magnetization. The susceptibility measurements overlap the resonance measurements by yielding the directional dependence of the magnet-

ization. In addition, the susceptibility measurements have the advantage of being more amenable to measurements as a function of temperature than are the resonance measurements, so that the former can more easily determine the temperature at which a localized picture becomes inappropriate than the latter, should magnetic ordering occur.

Using symmetry arguments, Willett and Rundle (Willett, 1962) developed a molecular orbital scheme for the $Cu_2Cl_6^{=}$ dimer (Figure 1). The highest occupied orbitals, namely the B_{1g}^{*} and B_{2u}^{*} are a degenerate, orthogonal pair. Calling the first of these orbitals ϕ and the second X, one sees that three configurations are possible, i.e., ϕ^2, X^2, and ϕX. The theoretical calculations will be based on these wave functions or combinations thereof.

In the present work, the electron spin resonance at room temperature and the magnetic susceptibility of $KCuCl_3$ powder and single crystals in the range 1.4 to 100°K and 1.4 to 70°K, respectively, have been measured. The results have been interpreted insofar as it has been possible to do so on the basis of the validity of the Willett-Rundle orbital picture.

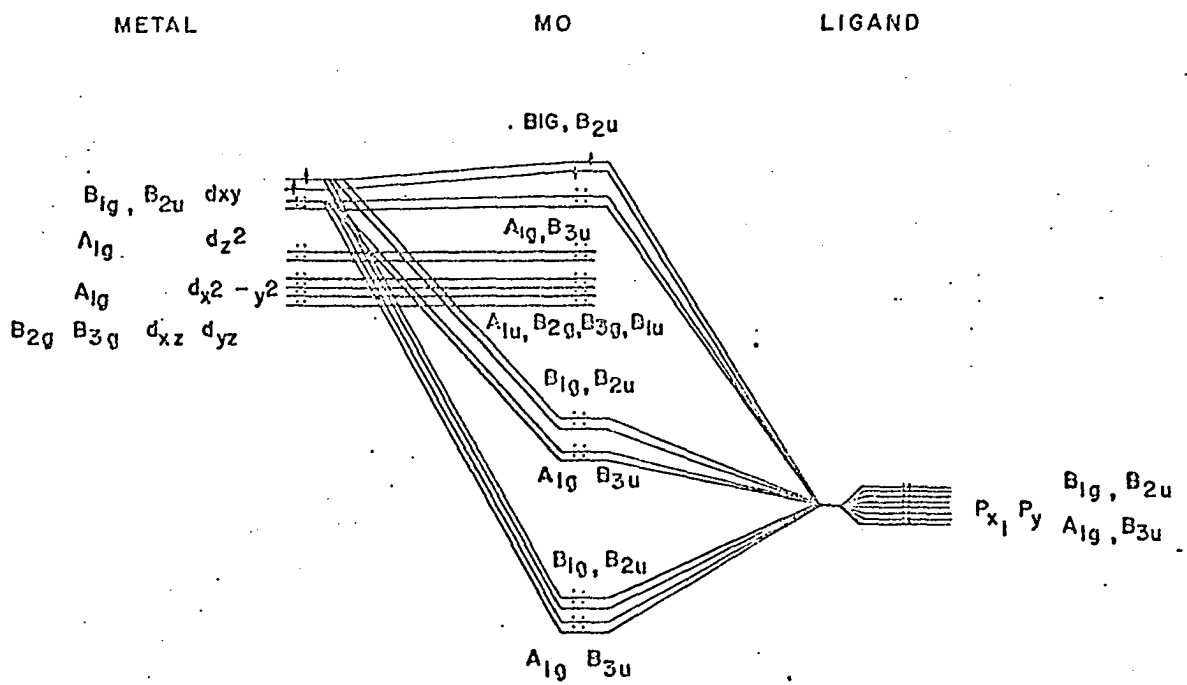

OMISSIONS:

1. DIRECT METAL - METAL INTERACTION
2. π BONDING
3. Cu 4s AND 4p ORBITALS

Figure 1. Molecular orbital diagram for the $Cu_2Cl_6^{=}$ dimer

LITERATURE REVIEW

The cupric ion and its salts have been a source of interest in recent years to physical scientists concerned with magnetism as applied to theories of chemical bonding. Compounds containing Cu and Cl atoms were observed to exhibit varied magnetic behavior below 300° K (Vossos, et al., 1963, Vossos, et al., 1960, Maass et al., 1967). The structures of many common cupric halide compounds have been published (Wells, 1962). The refined structures of $CuCl_2$ and $CuBr_2$ have been determined (Wells, 1947, Helmholz, 1964) to be layer chains with the copper-halogen distances equal to 2.28 and 2.40 Å, respectively. The magnetic susceptibility of these two salts was determined in the range 400 to about 20°K and the behavior of both was reported to be paramagnetic in the higher temperature regions, with antiferromagnetism being observed at lower temperatures (Barraclough, 1964). The distorted rutile CuF_2, with four Cu - F bonds of 1.93 Å and two Cu - F bonds of 2.27 Å, was reported to have a Néel point at 69°K with ferromagnetic ordering beginning below 40°K (Joenk, 1965).

The magnetic moments of all Cu(II) complexes which had been done prior to 1964 have been tabulated in an exhaustive work (Kato et al., 1964). Antiferromagnetism in $CuCl_2 \cdot 2H_2O$ was described in an NMR study by Rundle (1957). Umebayashi et al., (1966) have described a canted spin antiferromagnetism for this compound in the range 1.7 to 4.3°K. The

diamagnetic susceptibility of Cu_2O single crystals at 25°C has been recently published (Czanderna, 1966). The susceptibility of $CsCuCl_3$ has been worked out very recently (Rioux 1967), the structure having been determined previously, (Schleuter, et al., 1966). $CsCuCl_3$ has a distorted octahedral structure with a very short (3.06 Å) Cu-Cu distance. Even at this short distance, however, the metal-metal overlap integral has been calculated to be less than 10^{-5} (Schleuter, et al., 1966). $KCuCl_3$, on the other hand, is composed of bridged $Cu_2Cl_6^{=}$ dimers arranged in infinite chains. Metal-metal overlap in this compound is surely negligible, as the Cu-Cu distance is the comparatively long 3.44 Å. $KCuCl_3$ was first synthesized by Meyerhoffer (1889), and its refined structure was determined by Willett et al., (1963) seventy years later. The details of the synthesis and of the structure are given in the materials section of this work. The magnetic susceptibility of $KCuCl_3$ was first measured at 290°K in 1925(Cotton-Feytis, 1945).

The powder susceptibility of $KCuCl_3$ in the range 1.5 to 70°K was first determined by Willett et al., (1963). He found a broad maximum in the susceptibility at about 30°K, a sharp rise below 10°K, and no linear region for 1/x vs. T up to 70°K. Willett, and others, (1963) presumed that the broad maximum was indicative of an antiferromagnetic transition, and that the sharp rise was possibly low temperature ferromagnetism.

The statistical methods used in the calculations in this work, i.e., the relation of energy levels of a given separation to a microscopic susceptibility, are well known (Fowler and Guggenheim, 1952)

The Curie Law stating that paramagnetic susceptibilities are inversely proportional to temperature can be easily derived. Many situations cannot be handled by this simple equation, however, if the energy levels of a system are known, the magnetic susceptibility may be calculated by application of Van Vleck's equation (1932). (See the calculations section of this work for an example.) Van Vleck's equation had also been applied to ions perturbed by both Zeeman effect and spin orbit coupling (Kotani, 1949). The Hamiltonian for this interaction is $H = \lambda \bar{L} \cdot \bar{S} + \beta \bar{H} \cdot (\bar{L}+2\bar{S})$. The mathematical details of operating with both of the terms in this Hamiltonian have been presented in detail by Ballhausen (1962). Stevens (1953) has presented a molecular orbital method of obtaining g values by utilizing the Coulomb interaction and spin-orbit coupling. Using Stevens' method, Owen (1955) developed a crystal field treatment for octahedral complexes and introduced weak σ bonding into his model to explain some of the discrepancies.

A simple model for spin-spin interaction has been described in several places, (Ballhausen, 1962, Figgis, 1956). The calculations for this model have been applied to situations where there is a thermally accessible state at an

energy of less than kT above a diamagnetic ground state. (Ewald et al., 1964).

The parameter D, which is a measure of zero field splitting has been related to magnetic susceptibility by the familiar statistical formula (Dorain, 1962). It is further observed that g values obtained from esr data can be used to obtain molecular orbital mixing coefficients, and some reference works exist on the method of calculation, (Chen and Das, 1966). A discussion of zero field splitting and the other principles of paramagnetic resonance can be found in the reference works of Pake (1962) and Schlichter (1963).

A modified perturbation method for problems in paramagnetism in which second order effects are comparable in magnitude with first order effects, where orthodox methods break down, has been described by Pryce (1950).

In the range where cooperative interactions occur, susceptibilities have been treated using the Heisenberg - Dirac - Van Vleck model, (1940), (Griffiths, 1961 and Newell and Montroll, 1953). An Ising model for an antiferromagnet of spin=1 has been worked out by S. Liu of the Physics Department of this university. In some recent work in antiferromagnetism, it has been pointed out that in an antiferromagnet with large anisotropy in exchange energy, magnetic fields can induce various order-disorder transitions (Keen et al., 1966), and that a one and two dimensional,

isotropic Heisenberg model with a finite exchange interaction can neither be a ferromagnet nor an antiferromagnet, (Mermin and Wagner, 1966). The details of the theories mentioned in this section, as they are applicable to the present work, are discussed in the calculations section of this thesis.

APPARATUS

Magnetic Susceptibility Measurements

In this work, magnetic susceptibilities were measured by an inductance technique using a Hartshorn (1925) type mutual inductance bridge. The bridge was constructed by the author, following the design of L. D. Jennings (1960). The circuit diagram for the bridge and related equipment is shown in Figure 2.

The amplifiers in the diagram were constructed under the supervision of W. Rhinehart of this laboratory. The first of these is a power amplifier which amplifies the signal from the Hewlett-Packard 202C oscillator set at 33 cycles (current output 0.01 amp) to send a current of 0.1 amp to the primary circuits of the bridge balancing coils (i.e., the transformer and the secondaries of the sample coils, the external inductor, the step inductor, and the fine inductor) through a 60 cycle filter into the Y terminals of an oscilloscope. As shown, the X sweep of the oscilloscope was externally synchronized with the oscillator signal, so that the inductive and resistive components of the amplifier signal could be independently identified. The transformer was a 1:200 gain transformer, model # KI 1117 manufactured by South Western Industrial Electronics Co., of Houston, Texas. The oscilloscope was a "Pocket-scope" model # S-11-A manufactured by Waterman Laboratories.

The external variable inductor (Hesterman, 1958) was wound as an astatic pair. The details of construction are given in Figure 3. The plexiglass disk shown in that figure can be rotated 360°, so that a variety of possible orientations of primary with respect to secondary can be achieved. The function of the external inductor is to place the signal coming from the sample coils in the proper range so that it can be balanced by the opposing inductance of the step and fine inductors.

The construction of the fine inductor is shown in Figure 4. The wiring for this inductor is given schematically in Figure 5. The primary consists of two thin strips of phosphor bronze sheet, each 0.015 in. wide, one on each side of the grooved ring. The secondary consists of two two-turn sections of # 32 Belden Formar covered copper wire. These sections are on opposite sides of the ring and are astatically wound. The axis of the rotor fits down the center of the handle shown in Figure 4. It is necessary that the primary, secondary, and rotor be coaxial in order that linearity of inductance with rotation angle be achieved. The rotor wire leads to two phosphor-bronze contacts (Figure 4) which are imbedded in the disks that fit into the ring from above and below. These contacts press against the primary in the ring. The ring itself plugs into the main control panel of the instrument. A grounded copper foil shield (not shown)

fits between the primary and secondary on each side of the ring. The calibrated disk indicates that the fine inductance was designed such that 200° of rotation changes the total inductance by one unit. One unit on the bridge corresponds to 0.24 μHenrys.

The step inductor consists of four secondary coils wound as a magnetic octupole surrounded by 13 pairs of primary coils, wound so as to make a quadrupole of each pair, following the type described by Jennings (1960). The coil configurations were calculated from a program worked out for the IBM 7074 by Al Miller and Cluin Cameron, both formerly of this laboratory. The program was based on the calculations explained by Grover (1946).

The overall construction of the step inductor is shown in Figure 6. The details of the primary and secondary windings are given in Figures 7, 8, and 9. The secondary was made with # 36 Nyclad covered copper wire. The primary was made with # 30 Nyclad covered copper wire. Each pair of primary coils is connected to a reversing switch. The following changes in mutual inductance can be achieved by reversing the primary current in the various pairs: 0.02, 0.1, 0.5, 1.0, 2, 4, 8, 10, 20, 40, 80, and 160. These are in the aforementioned bridge units. The first four of these are for calibrating and checking the linearity of the continuously variable inductor.

Unfortunately, the primary of the step inductor had

to be built first. If the secondary had been built first, it would have been possible to arrange the primary windings so that the changes in mutual inductance would be exactly the units listed above. As it was, even with the help of the trimming coils, the following table represents the best correspondence obtainable.

Table 1. Comparison of step inductor units to fine inductor units (1 fine inductor unit = 0.24 Henry)

Units on Step Inductor	Units on Fine Inductor
1	0.980
2	2.430
4	4.350
8	8.560
10	10.680
20	23.870
40	44.560
80	99.610
160	184.260

For example, if the two and the four switch are in the "in" position for one reading and in the "out" position for the next reading, i.e., the current is reversed in these two pairs, then the difference in mutual inductance between the two readings is 2.430 + 4.350 = 6.780 bridge units, as previously defined.

The sample coils were wound to give a net mutual inductance of zero in the absence of a sample. The dimensions were obtained from the same computer program mentioned in connection with the step inductor.

The secondary of the sample coil was wound in three sections, using Belden # 30 Nyclad covered copper wire. The first and third sections were wound clockwise over a distance of 2.019 in., and contained 177 turns per layer in each of four layers. The second section was wound counterclockwise over a distance of 3.962 in., and contained 348 turns per layer in each of its four layers. A one inch space separated each of the three sections. A 0.001 in. copper foil was wrapped over the secondary. The shield had slits in it to reduce eddy currents, and was grounded to prevent capacitative coupling between the primary and the secondary.

The primary of the sample coil was wound over the secondary and the grounded shield. The 12 inch long primary consisted of 8000 turns, in four 2000 turn layers, of Belden # 36 Nyclad covered copper wire.

At room temperature, the resistance of the secondary is about 80 ohms; that of the primary is about 1000 ohms.

It is to be noted that the coils were wound on a one inch diameter winding form wrapped with one layer of 0.005 in. thick paper. This same paper was used between every layer of primary and secondary winding, and on both sides of the grounded shield. Thus the mean diameter of the secondary was 1.054 inches, and that of the primary was 1.160 inches.

Figures 10 and 11 are photographs of the front of

the bridge assembly and of the inside of the main control panel.

The sample coils, being rather aloof, live in a helium dewar, which, in turn, looks out at the world through the nitrogen dewar which surrounds it. This dewar system, plus the sample support and cryostat top, is pictured in Figure 12. The helium dewar, including Kimax tapered seal by which it is supported, measures 35 in. long with an i.d. of 1-3/4 in. and an o.d. of 2-1/2 in. The nitrogen dewar is 36 in. long and has an i.d. of 4 in. and an o.d. of 4-3/4 in. Both dewars were made from pyrex tubing by E. McKenna of the glassblowing shop, and they were strip silvered by the author according to the method of Hoare, Jackson and Kurti (1961). Since helium diffuses through pyrex, the helium dewar was equipped with a port through which it could be evacuated at regular intervals. The brass disks and rubber ring pictured at the top of the dewars in Figure 12 were designed to prevent water vapor from condensing in nitrogen dewar. The helium dewar made a vacuum seal to its support via a natural rubber gasket on top of the Kimax tapered joint. The sample coil mounting was a 25 mm o.d. pyrex tube which made a vacuum seal to the top of the cryostat through a Cenco vacuum coupling.

The sample holders were small Vycor tubes. For the powder susceptibility the sample was sealed in a Vycor tube under helium pressure. For the single crystal

susceptibilities, a small Vycor tube with a plexiglass plug in the top was used. The holders were attached to a bakelite rod by means of threads. The bakelite rod, in turn, was vacuum sealed through a rubber disk in the Cenco seal at the top of the 3/4 inch stainless steel tube, and was held in place by a dowel (see Figure 12). The stainless tube was open at the bottom end and short enough so that, in its lowest position, it would not come within 15 inches of the top of the sample coils. The tube was equipped with a side arm near the top, through which the wires to the sample heater and thermocouple could be run. A clamp around a small piece of rubber tubing vacuum sealed these wires.

The thermocouple was an alloy of 2% gold cobalt coupled to # 36 Belden Nyclad covered copper wire. The gold-cobalt wire was obtained from the Sigmond Cohn Corporation of Mt. Vernon, New York. The temperature vs. E.M.F. curve for the region 4.2 to 300°K was determined by M. D. Bunch of the National Bureau of Standards at Boulder, Colorado. In all cases, it was found that the sample holder plus thermocouple had no measureable contribution to the susceptibility.

The sample heater was composed of an alloy of #40 Cu-Be wire, having a resistance of seven ohms/foot, coupled to # 36 Nyclad covered copper wire. The copper wire and the alloy were wrapped, turn for turn, beside

each other, so that the pair formed a non inductive winding. Two heaters were used in the susceptibility work. One had a negligible contribution to susceptibility, and the other had a small, but reproducible contribution. In all cases where the latter was used, its contribution to the magnetic moment was subtracted, so that only the changes in mutual inductance due to the sample by itself are tabulated in this work. A circuit was built to convert the 120 volt DC line to the 30 volt, 0.030 amp line which the sample heater uses. (See Figure 13, the part enclosed in dotted lines.) The rest of Figure 13 refers to a circuit on the mutual inductance bridge control panel that connects the power source to the sample heater.

A schematic diagram of the pumping system for the sample chamber has been published (Gerstein, 1960). Figure 14 is a photograph of the top of the cryostat and the pumping lines leading to the sample chamber. This pumping system consists of a Consolidated Electrodynamics Corp. VMF 11 air cooled diffusion pump, a model 1400B Duoseal forepump, and the copper pipe line which connects them to the top of the cryostat.

The manometer system consisted of a standard mercury manometer connected in parallel with an oil manometer, each having a common low vacuum side to the helium dewar. The oil manometer was used for pressures below 20 mm of mercury.

The pump used to reduce the pressure in the helium dewar was a Kinney DVM 12814, and was connected to the cryostat by 40 ft. of two inch copper pipe. A manostat to control the pressure over the helium bath was constructed by R. Wagner, formerly of this laboratory, from plans obtained from D. Finnemore of the Physics Department. The manostat, Figure 15, was connected in parallel with the main pumping line leading to the helium dewar. The connection was made into the openings in part 1 (Figure 16). A pressure gauge and a "T" with two needle valves were soldered into the openings in part 5 (Figure 20). One of the needle valves goes to a pump, the other to the atmosphere. A thin rubber sheet fits between part 1 and parts 2 and 3. The needle valves can be adjusted so that the pressure in the control chamber (part 4, Figure 19) is less than the pressure in the cryostat. The rubber sheet will then be drawn up against part 3 (Figure 18) and pumping will occur until the system and control chamber pressures are equal. Temperatures below 4.2°K were determined by measuring the vapor pressure over the helium bath and converting vapor pressure to temperature via the 1955 tables (Clement, 1955).

A Rubicon potentiometer, catalogue number 2781, was used to measure the e.m.f. of the thermocouple. The galvanometer was a Leeds and Northrup catalogue number 2430-A. It had a sensitivity of 4.7 microvolts per cm.

The standard cell was an Eppley Laboratories #100, having an e.m.f. of 1.01945. The power supply for the potentiometer was a three volt "Even Volt" #252-05 from Instrulab. The motor used to raise and lower the sample was a Bodine KCI - 22RC reversing motor.

A transfer tube and transfer tube extension were constructed by the author. They were made of concentric 3/8 in. and 1/4 in. O.D. stainless tubing, with provisions made to evacuate the space between them. Copper tubing, 3/8 and 1/4 in. i.d. was used wherever bends were necessary, with teflon spacers used to keep the tubes apart. The efficiency of the transfers is such that approximately four liters of liquid helium is needed to fill the 1½ liter helium dewar on the first transfer of the day, and approximately two liters for each successive transfer.

Overall photos of the cryostat system are shown in Figure 21.

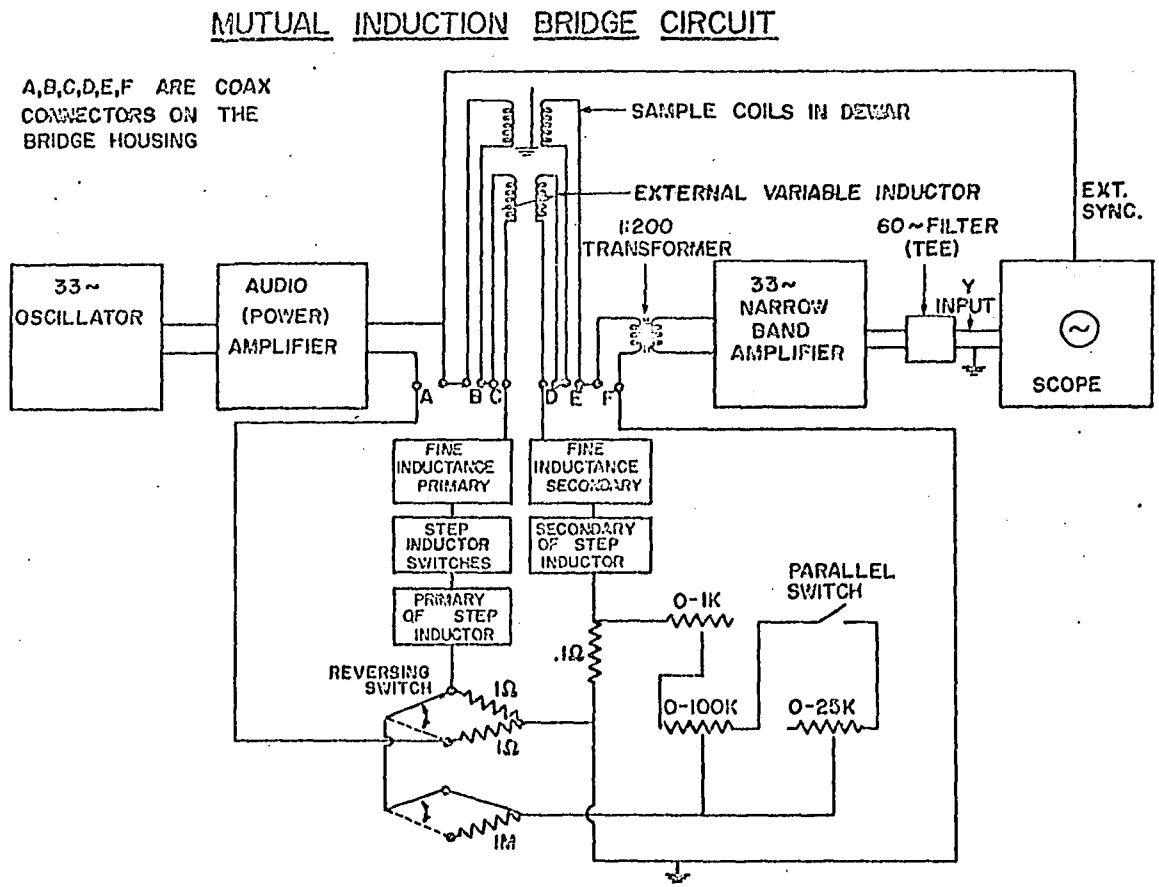

Figure 2. Circuit diagram for the overall bridge assembly.

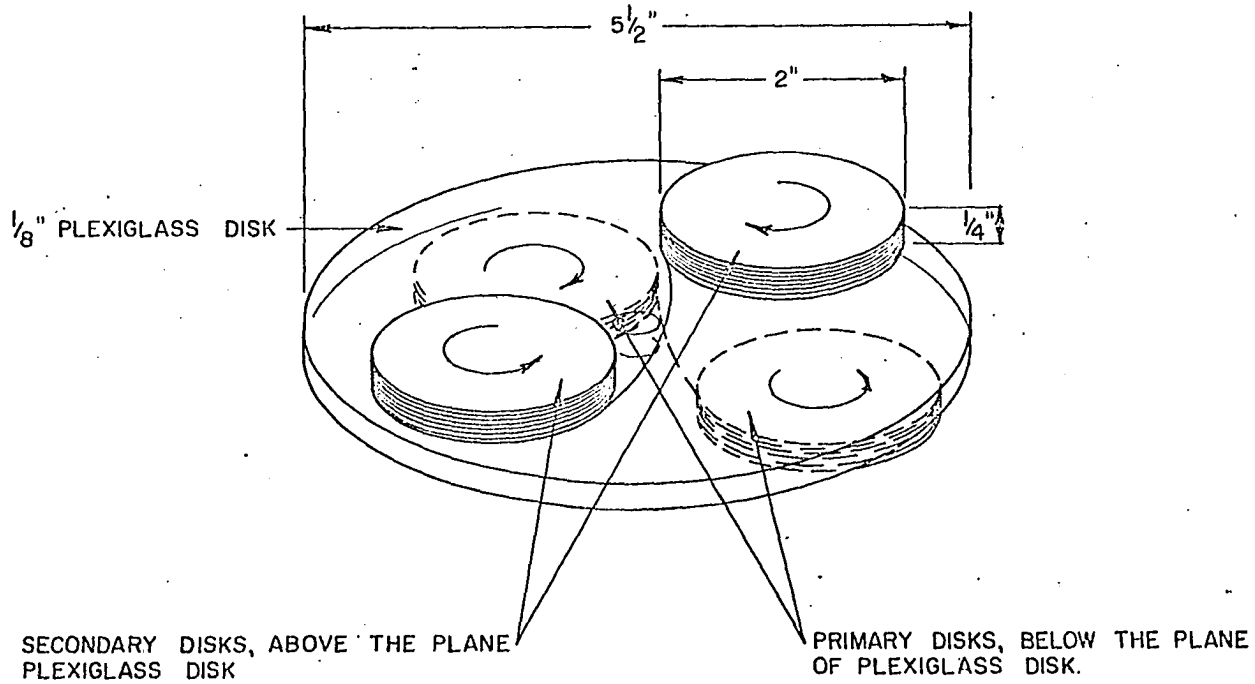

Figure 3. The external inductor

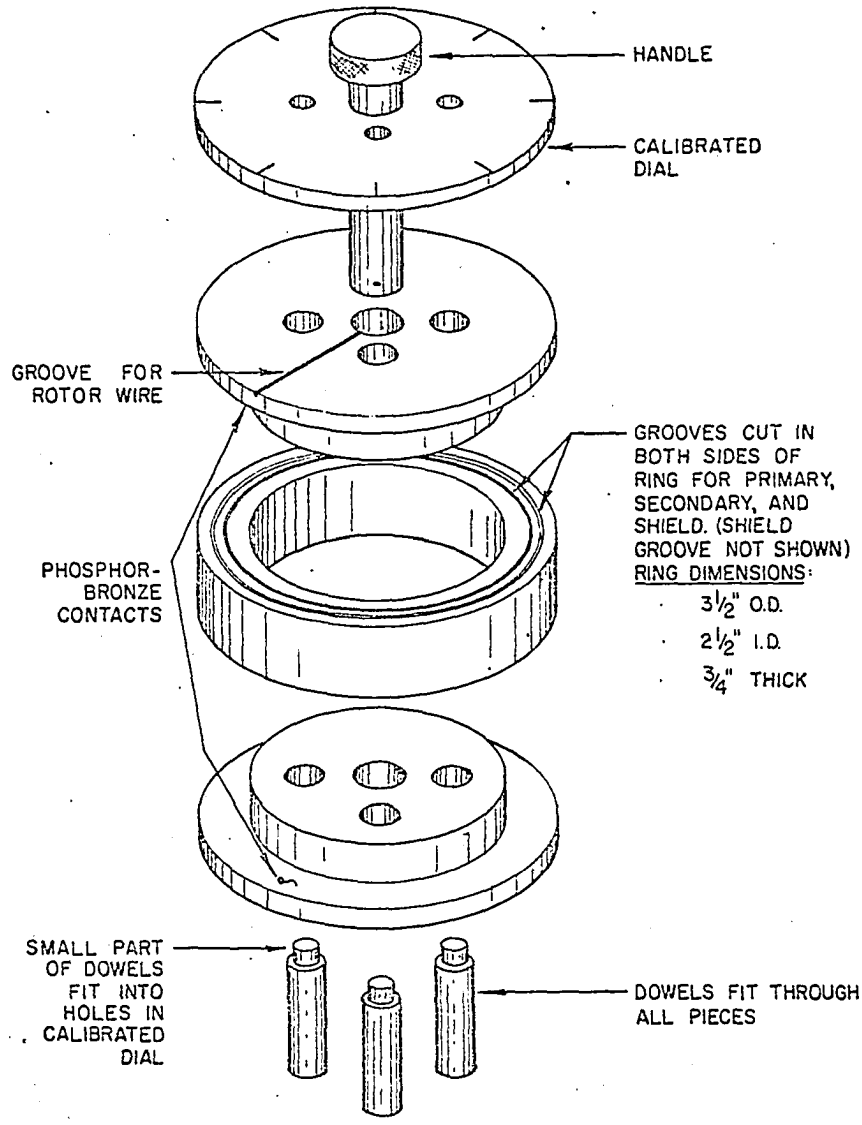

Figure 4. Fine inductance assembly

WIRING OF FINE (CONTINUOUS) INDUCTOR

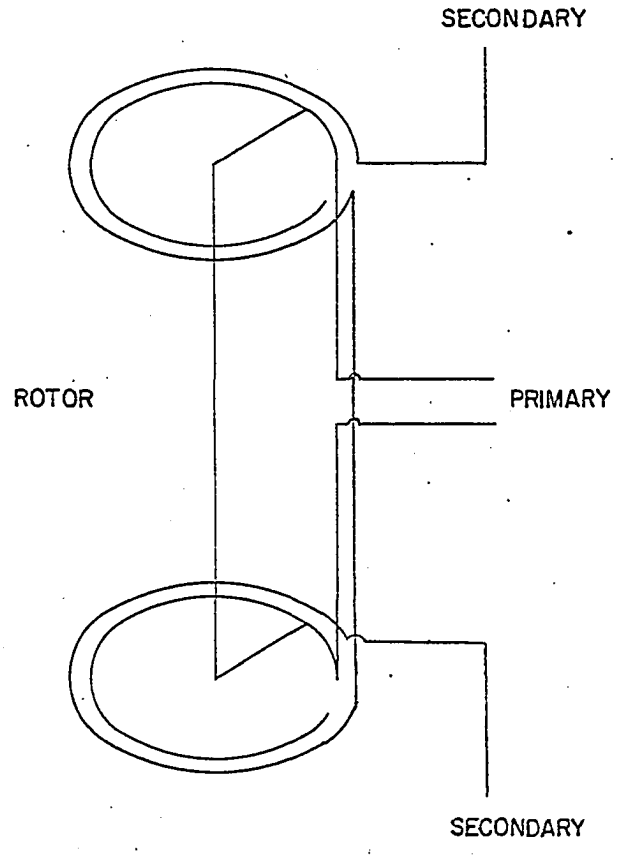

DIAMETER OF PRIMARY LOOP = 3"
" " SHIELD " = 3 1/8" (NOT SHOWN)
" " SECONDARY " = 3 1/4"

Figure 5. Fine inductor circuit

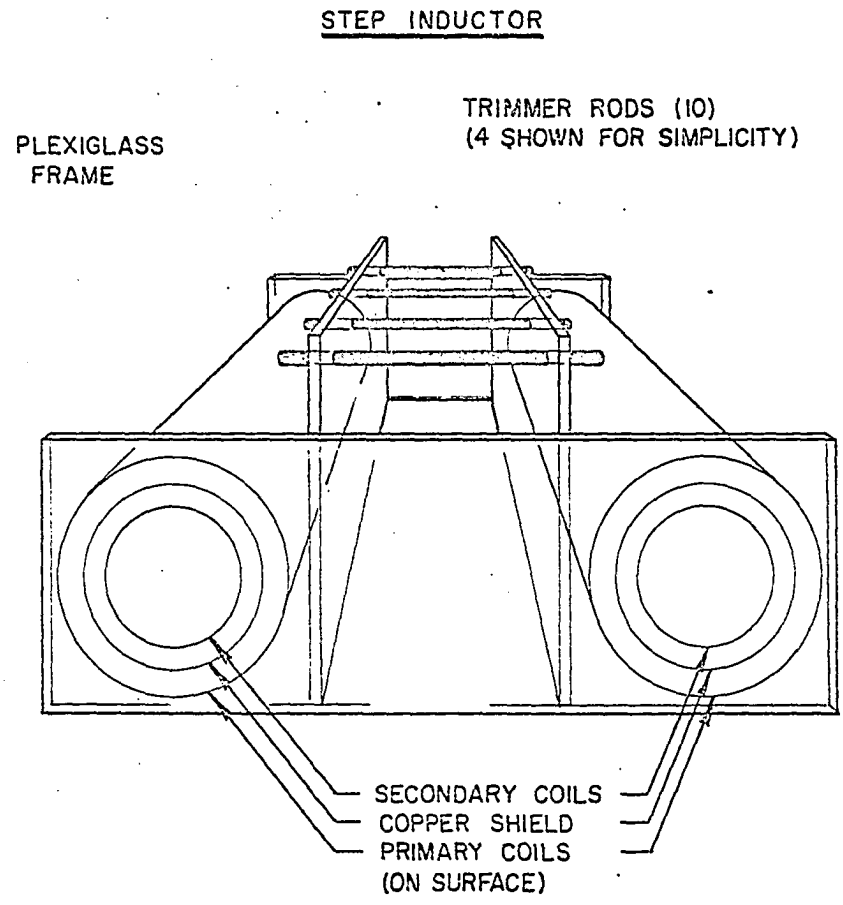

Figure 6. The step inductor and supporting plexiglass frame

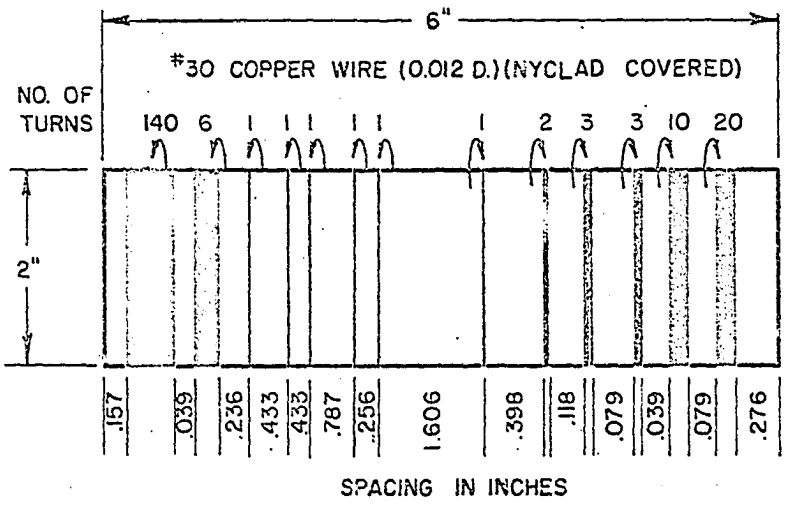

Figure 7. Placement of individual coils in the step inductor primary

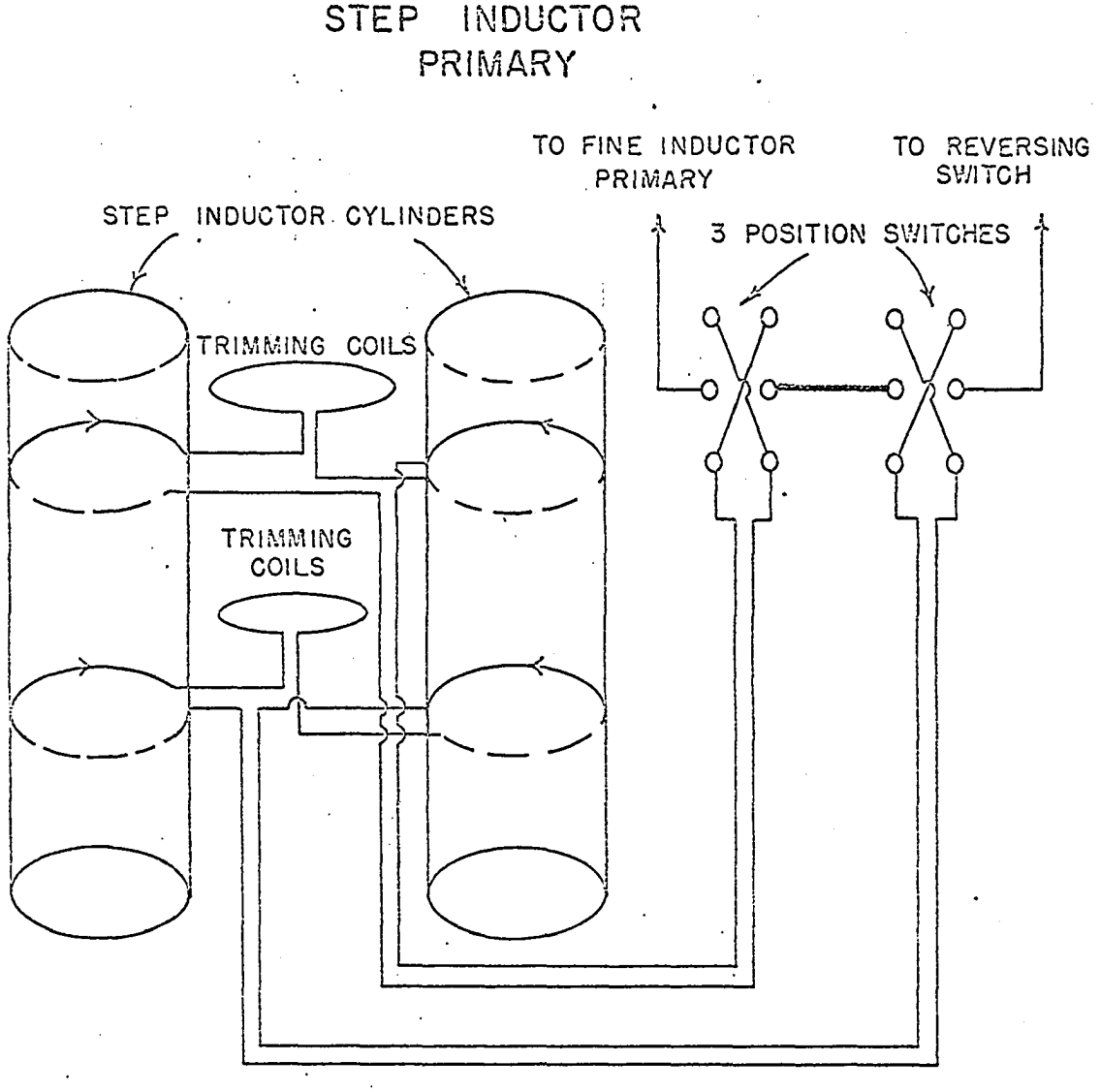

FOR SIMPLICITY, DIAGRAM SHOWS ONLY TWO OF THE 13 PRIMARY SECTIONS. TRIMMING COILS CAN BE ROTATED AN AXIS PERPENDICULAR TO THE AXES OF BOTH CYLINDERS.

Figure 8. Circuit diagram for step inductor primary

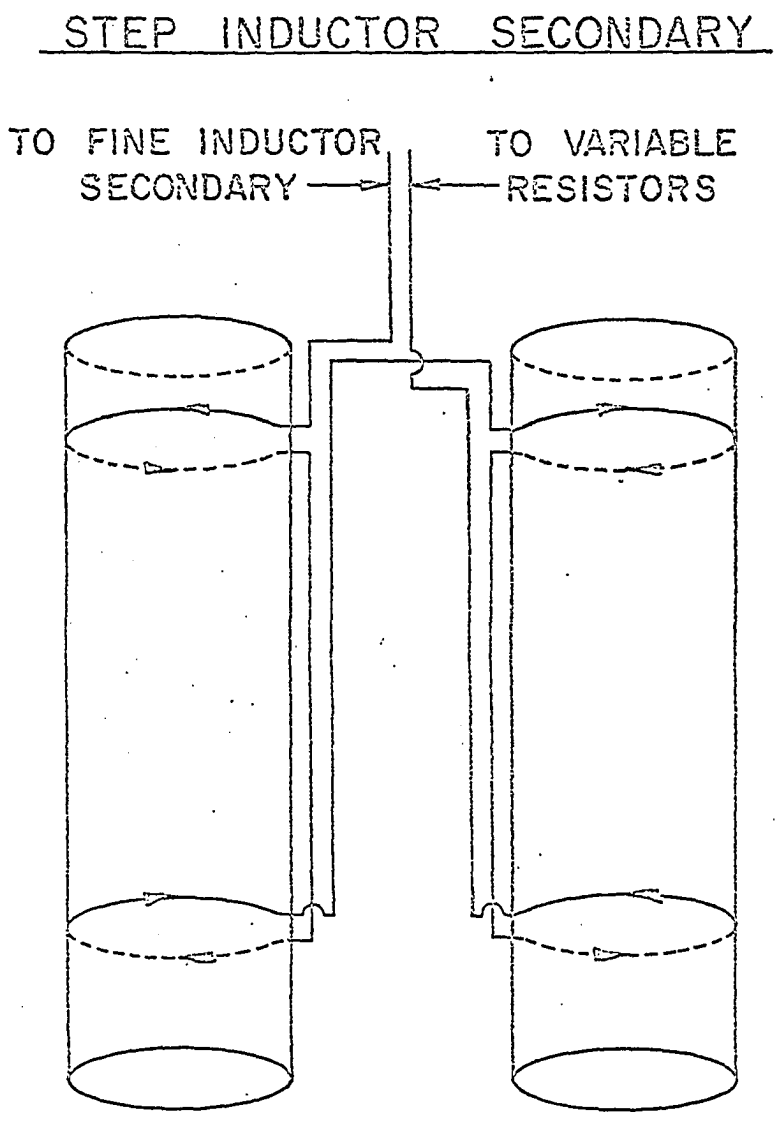

Figure 9. Circuit diagram for step inductor secondary

Figure 10. Mutual inductance bridge assembly

A. Power supply for amplifier

B. Heater control panel

C. Narrow band amplifier. Note that it is kept separate from the power supply to minimize noise pickup.

D. Step inductor

E. Fine inductor

F. Resistive circuit

G. External inductor

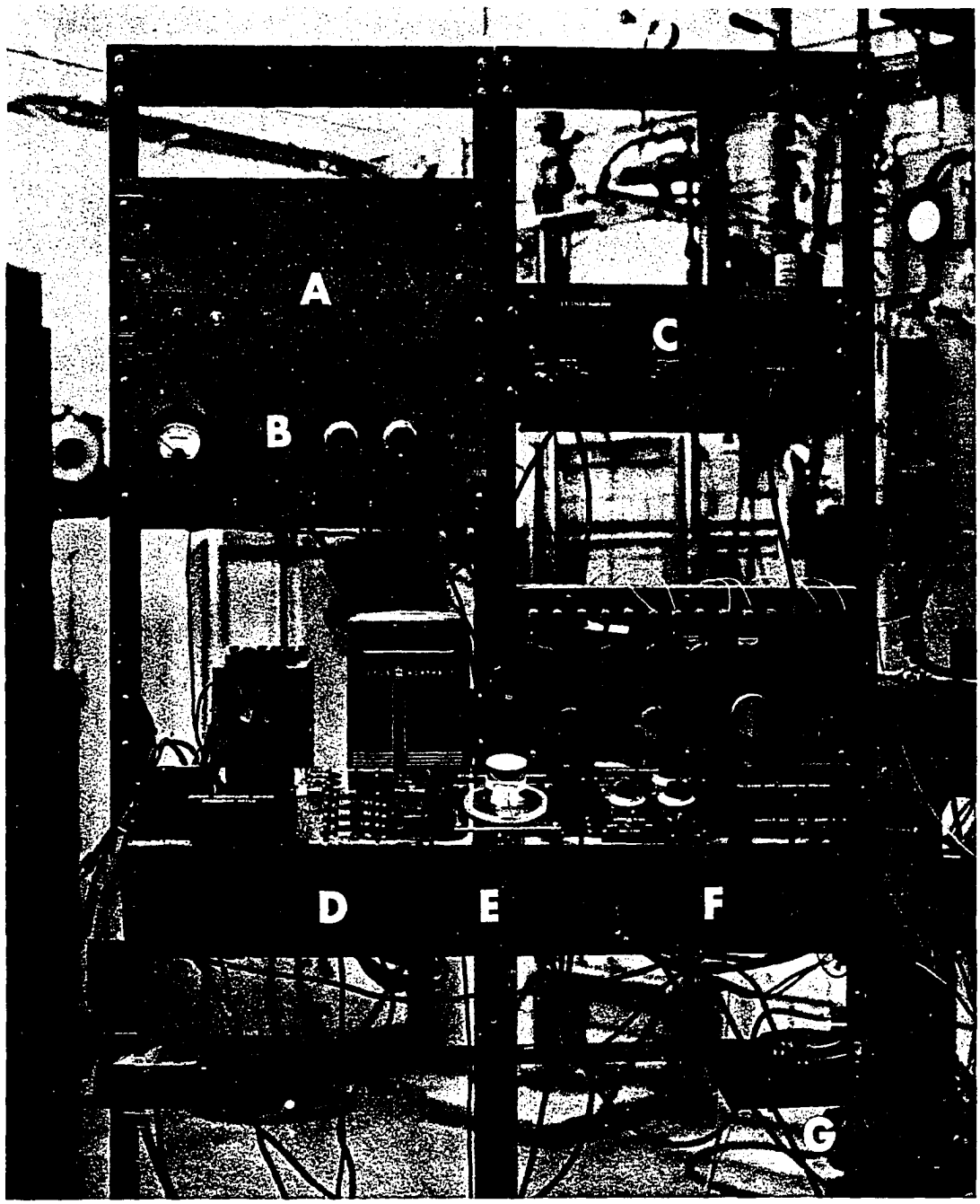
A
C
B
D
E
F
G

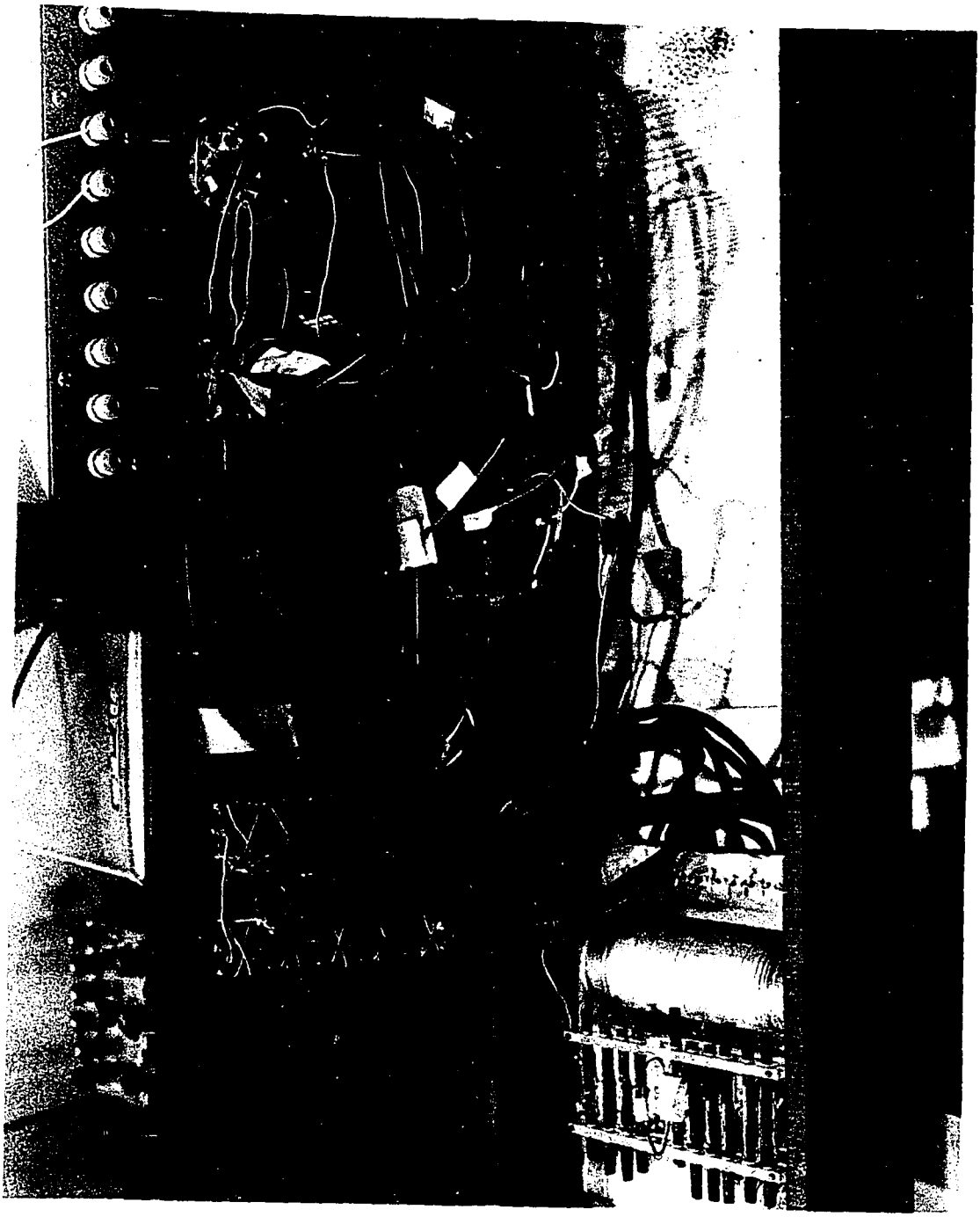

Figure 11. Inside of bridge panel

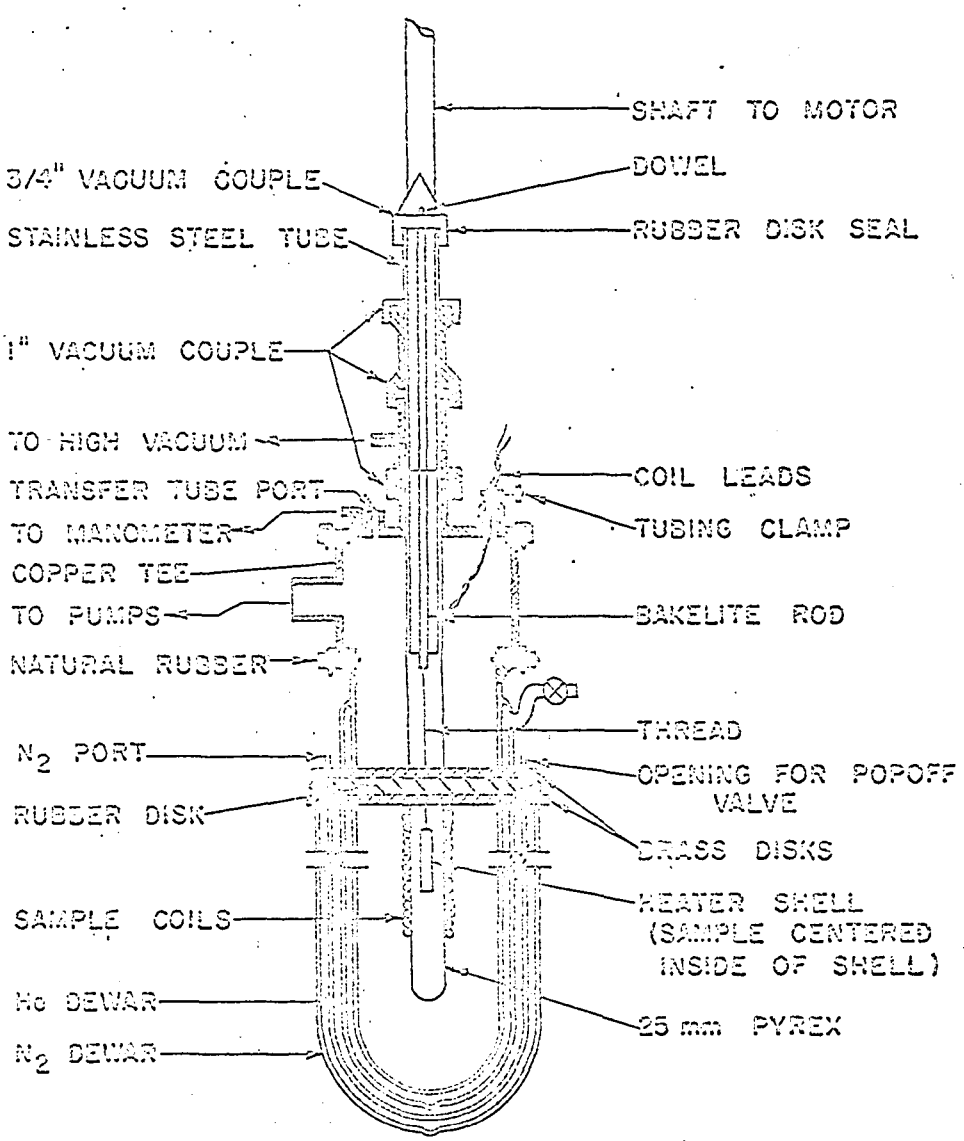

CRYOSTAT SYSTEM AND SAMPLE ARRANGEMENT WITHIN THE COIL.

Figure 12. Cryostat

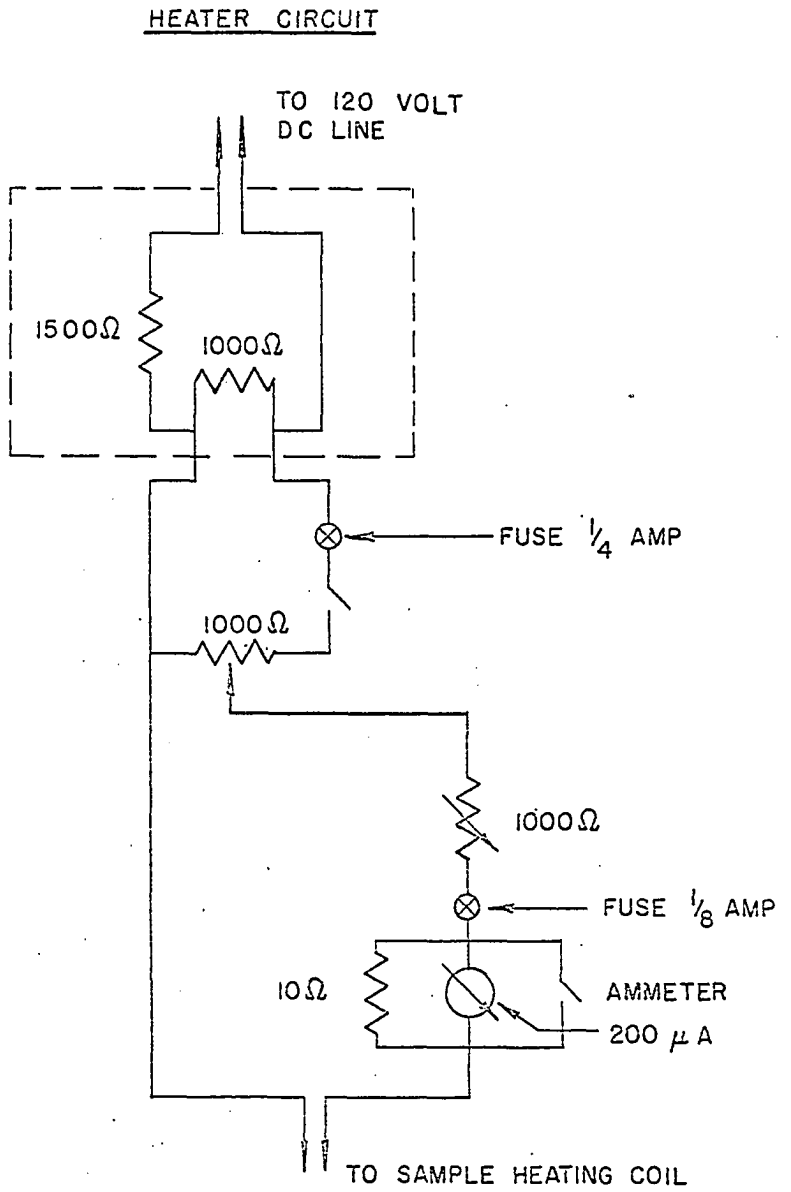

Figure 13. Circuit for supplying heat to the sample chamber

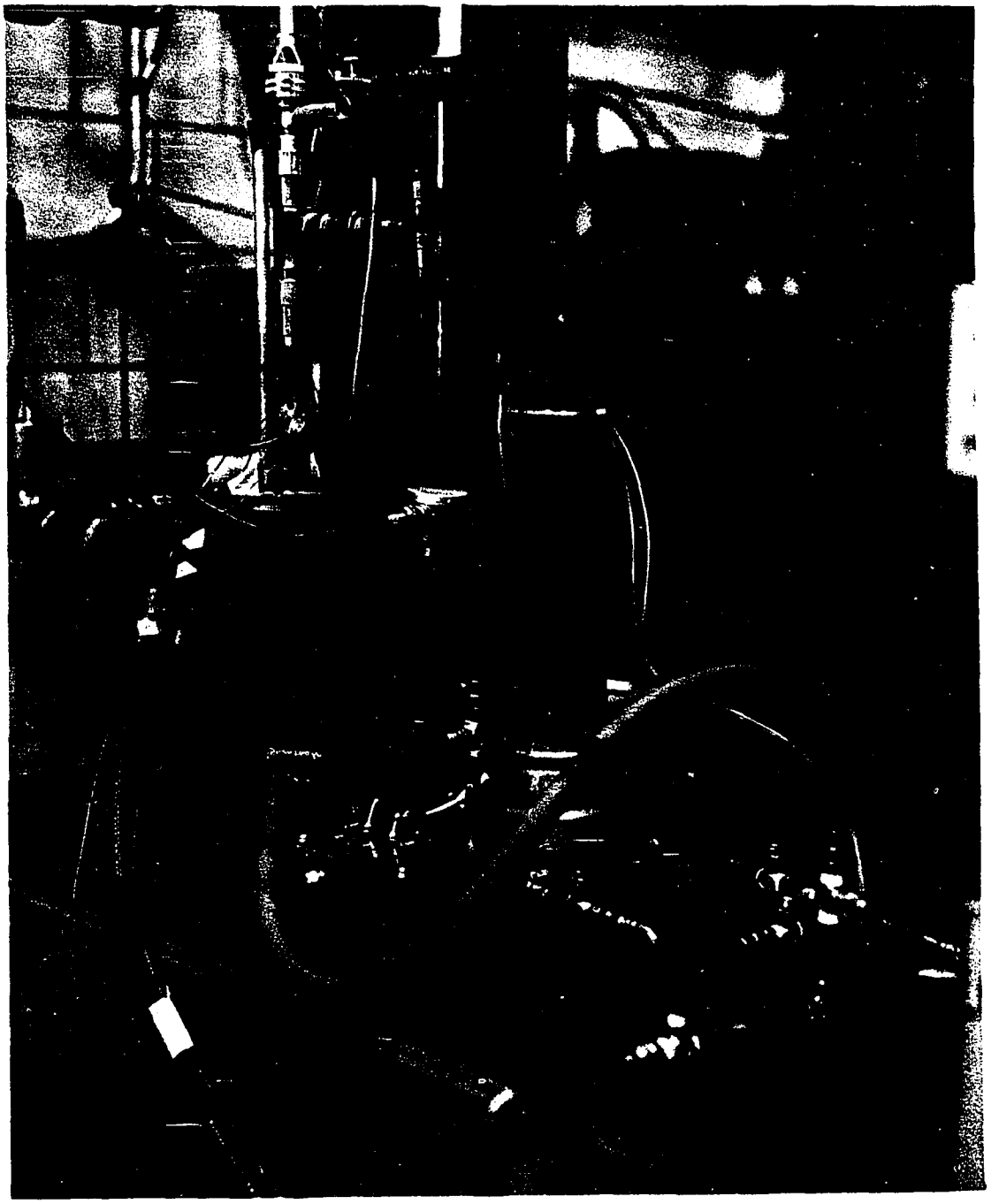

Figure 14. Pumping lines leading to top of cryostat

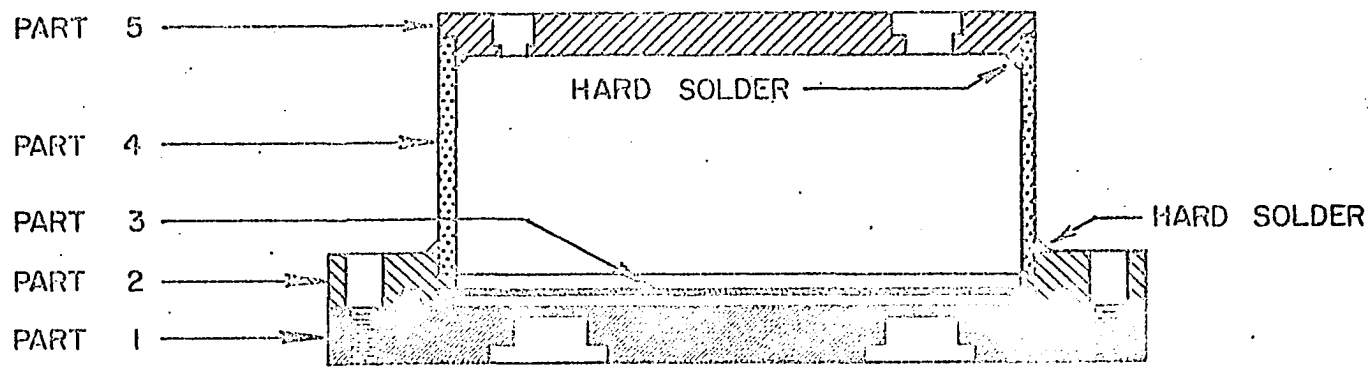

Figure 15. Manostat assembly

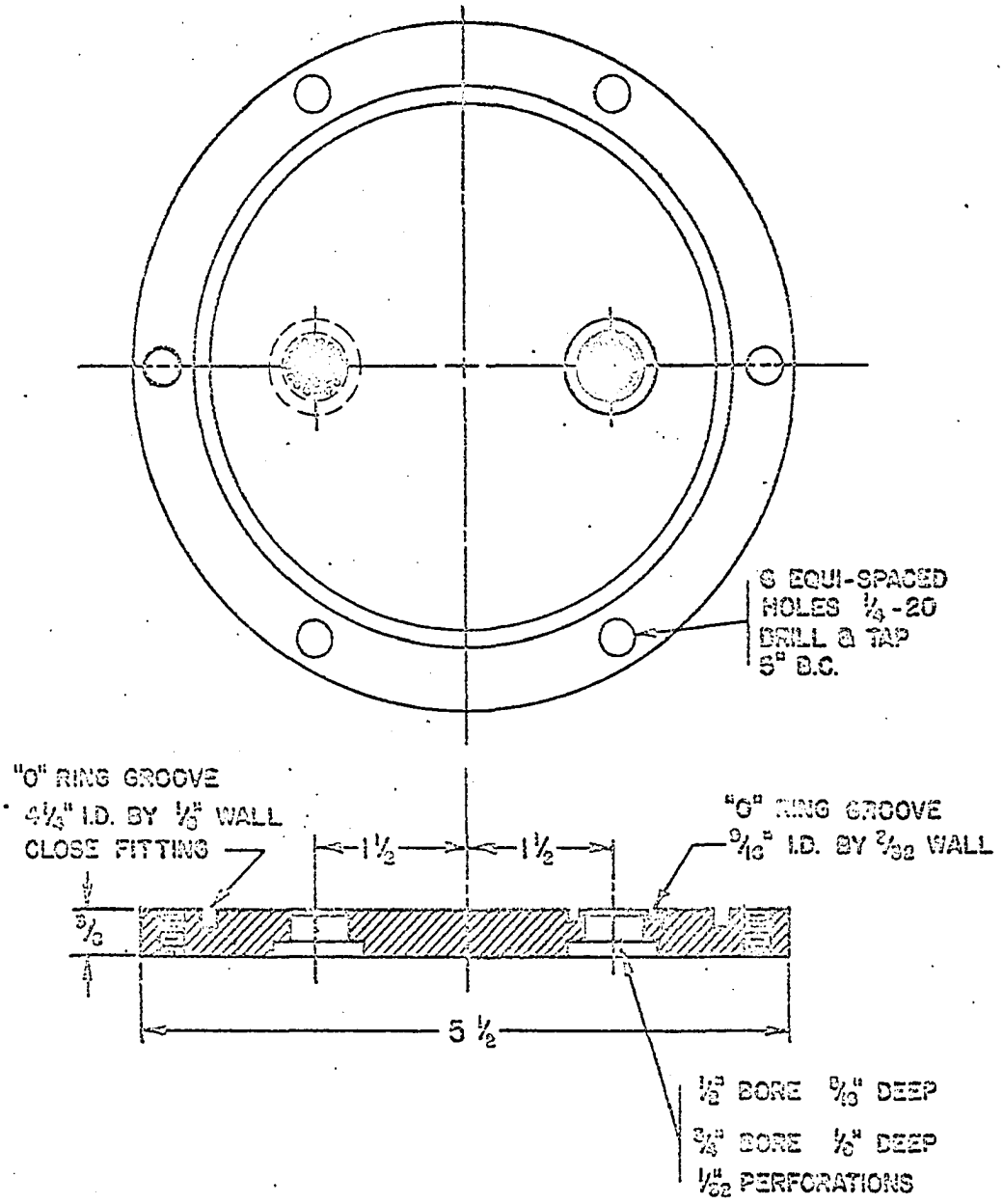

PART 1

Figure 16. Manostat component

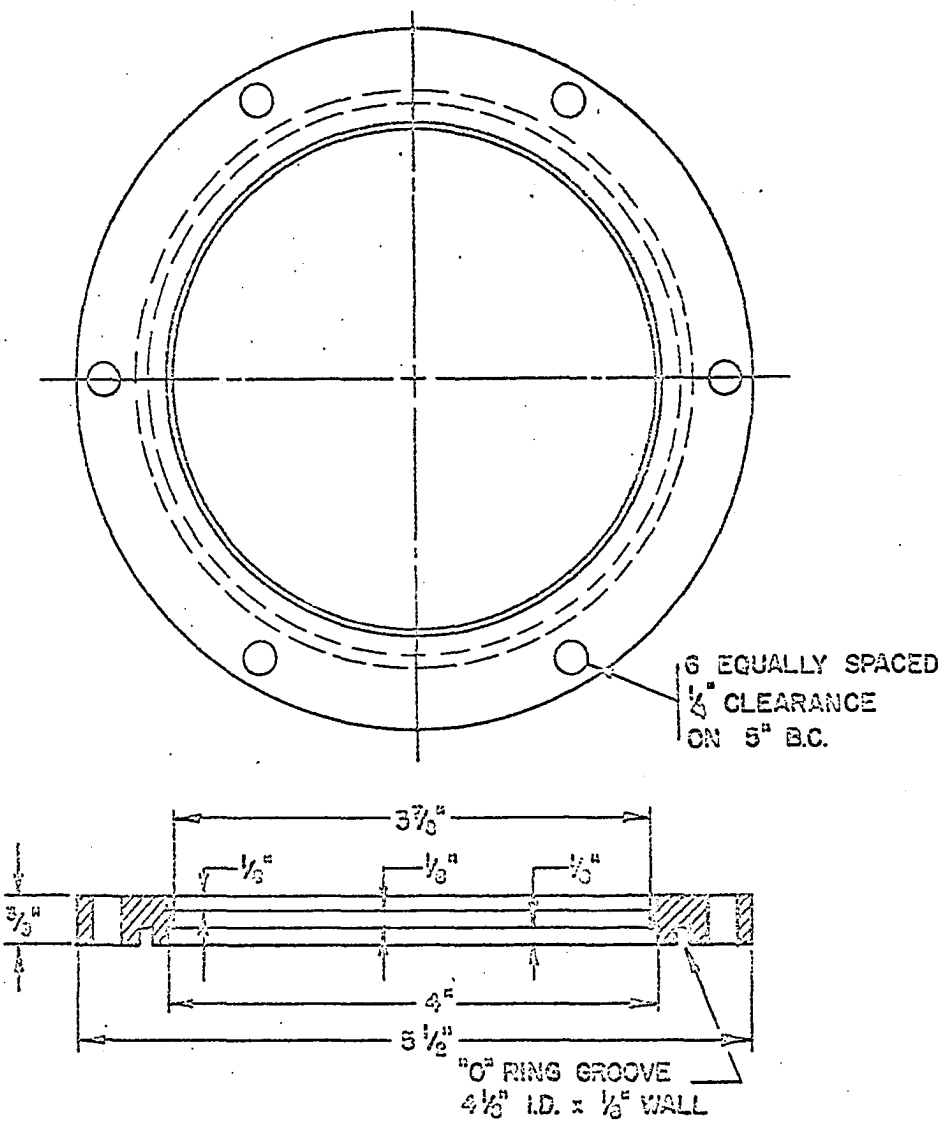

PART 2

Figure 17. Manostat component

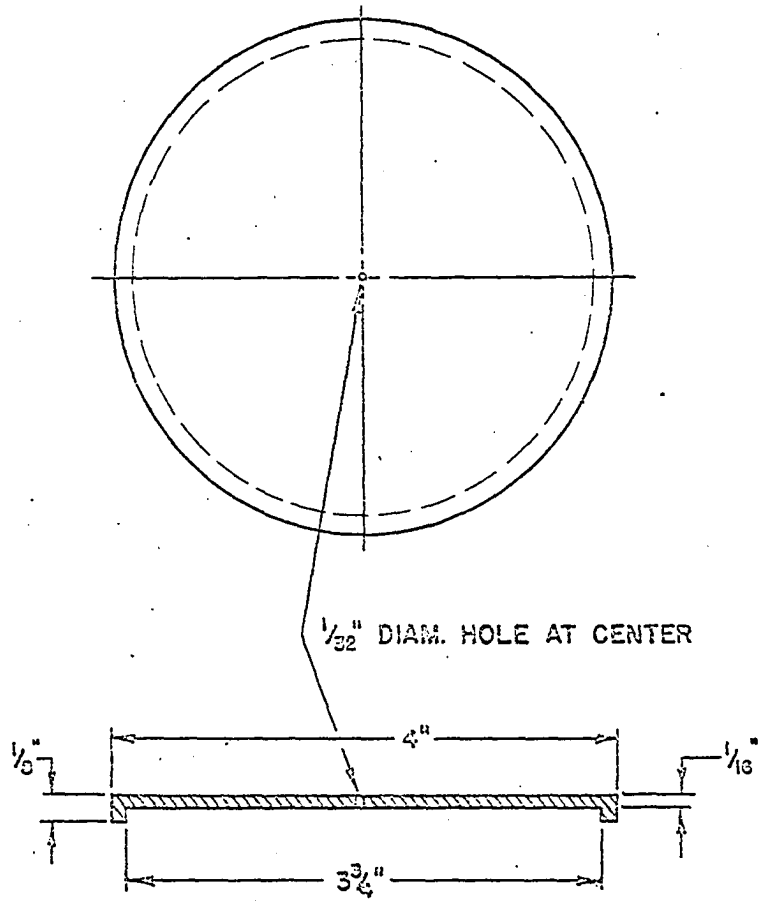

PART 3

Figure 18. Manostat component

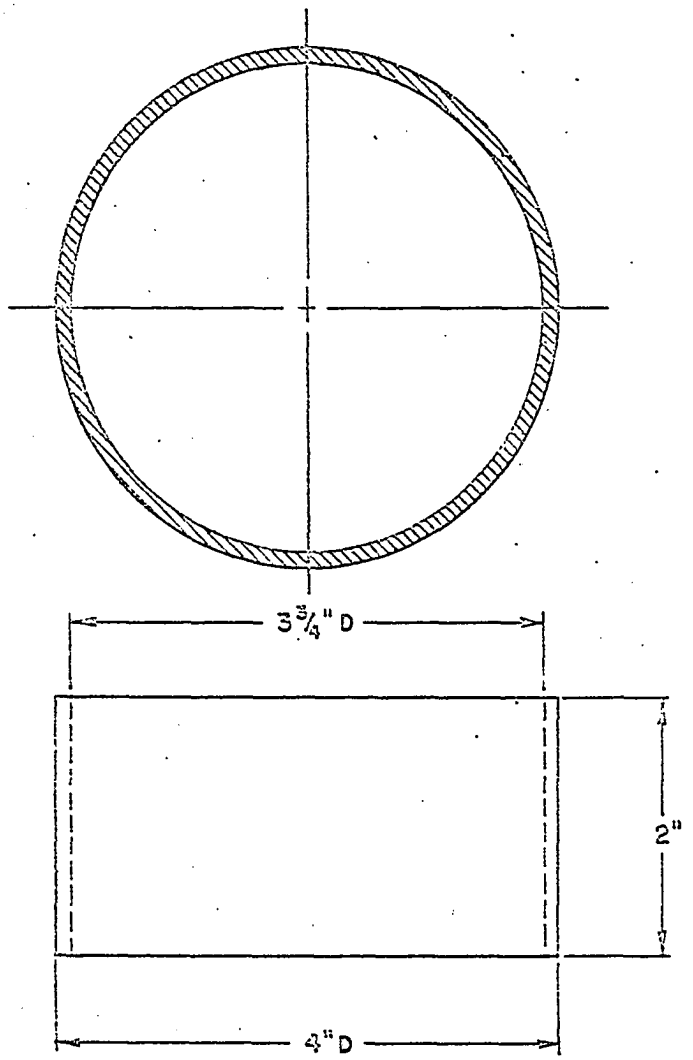

PART 4

Figure 19. Manostat component

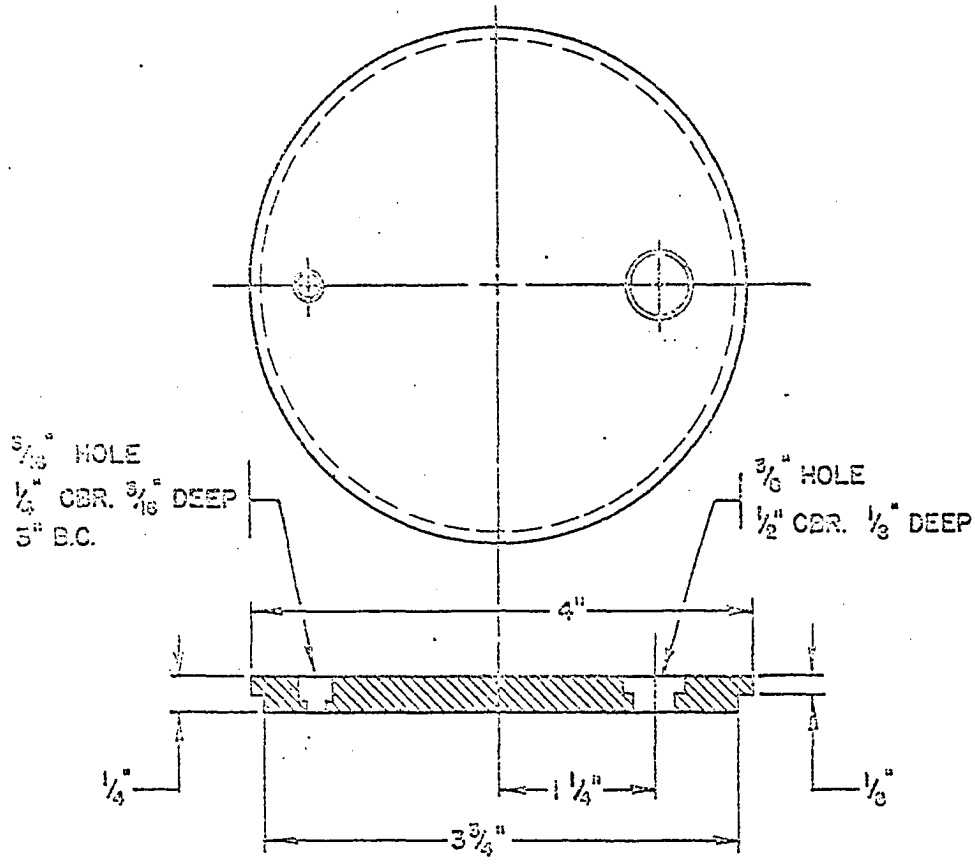

PART 5

Figure 20. Manostat component

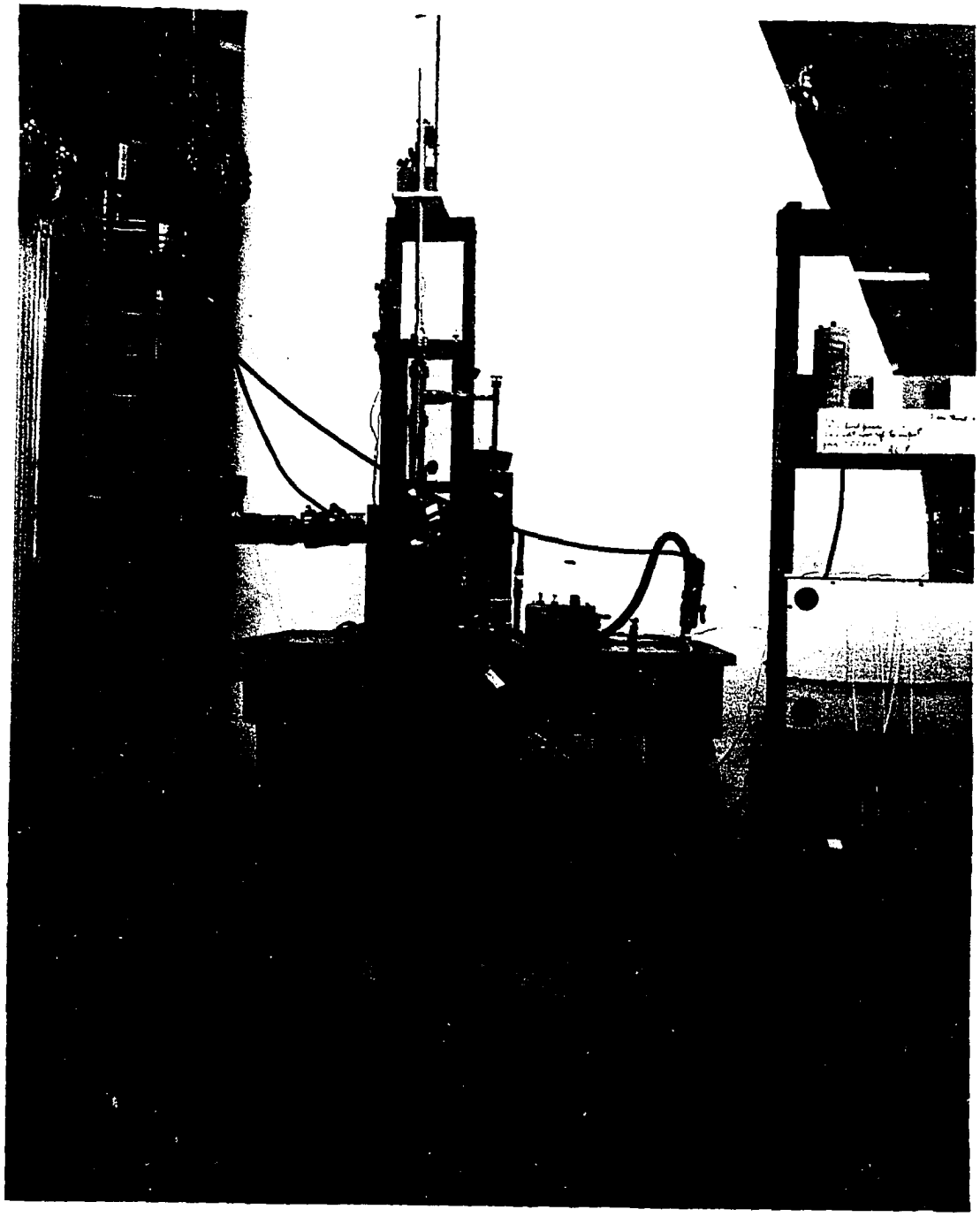

Figure 21. Cryostat and related equipment

Paramagnetic Resonance Experiments

The apparatus consists of a microwave bridge, one arm of which consists of the sample in the resonant cavity, the other a phase shifter. The two arms join in a balanced mixed detector. The difference in output from the arms is fed into a narrow band amplifier, at the modulation frequency, and then to a phase sensitive detector, filters and the recorder. A block diagram for the system can be found on page 46 of Pake (1962).

Figure 22 gives an overall view of the entire apparatus used for making paramagnetic resonance measurements. The principle components are listed below.

ESR Spectrometer:

602 B/X X band spectrometer, (Strand Laboratories, Cambridge, Mass.)
Klystron - 602 B/X S/N 111

K - 12 Power Supply

S - 20 Signal Amplifier

M - 20 Modulation Amplifier

Magnet Control:

HS - 136 5B Magnion Inc. Harvey Wells.

Magnet:

12. inch magnet with power supply and field control. Magnion Inc., Burlington, Mass.

Recorder:

Model 20XY Recorder Mosley Co., Pasadena, Calif.

Cavity:

Strand Labs room temperature cavity number SC-10-X.

Sample Holder:

The sample holder consisted of a quartz rod whose end surface was carefully cut and polished. The single crystals were affixed to this end surface with silicon grease, and were microscopically aligned. To the top of the rod, a pointer was attached, which indicated the orientation of the crystal with respect to the external field by means of a dial calibrated in degrees. Figure 23 shows the wedge, of the type used by Hutchinson and Mangrum (1961), which was affixed to the quartz rod for the measurements along one of the molecular orientations. When the 010 face was placed against the side and the 100 face against the bottom, one of the molecules was aligned with the field. That is, the Cu-Cu vector in one of the two dimer orientations could be aligned parallel to the field.

Figure 22. Electron spin resonance spectrometer and magnet

WEDGE FOR ORIENTING CRYSTAL

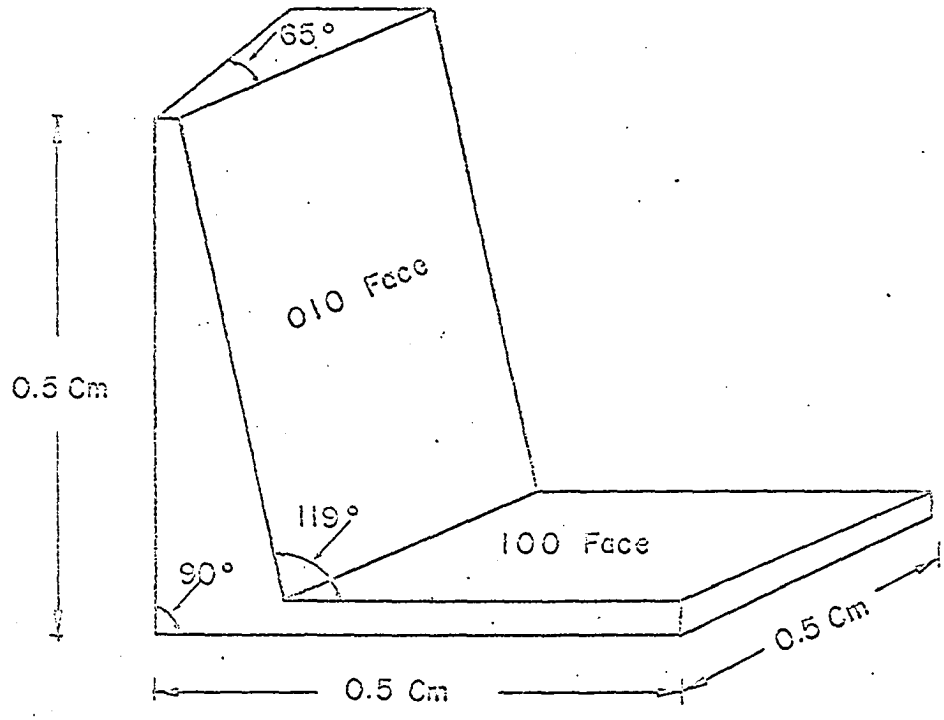

Figure 23. Device for aligning one of the dimers in the unit cell with the magnetic field

Material Preparation

$KCuCl_3$ was prepared according to the method of Groger (1393). In this method, $CuCl_2 \cdot 2H_2O$ and KCl were dissolved in concentrated HCl in a 2:1 mole ratio. The solution was allowed to evaporate in a desiccator over anhydrous $Mg(ClO_4)_2$. The crystals formed were removed from solution in a polyethylene bag under an atmosphere of dry nitrogen. The crystals were thoroughly dried on filter paper, and stored in a desiccator. The pure dry crystals were somewhat unstable to atmospheric moisture, but the crystals which were saturated with mother liquor were quite unstable, decomposing almost instantly to $K_2CuCl_4 \cdot 2H_2O$.

The crystals were analyzed by J. O'Laughlin and J. Connely of this laboratory, and the lattice constants were determined by J. Ugro of the Chemistry Dept., and were found to agree with the published data (Willett et al., 1963) within experimental error. Table 2 indicates the purity of the material.

The work of Willett, Dwiggins, Kruh, and Rundle (1963) states that the a axis of the crystal was chosen to be the needle axis, and that the crystals grow with the (010), (011), (01$\bar{1}$), and (100) faces well developed. That work also indicates the orientation of the molecule with respect to the crystal axes. Thus, a knowledge of the crystal axes and the molecular orientation can be obtained by the use of a polarizing microscope alone, as dis-

cussed below.

Table 2. Purity of $KCuCl_3$

Component	Theoretical composition	Actual composition (analytical average)
K	18.71%	18.50%
Cu	30.40	30.00
Cl	50.89	51.50
Principle impurity (Fe)	0	0.0019

Less than 1% of the total magnetic moment of the compound is due to the iron impurity, and the iron impurity is very much larger than the sum of all other impurities.

The projection of the Cu - Cu vector of the dimers on to the (010) plane makes an angle of 56° with the a axis and 41° with the c axis. Therefore, if the crystal is aligned in a magnetic field with the a axis parallel to the field and the b axis perpendicular to the field, then rotating about the b axis 56° in one direction aligns the plane of the Cu - Cu vector with the field. Alternatively, starting again with the a axis parallel to the field and the b axis perpendicular to the field, rotating 34° about the b axis in the opposite direction to the one described above, places the plane of the Cu - Cu vector perpendicular to the field. One can easily tell if he has rotated the crystal in the proper direction, since, under a

polarizing microscope, maximum extinction occurs when the electric vector is parallel to the plane of the Cu - Cu vector in the dimer.

Table 3 gives the coordinates of the positions of the copper and chlorine atoms for two dimers. Figure 24 shows the positioning of the dimers with respect to the crystal axes.

The $Mn(NH_4)_2(SO_4)_2 \cdot 6H_2O$ used in the calibration of the susceptibility apparatus was prepared by the author from a stoichometric mixture of the two sulfates in water. This alum can be roasted to $MnSO_4$ by keeping it in the temperature range 200 to 900°C for a few days. The weight lost on heating established that the original sample corresponded to the hexahydrate to within 0.07%.

Table 3. Atomic positions within the $Cu_2Cl_6^{=}$ dimer (Relative to the axes pictured in Figure 24)

Atom	A Axis	B Axis	C Axis
Cu	0.970 Å	0.690 Å	1.363 Å
Cl_1	1.108	2.743	2.300
Cl_2	2.730	-0.097	2.820
Cl_3	-0.725	1.365	0.389
Cu'	-0.970	-0.690	-1.363
Cl_1'	-1.108	-2.743	-2.300
Cl_2'	-2.730	0.097	-2.280
Cl_3'	0.725	-1.365	-0.389
Cu''	-0.970	7.590	3.010
Cl_1''	-1.108	9.643	2.070
Cl_2''	-2.730	5.003	1.550
Cl_3''	0.725	8.265	3.981
Cu'''	0.970	6.210	5.673
Cl_1'''	1.108	4.157	6.670
Cl_2'''	2.730	6.997	7.190
Cl_3'''	-0.725	5.535	4.759
K	3.155	2.358	4.868

Figure 24. Orientation of the $Cu_2Cl_6^{=}$ dimers with respect to the crystal axes

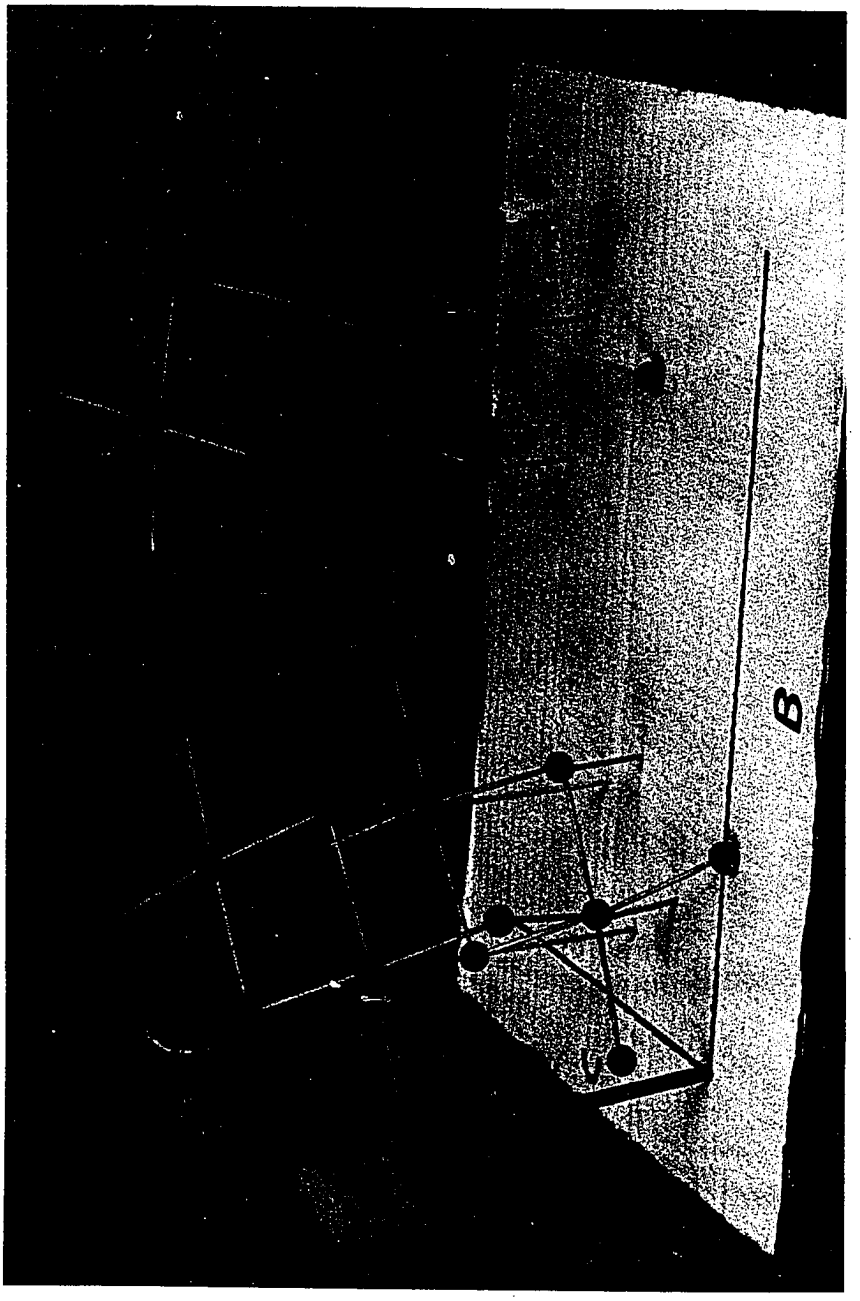
B

EXPERIMENTAL PROCEDURE

Magnetic Susceptibility Measurements

When a current is passed through the primary of the sample coils, a magnetic field, $\bar{B}$, is set up. This gives rise to a flux linkage, ϕ, (where $\phi = \int \bar{B} \cdot \bar{A}$) between the primary and the secondary. Call this ϕ_{12}.

For an alternating current, Lenz's law gives the voltage induced in the secondary.

$$E_2 = -n \frac{d\phi_{12}}{dt}$$

But this voltage is also equal to the time rate of change of primary current times a factor, M_{12}, called the MUTUAL INDUCTANCE.

$$E_2 = -n \frac{d\phi_{12}}{dt} = -M_{12} \frac{dI_1}{dt}$$

$$\therefore \quad M_{12} = n \frac{d\phi_{12}}{dI_1}$$

When a sample is introduced into the center of the coils, the flux linkage changes, therefore the mutual inductance does too. It can be shown (Gerstein and Spedding, 1960) that this change in mutual inductance is related to the macroscopic magnetic susceptibility. In the limit $\frac{4}{3}\pi\chi \ll 1$, this relation has the form:

$$\chi_m = \frac{\Delta M}{N\gamma}$$

where N is the number of moles of sample, and γ is a

constant for a given set of coils. γ is most easily determined by comparison with a sample of known susceptibility.

The salt chosen for this purpose was the manganese ammonium sulfate hexahydrate mentioned earlier. Paramagnetic down to 1°K, the salt is cubic, which means that the demagnetization field is equal, but opposite in sign, to the Lorentz field so that the total field is simply the external field. Using this calibration, the susceptibility of an unknown compound can be determined, assuming that the Lorentz field cancelling the demagnetization field is also a good approximation for the unknown.

So that the sample could be located in the region of uniform field, the center of the coils was located by lowering a paramagnetic salt into the coils, and recording the inductance at frequent intervals. The results are illustrated by Figure 25. Relative to infinite separation between sample and coil as the zero of ΔM, ΔM was found to vary by less than 0.1% over 1½ inches in the center region of the sample coils.

The process of making magnetic susceptibility measurements essentially consisted in measuring the mutual inductance of the sample coils with the inductive and resistive components of the bridge, and then remeasuring the mutual inductance with the sample withdrawn far enough from the coils so that its position no

longer has any effect on the signal. The difference in the two measurements ($M_{in}-M_{out}=\Delta M$) is related to susceptibility by calibrating the bridge with known paramagnetic susceptibility, i.e. the $Mn(NH_4)_2(SO_4)_2 \cdot 6H_2O$. The relationship is as follows:

$$\frac{\Delta M}{n\gamma} = \chi_m = \frac{N_o g^2 \beta^2 S(S+1)}{3kT - \theta}$$

where n is the number of moles of sample. A plot of $n/\Delta M$ vs. T yields a straight line, in the Curie - Weiss region, whose slope $= \frac{3k}{N_o g^2 \beta^2 S(S+1)}$. From this information, γ, the constant which calibrates the bridge, can be obtained. The value of γ was determined to be 30,800 ± 150.

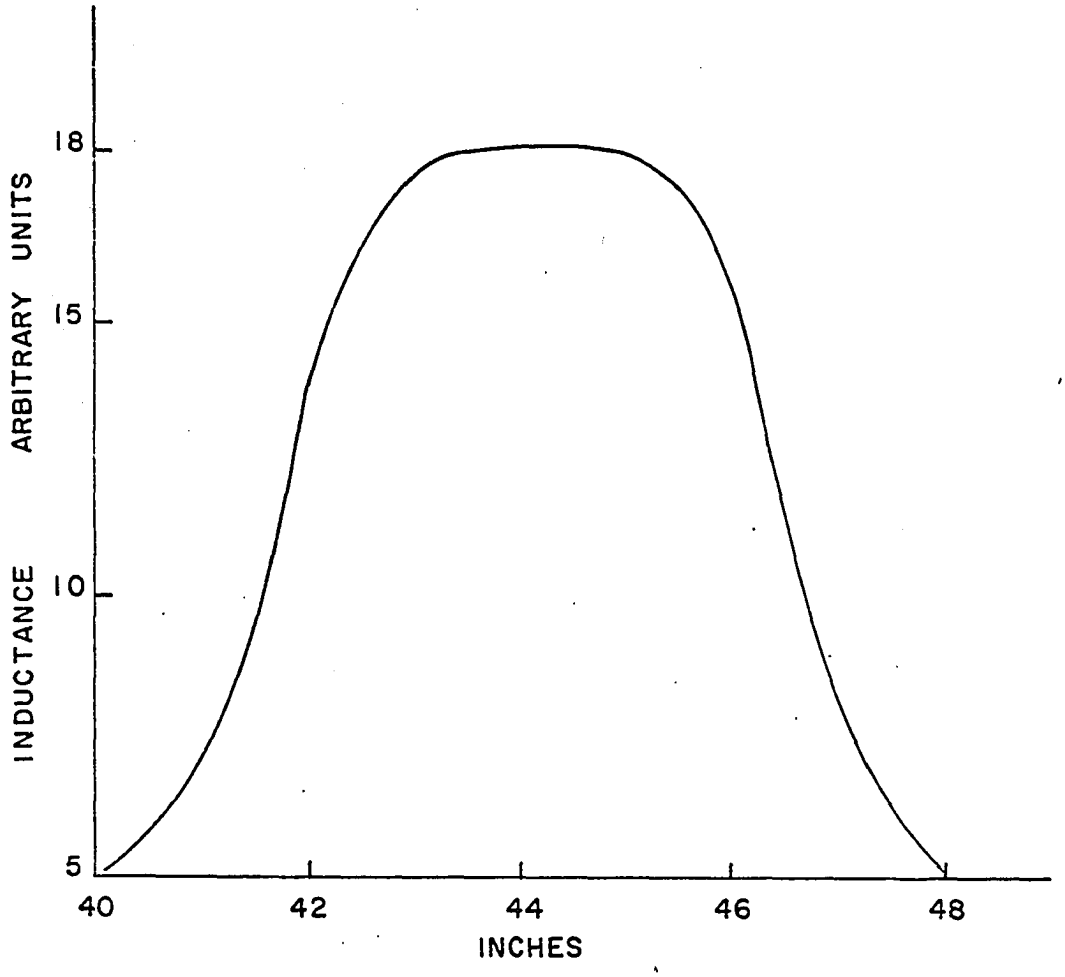

Figure 25. The center of the sample coil is 44 inches from a reference point at the top of the cryostat

As the manometer system is connected to the helium dewar, the vapor pressure over the helium bath was used as a measure of temperature for the runs below 4.2°K. The sample chamber was cooled to 4.2°K by admitting helium exchange gas to said chamber which is in contact with the liquid helium bath. Readings on the bridge were taken when thermal equilibrium was obtained, as evidenced by the constancy of the signal from the bridge. The temperature was lowered by pumping on the helium bath, and inductance measurements were taken for each in reading. This procedure was necessary, since the out readings change by several hundredths of a bridge unit for each degree the bath temperature changes due to the changing susceptibility of the pyrex tube on which the sample coils were mounted.

Above 4.2°K, the thermocouple was used as a thermometer , the tip of the thermocouple being imbedded in the sample. The temperature vs. e.m.f. table of Bunch, which was previously mentioned, was employed by obtaining a calibration point for the thermocouple at 4.2°K, and relating this to the data in the table.

Both cooling and heating mutual inductance measurements were made for the range 4.2°K to 78°K. The cooling measurements were made by introducing small amounts of exchange gas into the sample chamber and slowly letting the temperature fall to 4.2°K. The rate of cooling

could be decreased by removing some of the exchange gas with the forepump - diffusion pump system. Temperature drifts faster than 1° per 10 minutes led to non-equilibrium data and were discarded. Heating measurements were made by both pumping out the exchange gas and by using the sample heater. Merely pumping out the exchange gas caused the temperature of the sample chamber to rise about 20°K. The sample heater had to be used above that temperature, but it was also used below 20° in conjunction with the pumps to check on the constancy of the method. Cooling runs were made with and without the heater shell in the sample chamber to confirm the contribution of the shell to the mutual inductance signal. Above 4.2° the bath temperature was constant, so the out readings also remained fairly constant and were only taken every 20-30°.

When the bridge is balanced, the inductive and resistive components of the bridge are equal and opposite to the reactance of the sample coils, either with or without sample, making the secondary voltage zero. Thus, one has two components to balance which are 90° out of phase with each other. The reversing switch (Figure 2) is provided to change the phase of the primary component tapped into the secondary. The circut equations are easily obtainable from standard a.c. circuit theory (Gerstein and Spedding, 1960), (Bleaney and Bleaney, 1957).

Paramagnetic Resonance Experiments

The bridge generator produces microwave quanta which are fed into the sample cavity, as described in the apparatus section. The frequency is held constant and the field is varied. When the magnetic field is swept through the resonance condition, the sample in the cavity absorbs energy. The first derivitive of the absorption is plotted as a function of field on the recorder. The resonance was recorded for $KCuCl_3$ powder, and for $KCuCl_3$ single crystals with their axes aligned at various orientations with respect to the magnetic field.

EXPERIMENTAL RESULTS

As has been discussed in the experimental procedure section, the mutual inductance measurements yield experimental values for magnetic susceptibilities as a function of temperature and crystal orientation. A conventional plot for this data is $1/\chi_m$ vs. T. This plot, in a paramagnetic region in which energy splittings are much less than kT, exhibits a straight line of the form

$$\chi_m = \frac{C}{T - \Theta} .$$

Figure 26 shows the experimental points for $KCuCl_3$ powder. In this figure, as in all the susceptibility plots in this work, χ_m means susceptibility per mole of $K_2Cu_2Cl_6$. The plot was used because the $Cu_2Cl_6^{=}$ dimer is the magnetic species of interest. In Figure 27, the solid curve is the fit of the theoretical plot based on a triplet level lying 55k above a singlet, to the experimental points for the powder. The agreement between the theoretical and experimental slopes is less than a 2% error.

The remaining figures and tables in this section, i.e., Figures 28 through 37, show the dependence of reciprocal molar susceptibility vs temperature, and the first derivative of the paramagnetic resonance spectra (intensity vs field) for various orientations of the single crystal with respect to field in each case.

Table 4. Reciprocal molar susceptibility of $KCuCl_3$ powder. $\frac{1}{\chi_m} = \frac{56.32}{\Delta M}$

Cooling Data			Heating Data		
ΔM	T	$\frac{1}{\chi_m}$	ΔM	T	$\frac{1}{\chi_m}$
0.400	101.0	140.8	1.100	4.2	51.2
0.403	93.3	139.7	0.811	8.2	69.4
0.434	85.3	129.7	0.638	11.0	88.3
0.423	82.6	133.2	0.597	12.8	94.3
0.470	77.8	119.9	0.538	15.3	104.7
0.465	71.3	121.1	0.495	16.1	113.8
0.512	64.2	110.0	0.481	17.0	117.1
0.542	59.7	103.9	0.523	18.6	107.7
0.559	56.6	100.8	0.564	20.2	99.9
0.577	53.4	97.6	0.586	22.3	96.1
0.583	50.1	96.6	0.661	24.4	85.2
0.624	46.8	90.3	0.705	26.9	79.9
0.646	43.3	87.2	0.767	31.5	73.4
0.682	39.7	82.6	0.746	35.6	75.5
0.735	35.9	76.6	0.679	40.6	82.9
0.744	32.8	75.7	0.639	46.7	88.1
0.763	31.1	73.8	0.625	50.0	90.1
0.742	27.2	75.9	0.559	56.6	100.7
0.755	24.4	74.6	0.510	62.6	110.4
0.695	23.3	81.0	0.483	68.4	116.6
0.638	22.2	88.3	0.471	74.1	119.5
0.586	21.7	96.1	0.460	79.7	122.5
0.537	21.1	104.9	0.425	55.2	132.5
0.549	19.9	102.6	0.597	12.8	94.3
0.536	18.8	105.1	0.538	15.5	104.7
0.524	18.4	107.5			
0.589	15.5	95.6			
0.722	14.0	78.0			
1.170	4.2	48.1			
1.134	4.2	49.7			
1.130	4.2	49.8			
1.730	3.1	32.6			
2.905	2.2	19.4			
5.205	1.4	10.8			

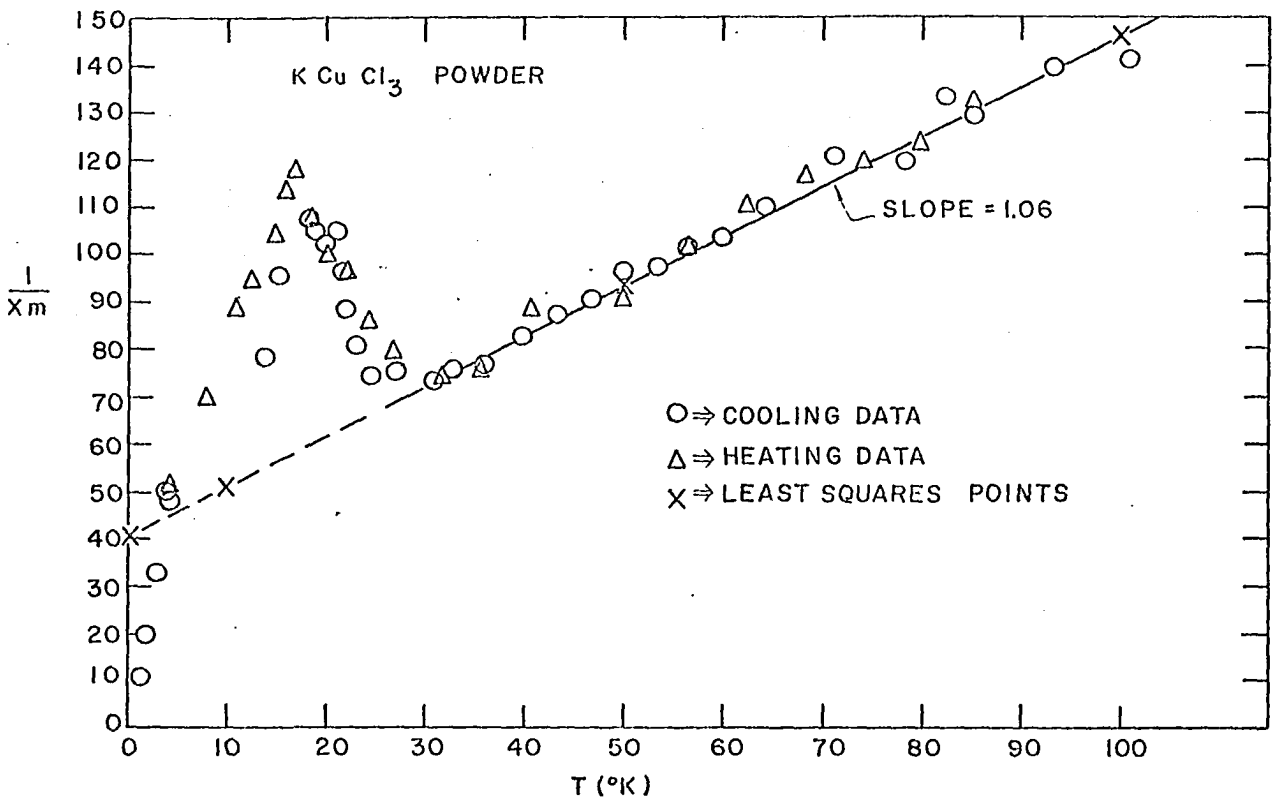

Figure 26. Reciprocal molar susceptibility vs. temperature for $KCuCl_3$ powdor

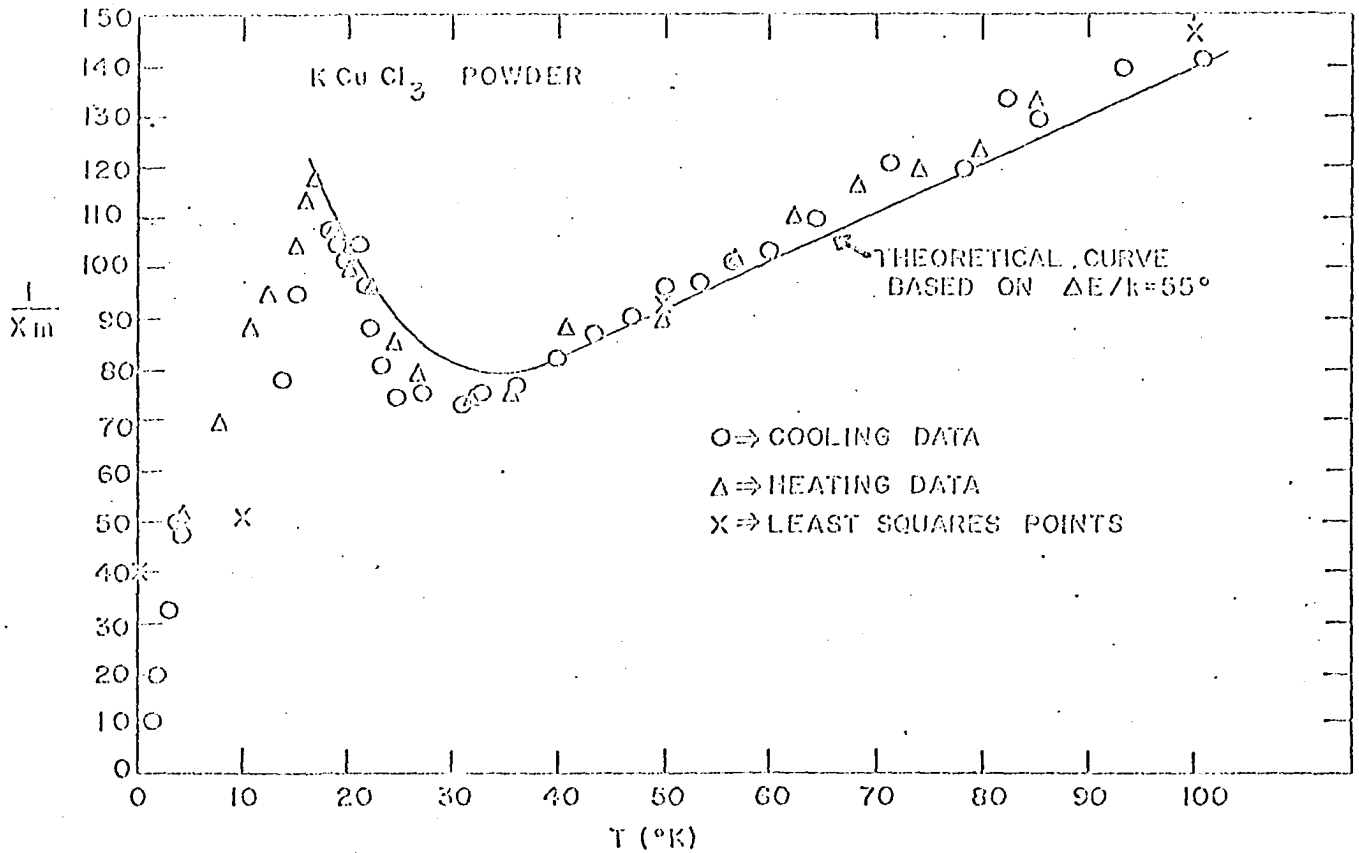

Figure 27. Experimental points and theoretical curves for susceptibility

Table 5. Reciprocal molar susceptibility of $KCuCl_3$ single crystal, sample #1, $\frac{1}{\chi_m} = \frac{11.79}{\Delta M}$, field parallel to a axis

Cooling Data			Heating Data		
ΔM	T	$\frac{1}{\chi_m}$	ΔM	T	$\frac{1}{\chi_m}$
0.146	49.8	80.8	0.350	4.2	33.6
0.160	44.1	73.7	0.162	8.4	72.8
0.171	35.7	68.9	0.144	9.6	81.9
0.185	31.1	63.7	0.112	12.6	105.2
0.196	26.5	59.9	0.110	15.3	107.2
0.184	21.8	63.9	0.106	16.5	111.2
0.176	18.7	67.0	0.109	18.2	108.2
0.180	15.3	109.2	0.187	21.3	63.0
0.128	12.5	92.1	0.188	26.5	62.7
0.150	10.0	78.6	0.180	31.1	65.5
0.177	7.0	66.6	0.179	35.3	65.9
0.350	4.2	33.6	0.174	39.3	67.8
			0.162	42.8	72.7
			0.150	46.4	78.6
			0.147	49.8	80.2

Table 6. Reciprocal molar susceptibility of $KCuCl_3$ single crystal, sample #2, $\frac{1}{\chi_m} = \frac{30.67}{\Delta M}$, field parallel to a axis

Cooling Data			Heating Data		
ΔM	T	$\frac{1}{\chi_m}$	ΔM	T	$\frac{1}{\chi_m}$
0.348	56.0	88.2	0.932	4.2	32.9
0.393	46.3	78.0	0.404	9.9	76.3
0.610	30.0	56.5	0.276	16.5	111.2
0.578	23.9	59.1	0.443	18.0	69.2
0.563	21.1	60.6	0.477	21.1	64.3
0.513	18.0	66.8	0.526	26.4	58.3
0.281	15.3	109.2	0.499	31.0	61.5
0.419	9.9	73.2	0.475	35.2	64.6
0.939	4.2	32.6	0.455	39.1	67.4
1.371	3.0	22.4	0.423	42.8	72.5
1.931	2.1	16.2	0.394	46.3	77.8
2.749	1.4	11.2	0.377	49.7	81.4

Figure 28. Reciprocal susceptibility vs. temperature for a $KCuCl_3$ single crystal with its a axis aligned parallel to the external field

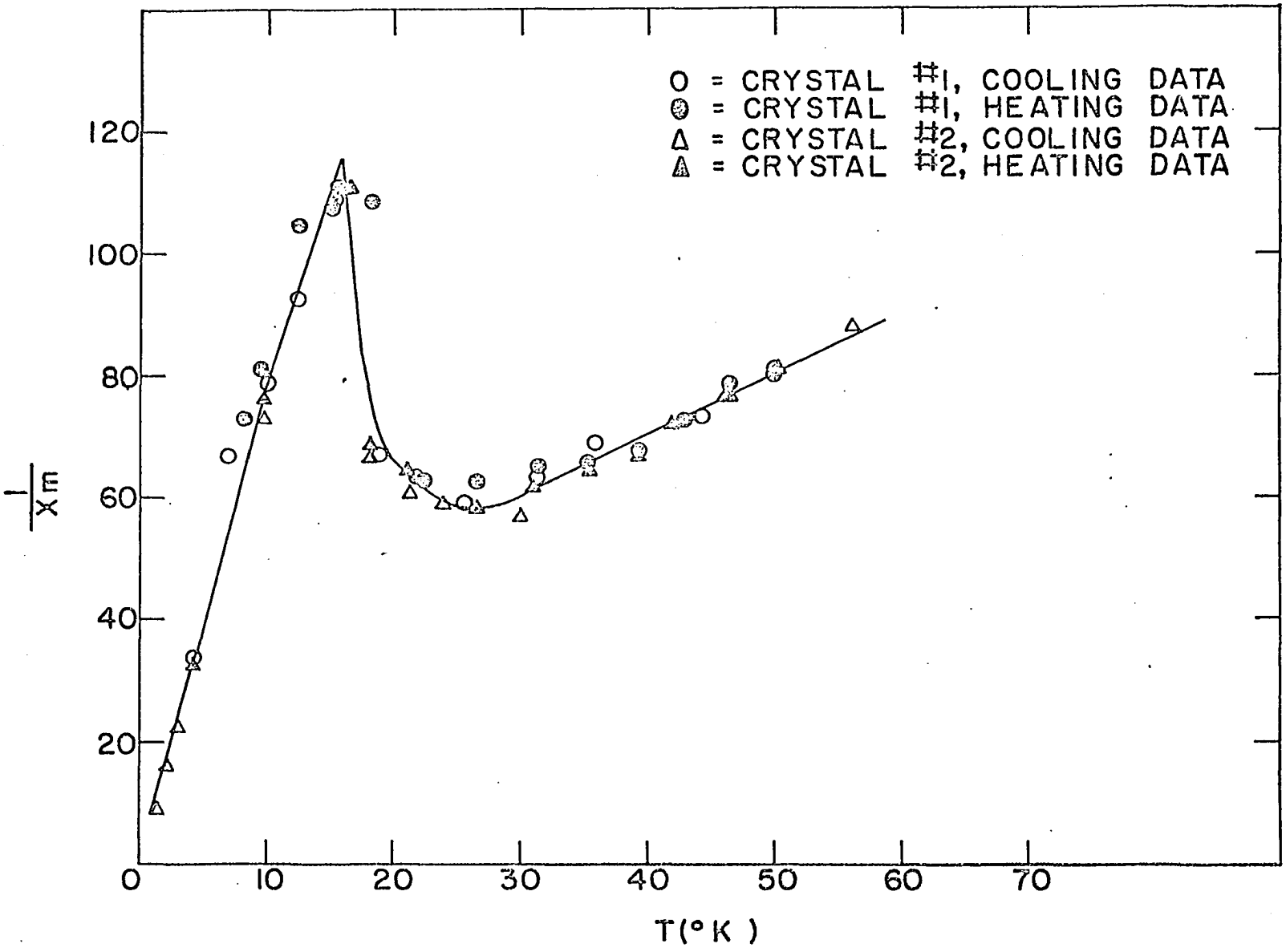
O = CRYSTAL #1, COOLING DATA
⊙ = CRYSTAL #1, HEATING DATA
Δ = CRYSTAL #2, COOLING DATA
▲ = CRYSTAL #2, HEATING DATA
1/Xm
120
100
80
60
40
20
0
10
20
30
40
50
60
70
T(°K)

Table 7. Reciprocal molar susceptibility of $KCuCl_3$ single crystal, sample #3, $\frac{1}{\chi_m} = \frac{20.30}{\Delta M}$, field parallel to b axis

Cooling Data			Heating Data		
ΔM	T	$\frac{1}{\chi_m}$	ΔM	T	$\frac{1}{\chi_m}$
0.226	50.0	89.8	0.659	4.2	30.8
0.238	46.7	85.3	0.276	11.0	73.5
0.245	43.2	82.9	0.235	13.2	86.4
0.263	39.5	77.2	0.220	15.2	92.3
0.270	35.6	75.2	0.215	17.0	94.4
0.297	31.5	68.4	0.225	18.6	90.2
0.286	26.5	70.9	0.241	21.2	84.2
0.245	21.2	82.9	0.244	21.7	83.2
0.224	18.1	90.6	0.268	26.5	75.7
0.203	17.6	100.0	0.290	31.1	70.0
0.208	17.0	97.6	0.277	35.3	73.3
0.221	15.2	91.9	0.265	39.5	76.6
0.226	14.6	89.8	0.255	43.2	79.6
0.290	11.0	70.0	0.241	46.7	84.2
0.332	9.7	61.1	0.222	50.0	91.4
0.648	4.6	31.3			
0.657	4.2	30.9			
0.858	3.1	23.7			
1.284	2.2	15.8			
1.750	1.4	11.6			

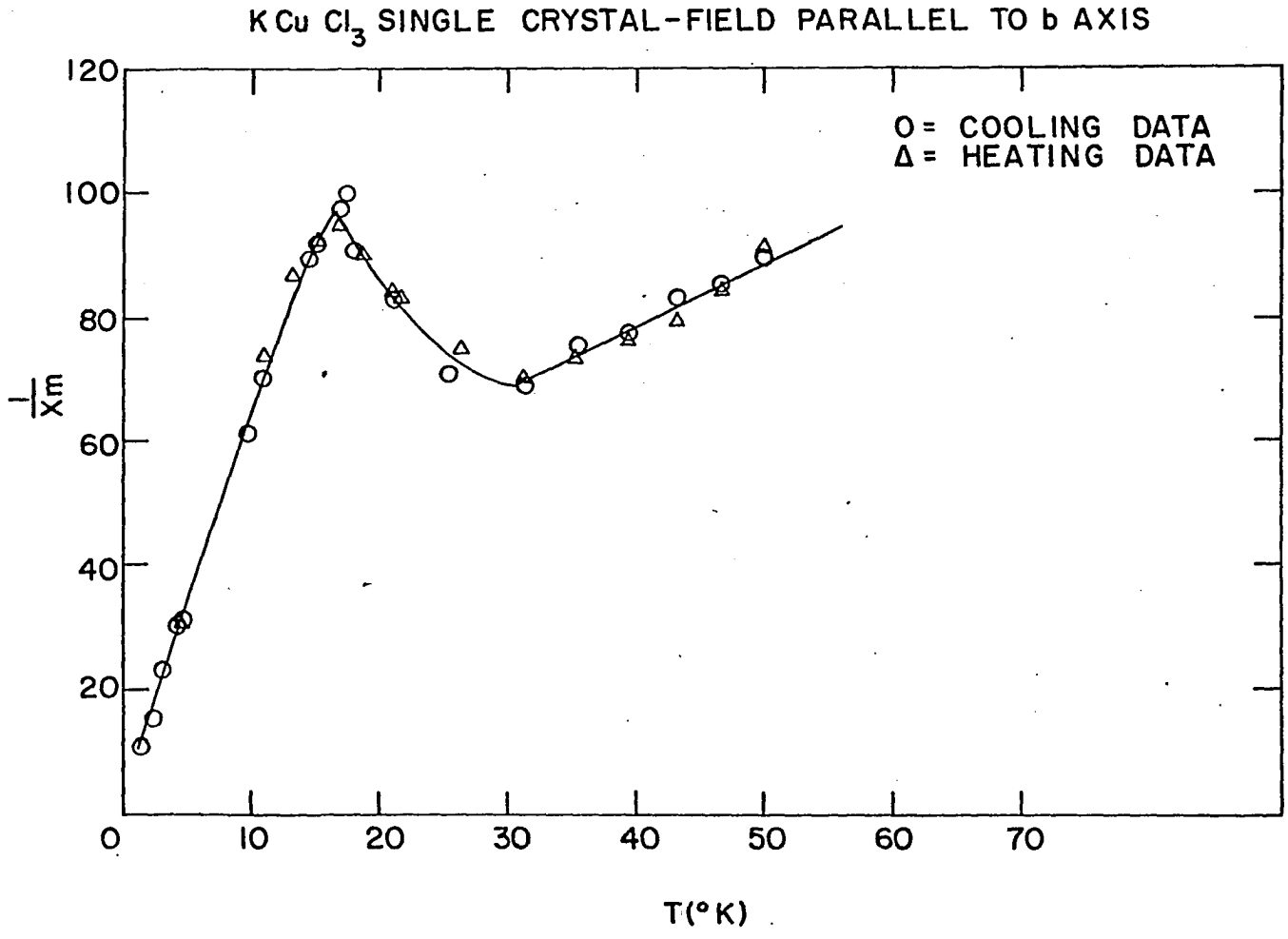

Figure 29. Reciprocal susceptibility vs. temperature for a $KCuCl_3$ with its b axis aligned parallel to the external field

Table 8. Reciprocal molar susceptibility of $KCuCl_3$ single crystal, sample #4, $\frac{1}{\chi_m} = \frac{27.96}{\Delta M}$, field perpendicular to a and b axes

Cooling Data			Heating Data		
ΔM	T	$\frac{1}{\chi_m}$	ΔM	T	$\frac{1}{\chi_m}$
0.255	49.6	109.6	0.649	4.2	43.1
0.260	49.3	107.5	0.658	4.2	42.5
0.268	46.3	104.3	0.362	7.7	77.2
0.278	42.8	100.6	0.377	7.7	74.2
0.279	42.7	100.2	0.300	10.0	93.2
0.287	39.1	97.4	0.301	10.0	92.9
0.299	35.2	93.5	0.334	12.3	83.7
0.303	55.1	92.0	0.330	12.3	84.7
0.306	31.6	91.4	0.350	14.5	79.9
0.309	30.9	90.5	0.355	14.5	78.8
0.313	28.8	89.3	0.354	18.1	79.0
0.318	26.3	87.9	0.364	18.1	76.8
0.335	26.2	83.5	0.374	21.1	74.8
0.354	21.0	79.0	0.352	21.1	79.4
0.373	20.4	75.0	0.334	26.4	83.7
0.355	17.9	78.8	0.332	26.4	84.2
0.374	17.7	74.8	0.315	31.1	88.8
0.354	14.3	79.0	0.345	31.1	81.0
0.350	14.1	79.9	0.299	35.3	93.5
0.345	12.2	81.0	0.303	35.6	92.0
0.301	9.8	92.9	0.297	36.5	94.1
0.334	9.5	83.7	0.306	39.2	91.4
0.400	7.6	69.9	0.290	39.2	96.4
0.666	4.2	42.0	0.286	42.9	97.8
0.671	4.2	41.7	0.278	42.4	100.6
0.883	3.1	31.7	0.255	46.4	109.6
1.223	2.1	22.9	0.267	46.4	104.7
1.745	1.4	16.0	0.263	49.8	106.3
			0.261	49.8	107.1
			0.259	50.0	108.0

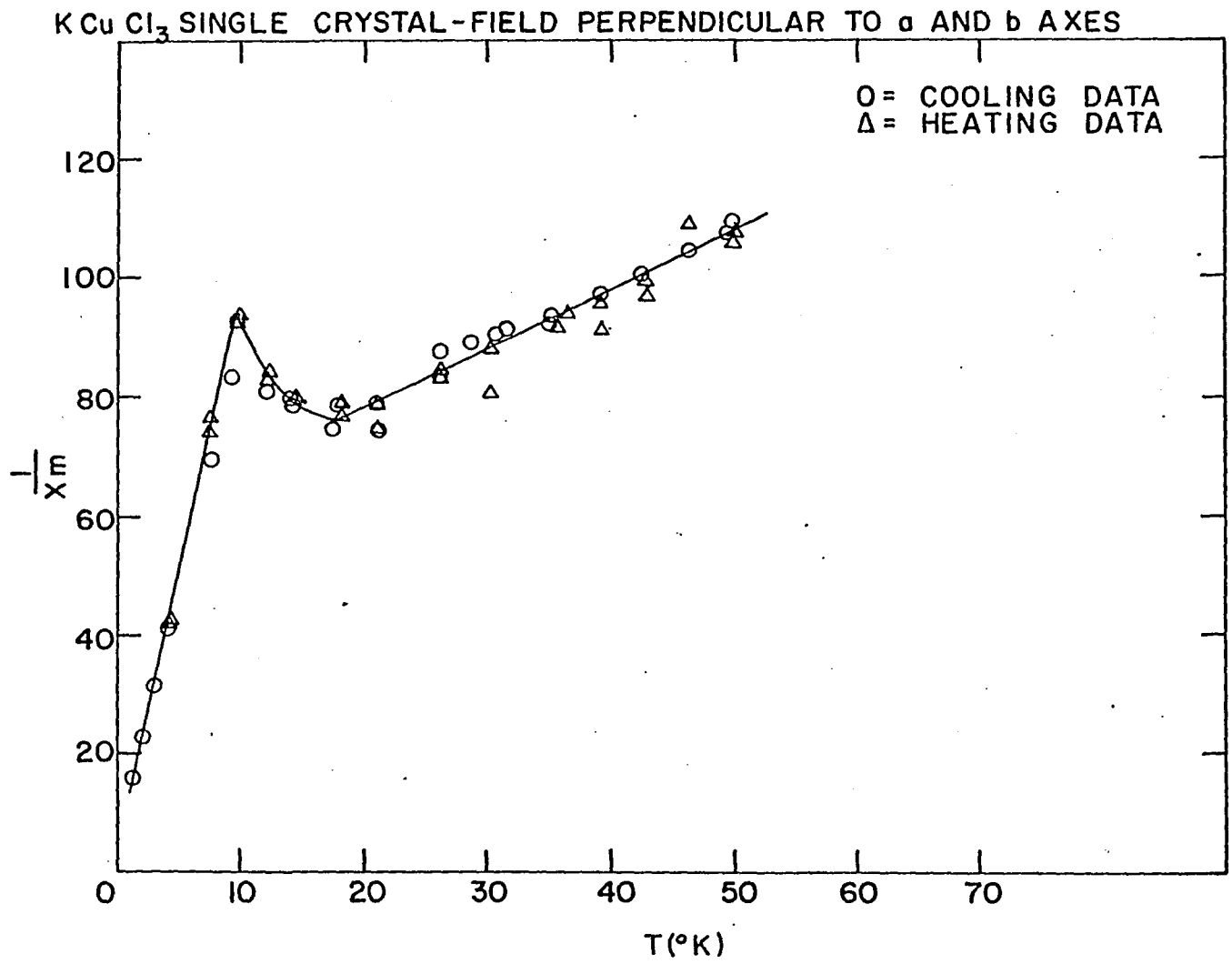

Figure 30. Susceptibility for a $KCuCl_3$ crystal with its a and b axes aligned perpendicular to the external field

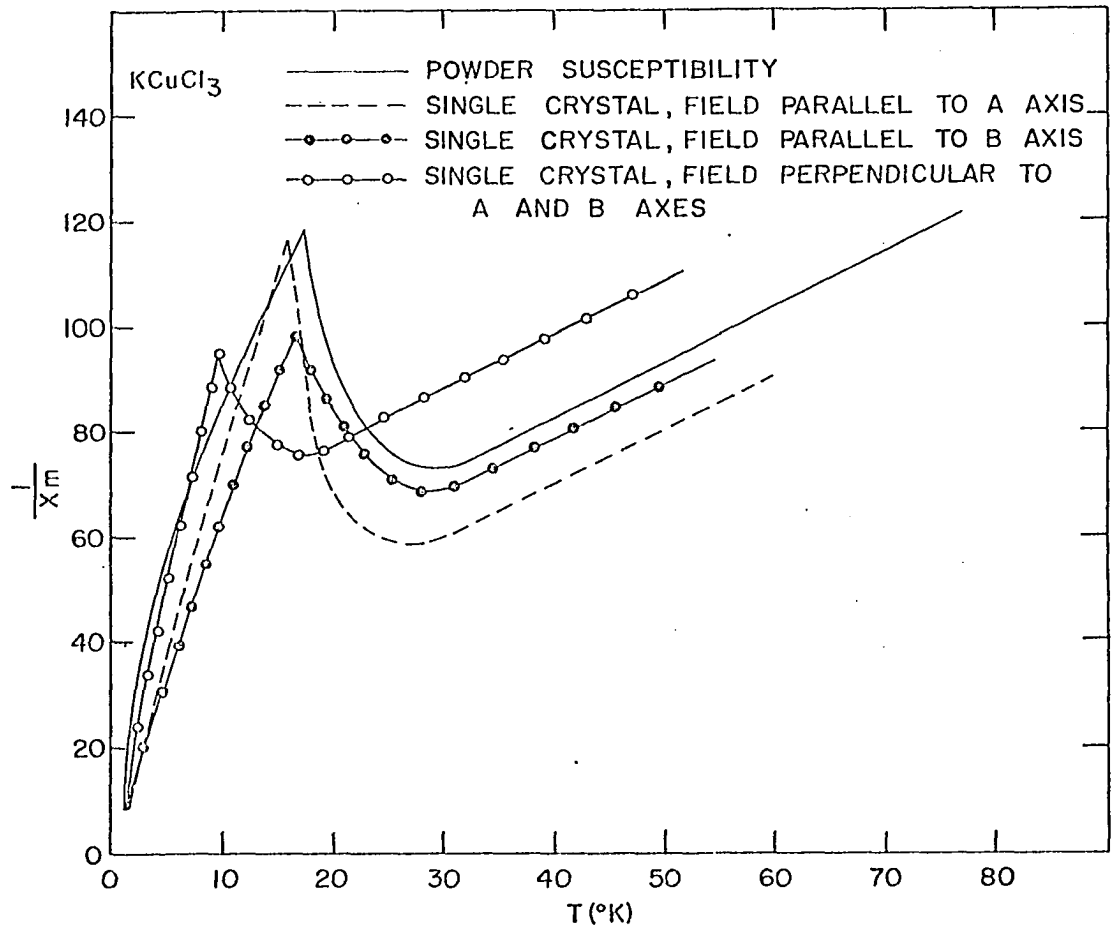

Figure 31. Comparison of susceptibility curves for $KCuCl_3$ powder and single crystals in various orientations

Table 9. Reciprocal molar susceptibility of $KCuCl_3$ single crystal, sample #5, $\frac{1}{\chi_m} = \frac{14.36}{\Delta M}$, field parallel to plane of Cu-Cu vectors

Cooling Data			Heating Data		
ΔM	T	$\frac{1}{\chi_m}$	ΔM	T	$\frac{1}{\chi_m}$
0.155	49.8	92.6	0.667	4.2	21.5
0.163	46.4	88.1	0.239	9.7	60.2
0.166	42.9	86.6	0.169	14.6	85.0
0.182	39.2	78.9	0.153	17.0	94.0
0.187	35.3	76.8	0.186	18.1	77.2
0.199	31.1	72.2	0.193	21.2	74.4
0.203	26.5	70.8	0.199	26.5	72.1
0.183	21.2	78.4	0.205	31.1	70.0
0.167	18.1	86.0	0.188	35.3	76.4
0.167	14.6	86.0	0.185	39.2	78.8
0.212	9.7	67.7	0.172	42.9	83.6
0.274	5.1	52.4	0.165	46.4	87.2
0.607	4.2	23.6	0.159	49.8	90.3
0.708	3.1	20.3	0.150	56.2	96.0
0.890	2.2	16.1			
1.410	1.4	10.4			

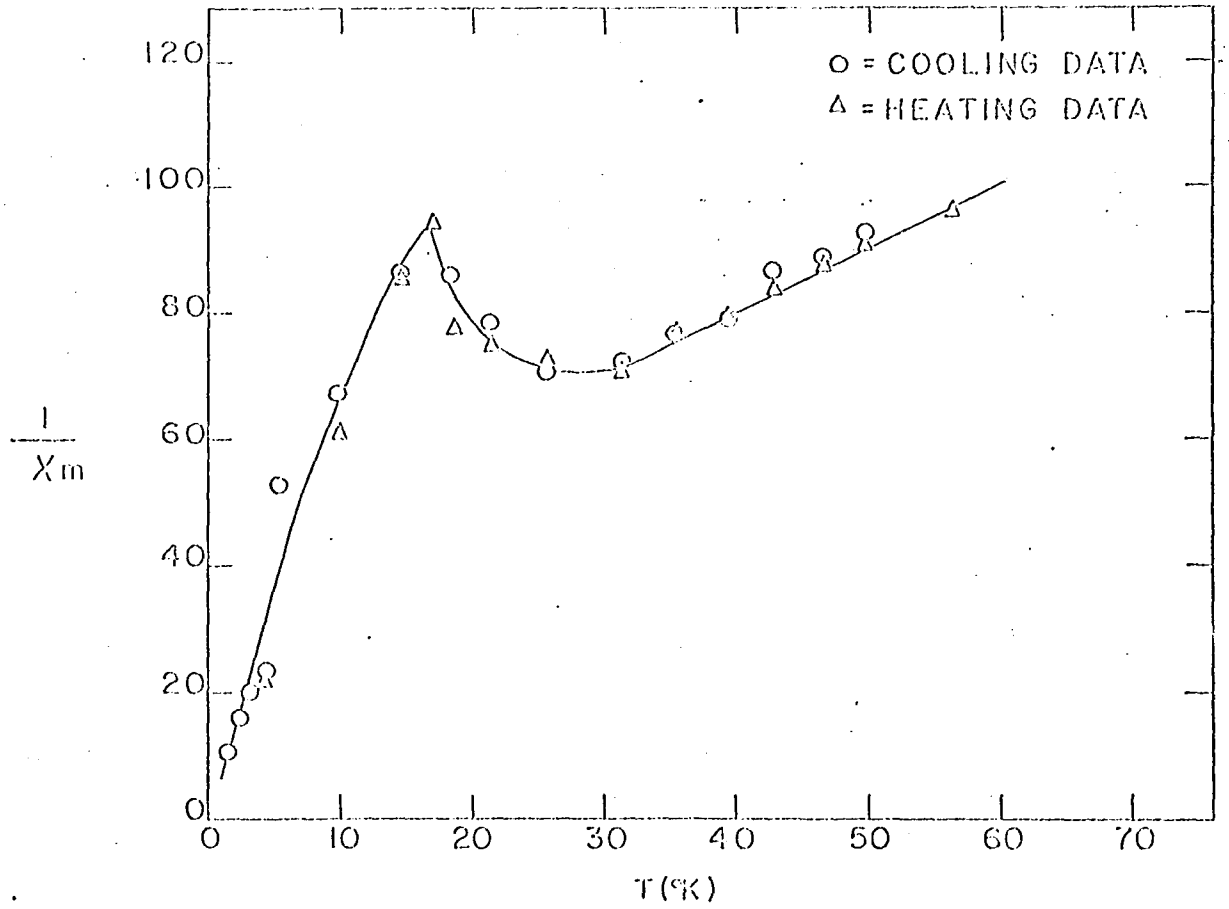

Figure 32. Susceptibility curve for the external field being parallel to the plane of the Cu-Cu vectors in the dimer

Table 10. Reciprocal molar susceptibility of $KCuCl_3$ single crystal, sample #6, $\frac{1}{\chi_m} = \frac{13.48}{\Delta M}$, field perpendicular to plane of Cu-Cu vectors

Cooling Data			Heating Data		
ΔM	T	$\frac{1}{\chi_m}$	ΔM	T	$\frac{1}{\chi_m}$
0.170	56.0	79.4	0.751	4.2	18.0
0.185	49.7	72.8	0.401	7.5	33.6
0.200	46.3	67.4	0.326	9.9	41.4
0.215	42.8	63.7	0.254	12.3	53.1
0.230	39.1	58.6	0.199	14.4	67.7
0.245	35.2	55.0	0.168	15.2	80.3
0.265	31.0	50.8	0.226	16.3	59.7
0.285	26.4	47.4	0.264	18.0	51.1
0.279	21.1	48.4	0.277	21.1	48.7
0.256	18.0	52.6	0.289	26.4	46.7
0.187	14.4	72.1	0.252	29.6	53.5
0.325	9.9	41.5	0.251	31.0	53.7
0.752	4.2	17.9	0.233	35.2	57.9
1.074	3.1	12.5	0.218	39.1	62.0
1.390	2.2	9.7	0.207	42.8	65.2
1.706	1.4	7.9	0.197	46.3	68.4
			0.187	49.7	72.1

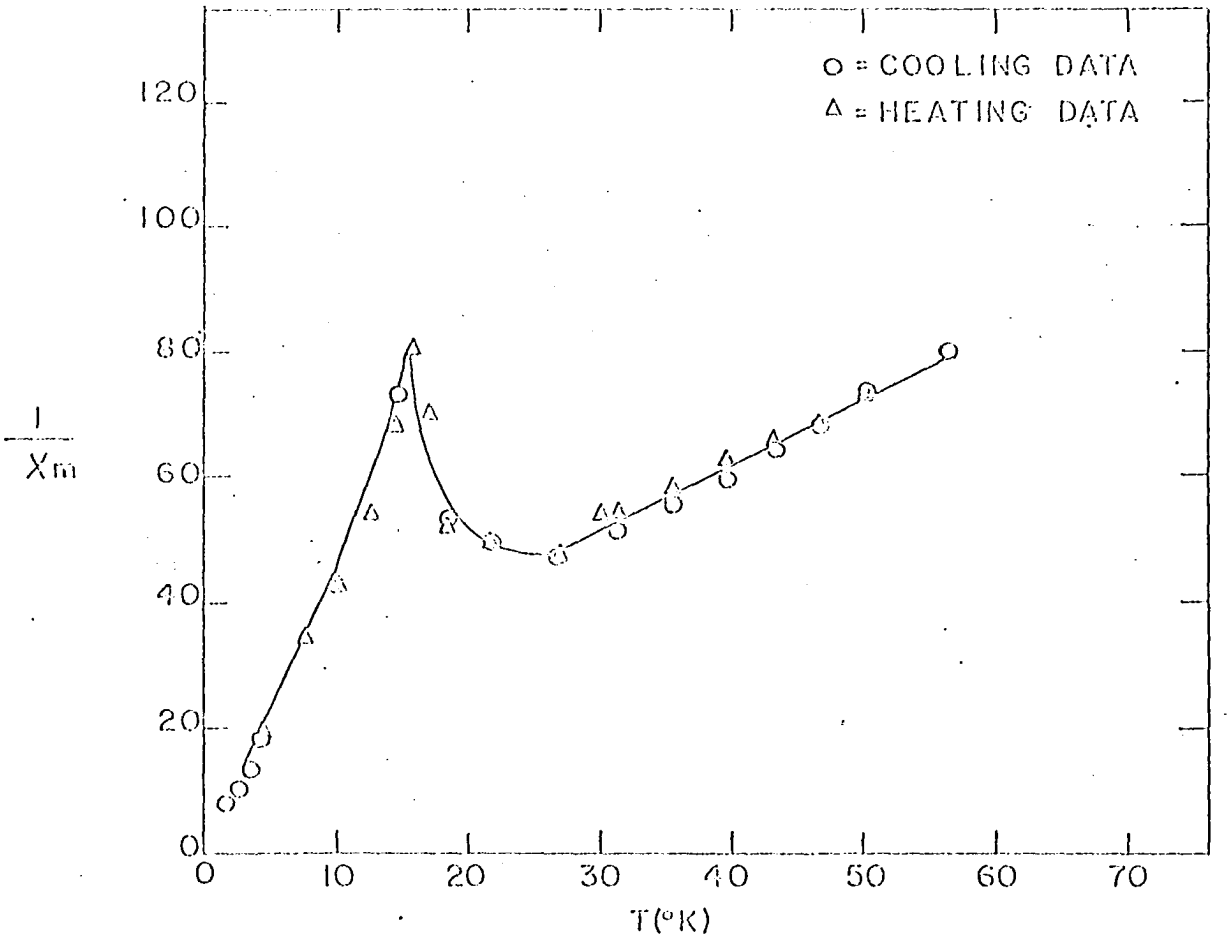

Figure 35. Susceptibility curve for the external field being perpendicular to the plane of the Cu-Cu vectors in the dimer

Table 11. Reciprocal molar susceptibility of $KCuCl_3$ single crystal, sample #2, field dependence-oscillator 40

$$\frac{1}{\chi_m} = \frac{30.67}{\Delta M}$$

ΔM	T	$\frac{1}{\chi_m}$
0.757	4.2	40.5
0.427	10.1	71.8
0.273	12.5	112.3
0.257	14.6	119.3
0.252	16.4	121.7
0.269	18.1	114.0
0.328	21.2	93.5
0.518	26.4	59.2
0.503	31.1	61.0
0.466	35.3	65.8
0.454	39.2	67.6
0.412	42.9	74.4
0.393	46.4	78.0
0.364	49.8	84.3

Figure 34. Susceptibility for the field parallel to the a axis at two different field intensities

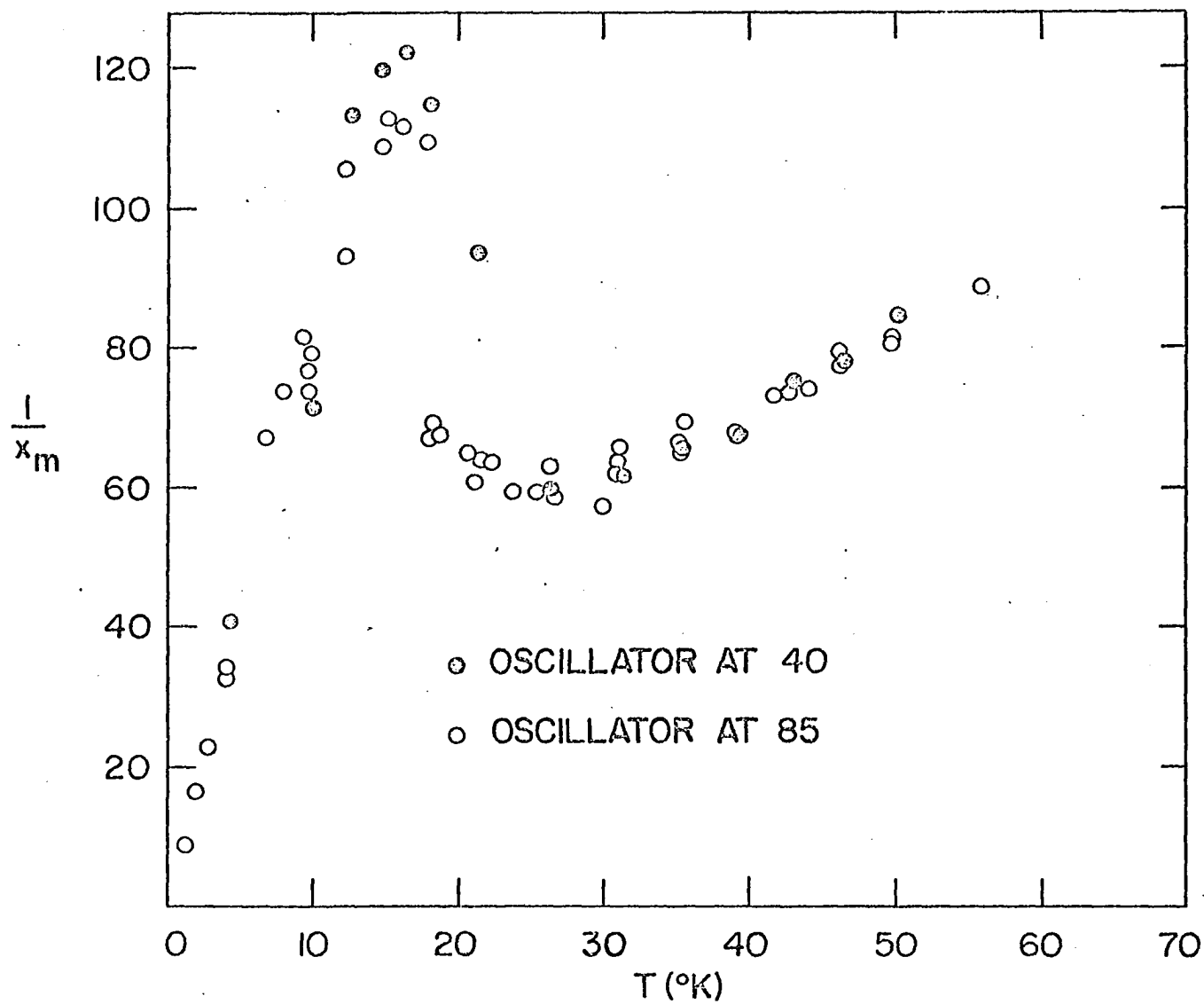
120
100
80
60
40
20
$\frac{1}{x_m}$
OSCILLATOR AT 40
OSCILLATOR AT 85
0
10
20
30
40
50
60
70
T (°K)

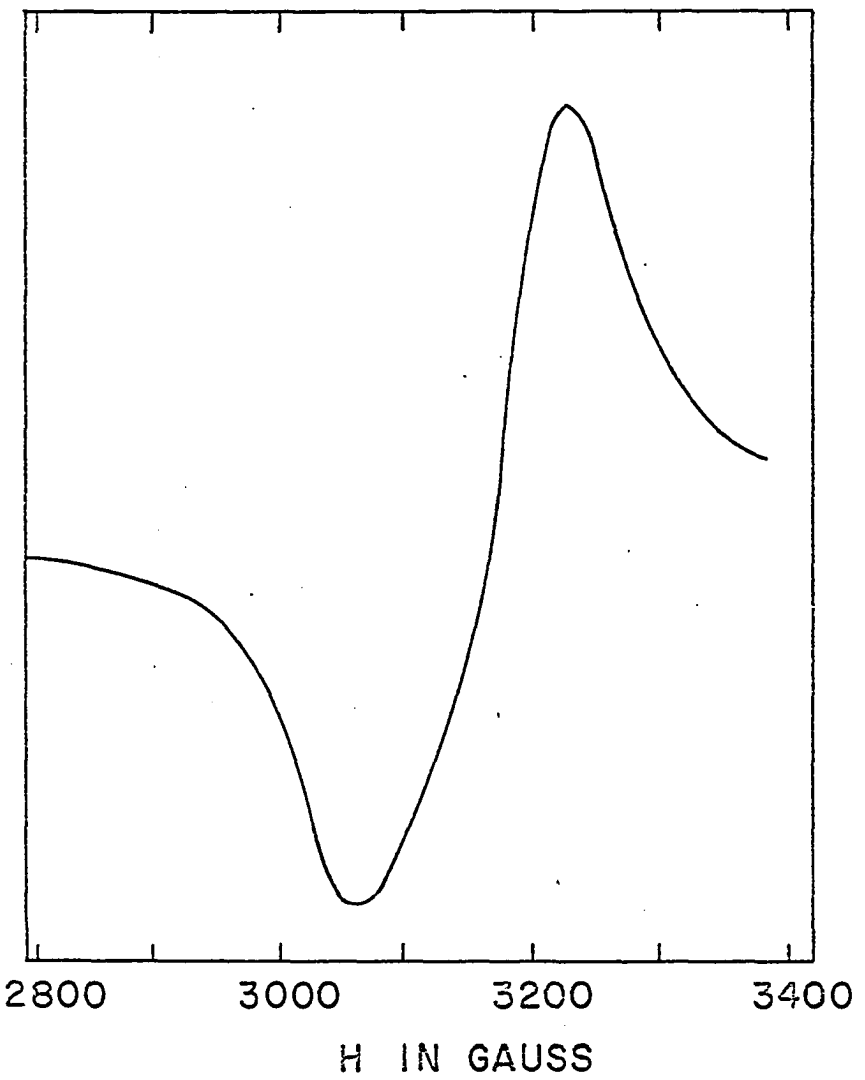

Figure 35. First derivative of ESR absorption for $KCuCl_3$ powder

Figure 36. First derivative of ESR absorption for a $KCuCl_3$ single crystal. 0^o means the external field is parallel to the X axis of one of the dimers in the crystal (see Figure 39 for axes). Note that the baseline has been shifted with each successive rotation

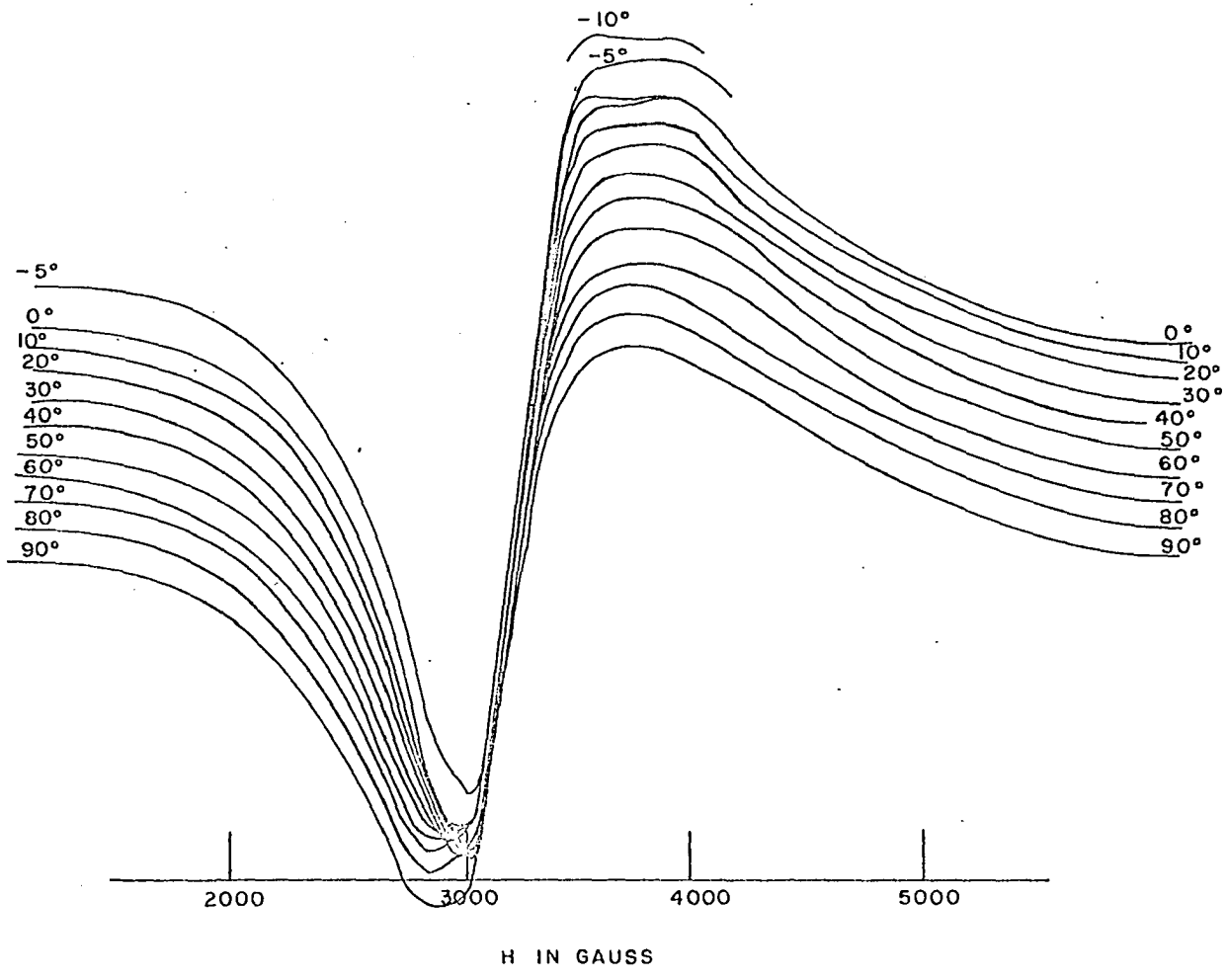
-10°
-5°
-5°
0°
10°
20°
30°
40°
50°
60°
70°
80°
90°
0°
10°
20°
30°
40°
50°
60°
70°
80°
90°
2000
3000
4000
5000
H IN GAUSS

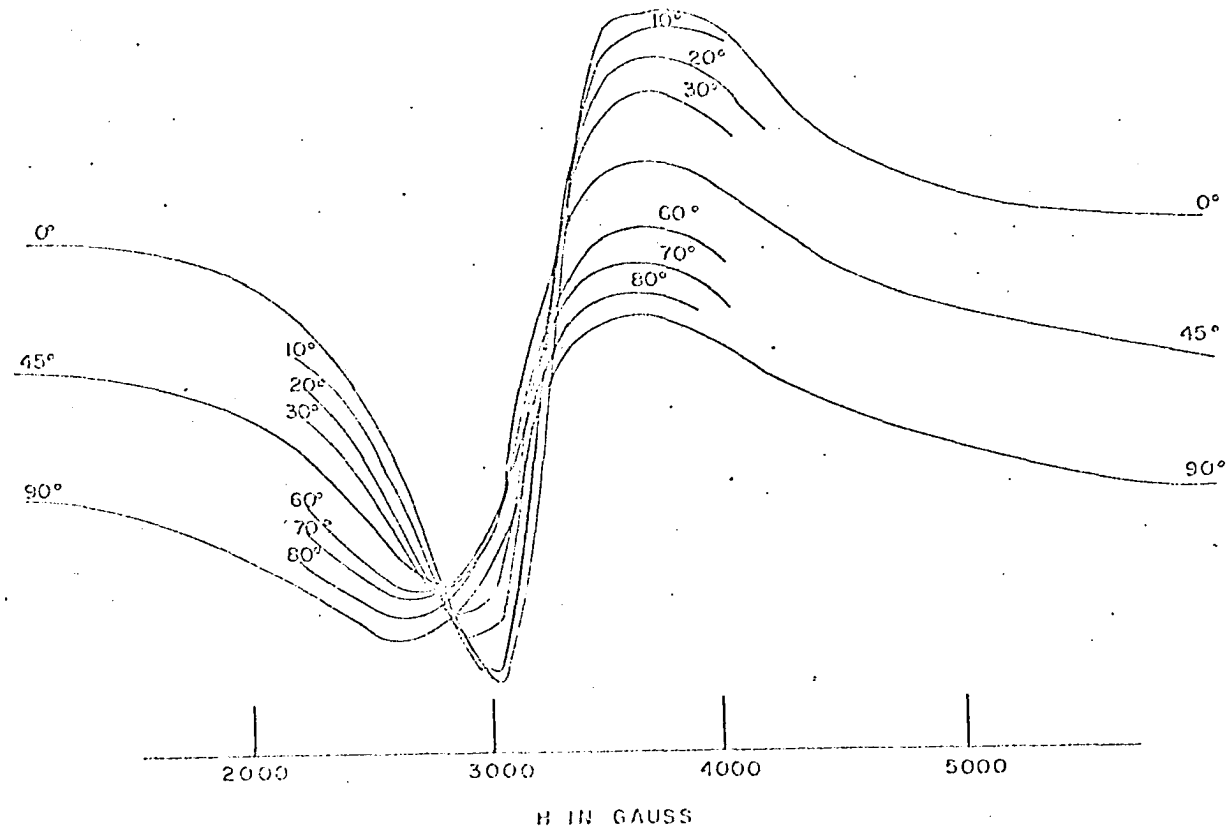

Figure 37. 90^{o} refers to the field being perpendicular to both the x and y axes in one of the dimers in the crystal (See comments on Figure 36)

CALCULATIONS

In this section we discuss results in terms of the Willett-Rundle LCAO-MO model. The model contains four parameters which can be adjusted in such a manner that the experimental data can be fitted to the theory. It is not the case that all four parameters are adjusted simultaneously, whereby any model might be made to fit the experiments, but that each calculation establishes the value of a different parameter, with each previously determined parameter being carried through to the next successive calculation, thus giving the model greater credibility.

To a first approximation there are three possible configurations for the ground state: B_{1g}^{*2}, B_{2u}^{*2} and $B_{1g}^{*}B_{2u}^{*}$. The first two are spin singlets; the last leads to a spin singlet and a spin triplet. The powder susceptibility measurements in this work are not in disagreement with the lowest two states being a triplet 55° above a ground singlet. A ground singlet has also been reported for $LiCuCl_3$ (Vossos et al., 1960). These orbitally degenerate, in the absence of zero field splitting, states are split in the presence of a magnetic field, the triplet degeneracy being removed, so that four levels result. These are designated by E_o, $\Delta - g\beta H$, Δ, $\Delta + g\beta H$. One can calculate a partition function from standard statis-

tical theory (Fowler and Guggenheim, 1952) for this system.

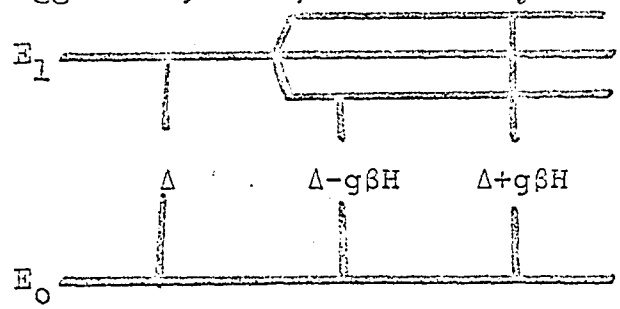

$$\sigma = \sum_i e^{-\varepsilon_i/kT} \qquad (1)$$

$$= e^{-E_o/kT}\left(1 + e^{-(\Delta - g\beta H)/kT} + e^{-\Delta/kT}\, e^{-(\Delta + g\beta H)/kT}\right)$$

$$= e^{-E_o/kT}\left(1 + e^{-\Delta/kT}\left(e^{a/kT} + 1 + e^{-a/kT}\right)\right) \qquad (2)$$

where $a = g\beta H$, $\frac{da}{dH} = g\beta$, g is a factor to be determined from the system wave functions, and β is the Bohr magneton.

Using $e^{-x} = 1 - x + \frac{x^2}{2!}$ ...., where terms of higher than second order in H are neglected, since these are small compared to unity for the fields in question, one obtains

$$\sigma = e^{-E_o/kT}\left(1 + e^{-\Delta/kT}\left(3 + \left(\frac{a}{kT}\right)^2\right)\right) \qquad (3)$$

Now

$$\chi = \frac{N\,kT}{H}\,\frac{\partial \ln \sigma}{\partial H} \qquad (4)$$

$$= \frac{N\,kT}{H}\,\frac{1}{\left(1+3e^{-\Delta/kT}\right)}\left(e^{-\Delta/kT}\,\frac{2g^2\beta^2 H}{(kT)^2}\right)$$

$$= \frac{2Ng^2\beta^2 e^{-\Delta/kT}}{\left(1+3e^{-\Delta/kT}\right)kT} \qquad (5)$$

$$\lim_{\Delta/kT \to 0}(\chi) = \frac{2Ng^2\beta^2}{4kT} = \frac{Ng^2\beta^2}{2kT} \qquad (6)$$

Slope of $\frac{1}{\chi}$ vs. T should be

$\frac{5.333}{g^2}$. Experimentally, the slope for the powder susceptibility was 1.04 leading to a value of 2.226 for the powder g factor.

Going back to equation (5) and substituting the values for the constants N, β, and the ESR value for g which is 2.16 for the dimer, one obtains,

$$\frac{1}{x} = \frac{T}{3.45}\left(e^{\Delta/kT} + 3\right) \quad (7)$$

Empirically the best fit of (7) to the experimental data was found for $\Delta/k = 55^{\circ}$, for which the slope was 1.06. Substituting these values the following table was obtained.

Table 12. Reciprocal susceptibility as a function of temperature for the singlet-triplet separation being 55k

T	$\frac{1}{X_m}$
100	136.7
70	105.6
40	80.9
30	80.4
25	87.9
20	107.8

This plot is the solid curve in Figure 27.

Comparison with a Spin = 1 One Dimensional Ising Model

For $CuCl_2$ and $CuBr_2$ (layer chains with smaller interchain distances) the one dimensional Ising model has been used to discuss the observed susceptibility (Barraclough and Ng, 1964). The thought occurred that the behavior

observed above 17°K in $KCuCl_3$ might as well be fitted by a one dimensional Ising model in which the nearest neighbor interaction was antiferromagnetic, as by our isolated binuclear spin one cluster model. As can be seen in Figure 38, however, the one dimensional Ising model gives a poor fit to the experimental curve for any value of J.

Figure 38 shows the curve for the reciprocal molar susceptibility of $KCuCl_3$ powder superimposed on the theoretical curves for the Ising model. The one dimensional Ising model was chosen because it is amenable to exact calculation, and because it was felt, in view of the stacking of the dimers in the crystal (i.e., one above the other along the a axis of the crystal) that this model might possibly approximately represent the system, if, indeed antiferromagnetic coupling is responsible for the behavior of the susceptibility above 17°K.

The formula for the susceptibility of an Ising model system of spin = 1 was derived by S. H. Liu of the Iowa State University Physics Department. Converting to the units for susceptibility used throughout this work, namely cm^3/mole, and taking the reciprocal, one obtains the formula:

$$\frac{1}{\chi_m} = AT\left[\frac{3\alpha^2 - 2\alpha(2e^{-\beta J}) - 2(1-e^{-\beta J}) - 2\sinh 2\beta J}{e^{-\beta J}\,\alpha + 1 - e^{-\beta J}}\right] \quad (8)$$

where $A = \frac{k}{2N_0(g\mu)^2} = 1/3$, $\beta = \frac{1}{kT}$, $g = 2.00$,

and $\alpha = \cosh \beta J + 1/2 + \left[\cosh^2 \beta J - \cosh \beta J + 9/4\right]^{1/2}$

Plots were obtained for three values of the adjustable parameter J.

Table 13. $1/\chi m$ as a function of T for the spin = 1 Ising model

T	J = 10 k	J = 22 k	J = 30 k
70	85.5	105.0	120.5
50	66.8	84.4	108.9
40		80.5	
30	49.4	76.0	106.3
20	34.5	81.8	
10	36.2	275.0	131.4

One notices that equation (7), based on a triplet lying 55° above a singlet, fits the experimental curve very well, while equation (8) gives a poor fit for any value of J. Since equation (7) describes an ensemble of weakly coupled dimers, and (8) describes a system in which dimer-dimer interactions are of the order of kT, one is led to believe that the $KCuCl_3$ system might be treated very well above 17°k as an assembly of discrete, weakly interacting dimer systems.

Experimental g Values

From ESR Data

In the last section, the first derivative plots of the paramagnetic resource curves were given. By integrating graphically, the absorption curves were obtained. The midpoint of the absorption curve (center of mass) is the

point where $\bar{g} = \frac{h\nu}{\beta H}$, with g being the average g value for the two dimer orientation in the crystal.

$$\therefore \bar{g} = \frac{h\nu}{\beta H_{midpt.}} = \tfrac{1}{2} \left(g_{xx}^2 \sin^2\theta_1 \cos^2\phi_1 + g_{yy}^2 \sin^2\theta_1 \sin^2\phi_1 + g_{zz}^2 \cos^2\theta_1 \right)^{\frac{1}{2}} + \left(g_{xx}^2 \sin^2\theta_2 \cos^2\phi_2 + g_{yy}^2 \sin^2\theta_2 \sin^2\phi_2 + g_{zz}^2 \cos^2\theta_2 \right)^{\frac{1}{2}} \quad (9)$$

Since three equations are needed to solve for the unknowns g_{xx}, g_{yy}, g_{zz}, three orientations of the crystal with respect to field were needed. The three chosen were with the field parallel to the three principal axes of one of the dimers in the crystal, i.e., θ_1 and ϕ_1 = either 0 or 90° in each case. The angles of the second dimer with respect to the field were obtained by trigonometric relationships based on a knowledge of the structure. The following average g values were obtained:

Field parallel to x axis of one dimer, $\bar{g} = 2.088$

Field parallel to y axis of one dimer, $\bar{g} = 2.120$

Field parallel to z axis of one dimer, $\bar{g} = 2.202$

The axis are as defined in Figure 40.

These average values, along with the measured angles of the dimers with the field give rise to the following equations:

$$2.088 = \frac{g_{xx} + (.368\, g_{xx}^2 + .413\, g_{yy}^2 + .218\, g_{zz}^2)^{\frac{1}{2}}}{2} \quad (10)$$

$$2.120 = \frac{g_{yy} + (.413\ g_{xx}^2 + .368\ g_{yy}^2 + .218\ g_{zz}^2)^{\frac{1}{2}}}{2} \quad (11)$$

$$2.202 = \frac{g_{zz} + (.103\ g_{xx}^2 + .115\ g_{yy}^2 + .781\ g_{zz}^2)^{\frac{1}{2}}}{2} \quad (12)$$

Solving, one obtains,

$g_{xx} = 2.057$.

$g_{yy} = 2.124$ The diagonal elements of the tensor.

$g_{zz} = 2.215$

Using these values for the diagonal g tensor, and the angles for the field being parallel to the plane of the Cu-Cu vector in both types of dimers (i.e., $\phi = 23°20$, $\theta = 76°05$).

$g_{parallel}$ is calculated to be 2.08

Similarly, for the field perpendicular to the plane of the Cu-Cu vector ($\phi = 23°20$, $\theta = 13°55$).

$g_{perpendicular}$ is calculated to be 2.21

There exists the possibility that there is a variation of ESR as a function of the orientation of the transition probability external field relative to each dimer. In this case, the elements of the g tensor for the individual dimers obtained from the center of gravity calculation would be in error. We infer that such is not the case from the agreement between the elements of the g tensor obtained from ESR and from susceptibility measurements (vide infra).

From Susceptibility Data

Using equation (5), derived at the beginning of this section, and substituting the smoothed curve values for $\frac{1}{\chi_m}$ and T for various orientations, experimental values for g are obtained. The following table shows the agreement between the g values so obtained and ESR g values.

Table 14. Comparison of g values calculated from Susceptibility Data and from ESR Data

Orientation	Susceptibility g	ESR g
parallel to a axis	2.21	2.20
parallel to b axis	2.12	2.13
parallel to plane of Cu-Cu vector	2.09	2.08
perpendicular to plane of Cu-Cu vector	2.28	2.21

Calculation of states arising from the configurations $(B_{1g}^*)^2$, $(B_{2u}^*)^2$, and $B_{1g}^* B_{2u}^*$

One now wishes to calculate the relative separation of the four states arising from the three configurations $(B_{1g}^*)^2$, $(B_{2u}^*)^2$ and $B_{1g}^* B_{2u}^*$ in the approximation that kinetic energy differences are negligible compared to the potential, and that the two electron Hamiltonian is therefore

$$H = -\sum_{i=1}^{2}\sum_{\alpha=1}^{8}\frac{Z_\alpha e^2}{r_{i\alpha}} + \frac{e^2}{r_{12}},$$

where α labels the nuclei and i labels the electrons. For a given nuclear configuration the nuclear-nuclear

terms contribute a constant and are neglected.

For states arising from a given configuration of electrons in molecular orbitals, energy differences due to one electron operators may be shown to vanish. The kinetic energy difference between states arising from different configurations may be shown to be small with respect to potential terms, as will be subsequently illustrated.

In detail, the B_{1g}^{*} and B_{2u}^{*} orbitals, expressed as a linear combination of atomic orbitals, are as follows:

$$B_{1g}^{*} = \frac{\alpha}{\sqrt{2}}(A + B) + (1-\alpha^2)^{\frac{1}{2}}\left[\frac{\beta}{2}(1-2-3+4) + \frac{(1-\beta^2)^{\frac{1}{2}}}{\sqrt{2}}(5-6)\right] = \emptyset \qquad (13)$$

$$B_{2u}^{*} = \frac{\alpha}{\sqrt{2}}(A - B) + (1 - \alpha^2)^{\frac{1}{2}}\left[\frac{\beta}{2}(1-2+3-4) + \frac{(1 - \beta^2)^{\frac{1}{2}}}{\sqrt{2}}(5' + 6')\right] = X \qquad (14)$$

Where α^2 is the molecular orbital coefficient indicating the electron density on the metal atoms, and where A and B are the dxy orbitals on the Cu atoms, 1 means a P_x orbital on 1 with its positive lobe pointing in the positive direction and -2 means a P_y orbital on 2 with its negative lobe pointing in the y positive direction, etc., as shown in Figures 39 and 40.

The antisymmetric space-spin wave functions arising from the configurations $(B_{1g}^*)^2$, $(B_{2u}^*)^2$ and $B_{1g}^* B_{2u}^*$ are, after proper linear combinations of the Slater determinants have been made to arrange these spin functions to be eigenfunctions of S^2 and S_z,

$$\phi^2 = \phi_1 \phi_2 (\alpha_1\beta_2 - \beta_1 \alpha_2)$$

$$X^2 = X_1 X_2 (\alpha_1\beta_2 - \beta_1 \alpha_2) \qquad \text{Singlets (15)}$$

$$\phi X = (\phi_1 X_2 + X_1 \phi_2)(\alpha_1 \beta_2 - \beta_1 \alpha_2)$$

and

$$(\phi_1 X_2 - X_1 \phi_2)(\alpha_1 \alpha_2)$$

$$(\phi_1 X_2 - X_1 \phi_2)(\beta_1 \beta_2) \qquad \text{Triplet (16)}$$

$$(\phi_1 X_2 - X_1 \phi_2)(\alpha_1\beta_2 + \beta_1 \alpha_2)$$

Normalization

It can be readily seen that the one electron molecular orbitals ϕ and X are normalized as they stand, since

$$\int \phi^2 dV = \int X^2 dV = N^{-2} = \frac{2\alpha^2}{2} + \frac{4\beta^2(1-\alpha^2)}{4} + \frac{2\beta(1-\beta^2)(1-\alpha^2)}{2} = 1.$$

Neglecting overlap, the normalization for the two electron space functions is as follows:

$$\Psi_1 = \frac{1}{\sqrt{2}} (\phi X + X\phi)$$

$$\Psi_2 = \frac{1}{\sqrt{2}} (\phi X - X\phi)$$

Later on we will make use of configuration interaction between the ϕ^2 and the X^2 singlets, and the normalization

for such a function is given by $\Psi_3 = \frac{1}{\sqrt{1 + k^2}} (\phi^2 \pm kX^2)$.

Our experimental results are not in disagreement with the idea that a singlet lies lower than the triplet by 55k. Choosing the ϕX configuration, one problem of interest was to see if the model would predict that the $(\phi X + X\phi)$ singlet would lie lower than the $(\phi X - X\phi)$ triplet. Thus, one wants to solve a secular determinant,

$$\begin{vmatrix} \frac{(\phi X - X\phi)}{\sqrt{2}} \left| m_1 + m_2 + R \right| \frac{(\phi X - X\phi)}{\sqrt{2}} - E & 0 \\ 0 & \frac{(\phi X + X\phi)}{\sqrt{2}} \left| m_1 + m_2 + R \right| \frac{\phi X + X\phi}{\sqrt{2}} - E \end{vmatrix} = 0$$

where the off diagonal elements disappear due to the orthogonality of the spin functions, and $m_1 = \frac{e^2}{r_{1\alpha}}$, $m_2 = \frac{e^2}{r_{2\alpha}}$, $R = \frac{e^2}{r_{ij}}$.

It should be noted that the one electron operators, m_1 and m_2, do not contribute to the energy level difference, as was previously stated. E.g., in the calculation of ΔE, the one electron operators are

$$\tfrac{1}{2} \left[(\phi_1 | m_1 | \phi_1) + (\phi_2 | m_2 | \phi_2) + (X_1 | m_1 | X_2) + (X_2 | m_2 | X_2) \right]$$

$$- \tfrac{1}{2} \left[(\phi_1 | m_1 | \phi_1) + (\phi_2 | m_2 | \phi_2) + (X_1 | m_1 | X_2) + (X_2 | m_2 | X_2) \right] = 0$$

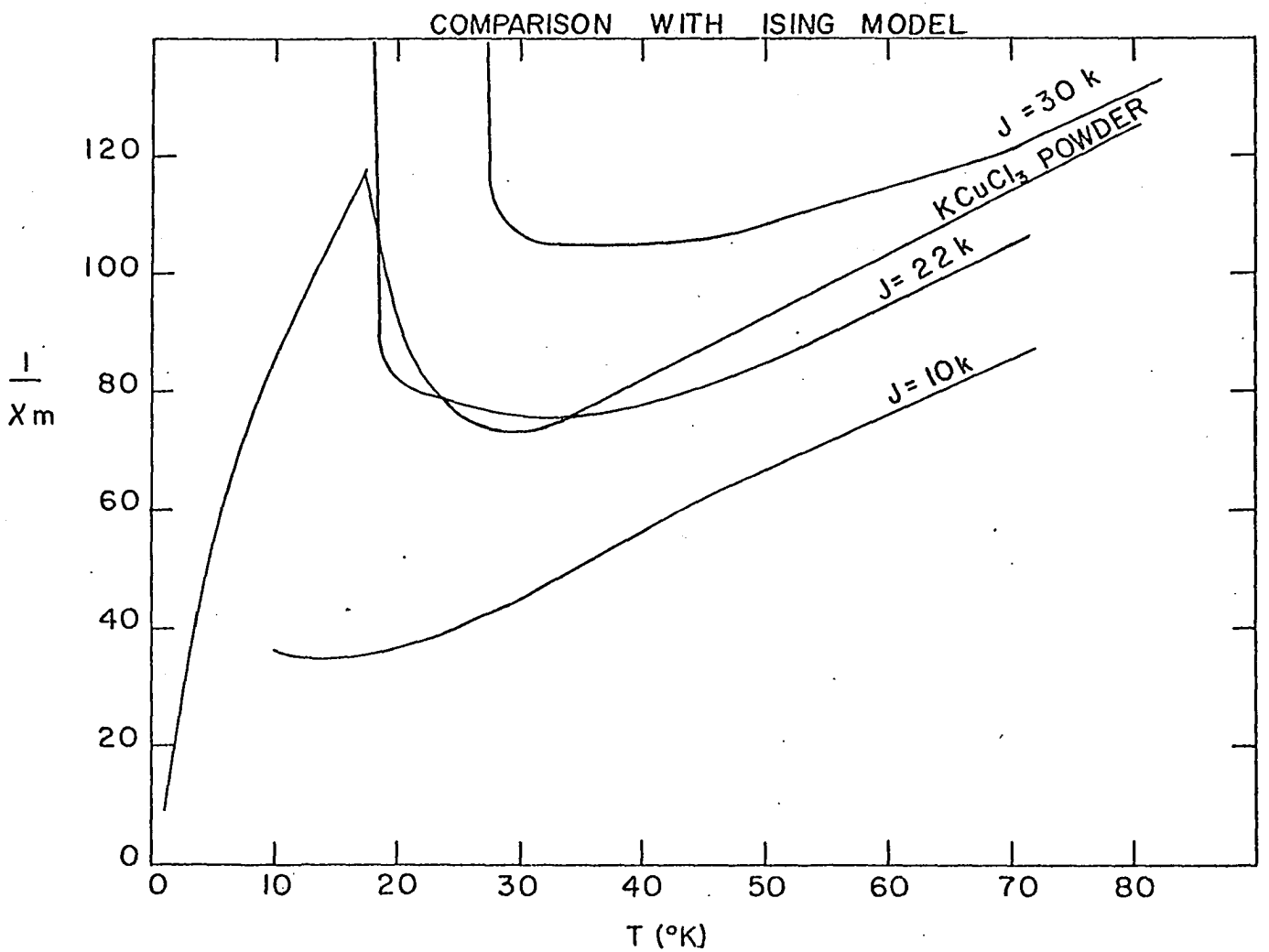

Figure 38. Experimental and Ising susceptibility curves

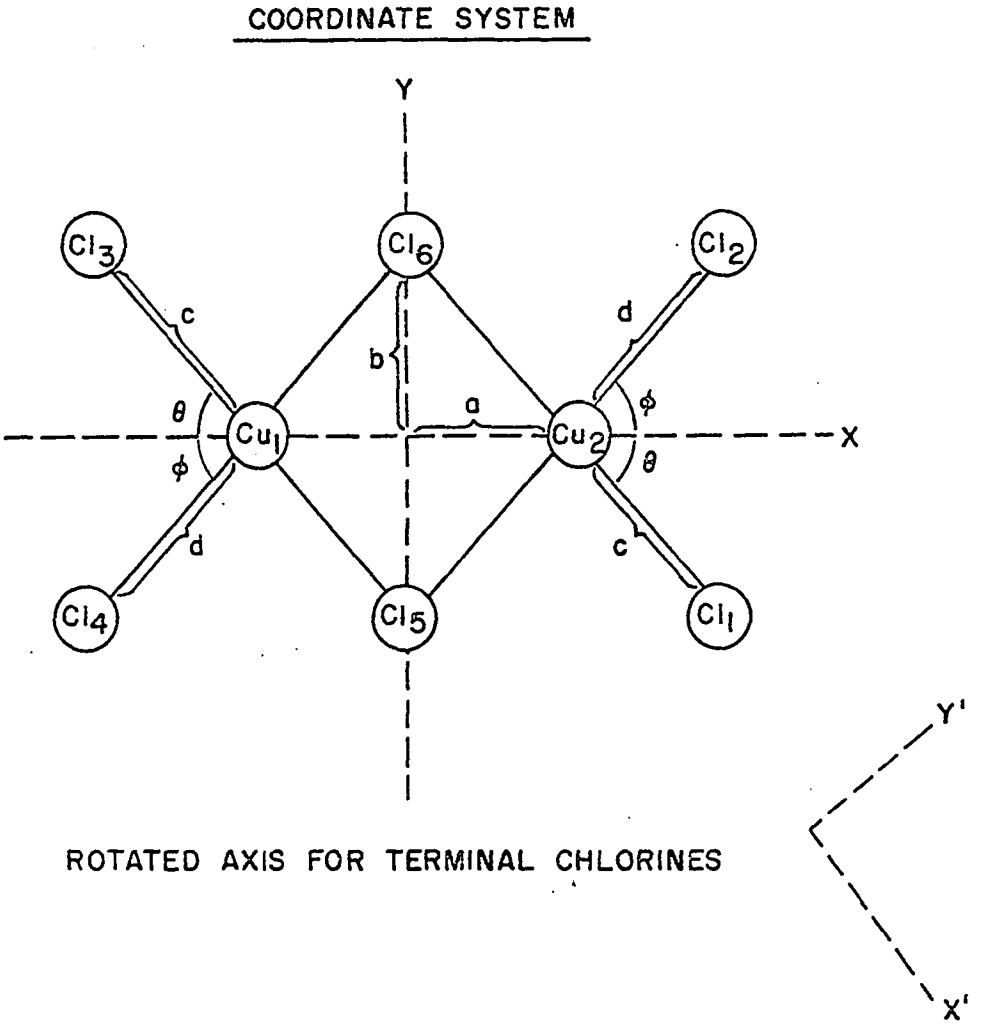

Figure 39. Coordinate system for the $Cu_2Cl_6^{=}$ dimer

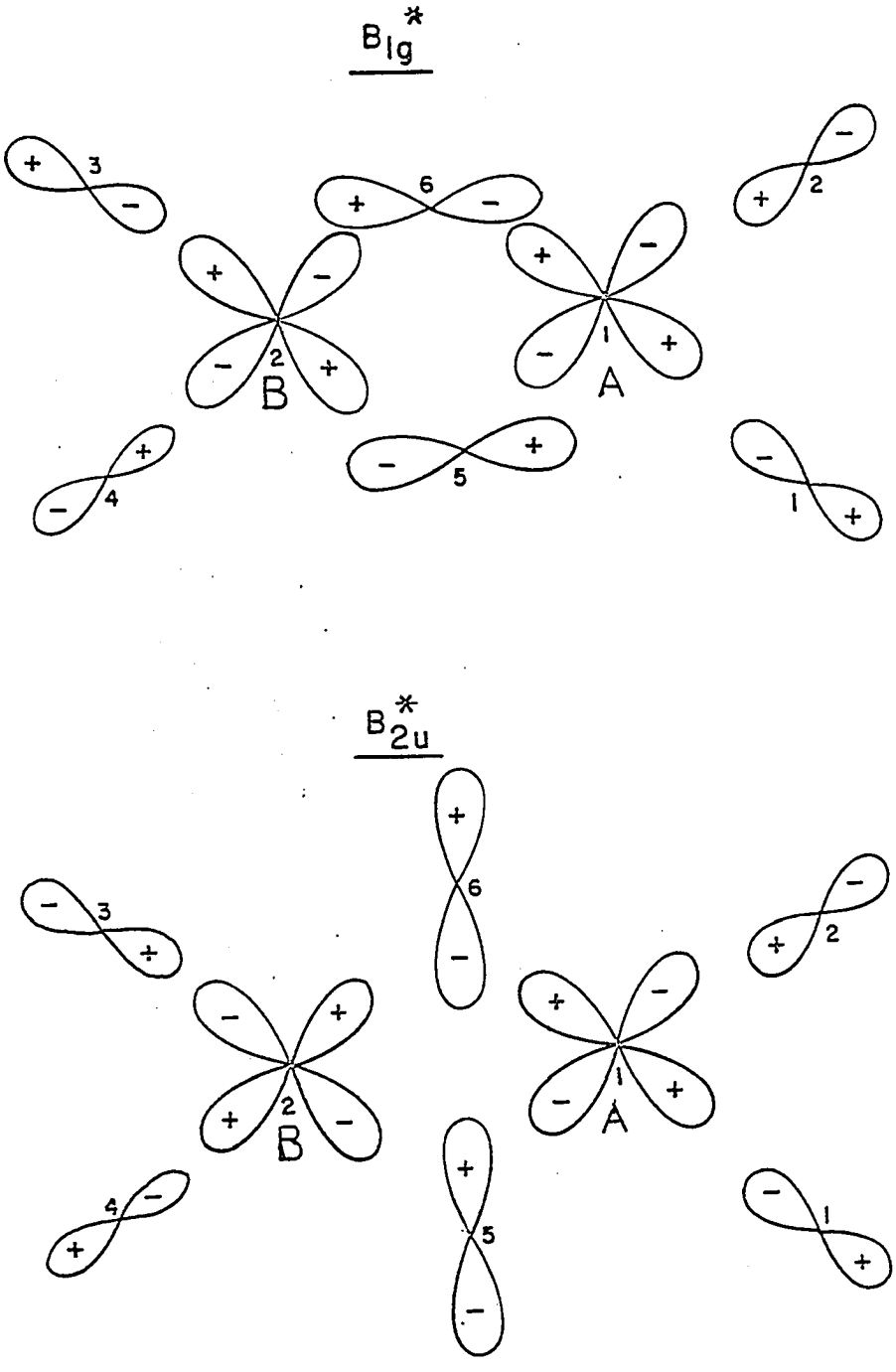

Figure 40. Atomic orbitals comprising the B_{1g}^* and B_{2u}^* molecular orbitals

Solving the determinant, one obtains

$$E_{triplet} - E_{singlet} = \Delta E = -2(\emptyset X|R|X\emptyset), \quad (17)$$

including normalization. Since the $\emptyset$ and X functions are linear combinations of eight atomic orbitals, the $\emptyset X$ product contains 64 terms. Thus, an integral of the type $(\emptyset X|R|X\emptyset)$ is actually the sum of 4096 integrals. Fortunately, for reasons of symmetry, overlap, or simple cancellation, most of these terms vanish or are small with respect to the leading terms. For example, it was observed that the two center integrals were 10^{-1} to 10^{-3} of the similar one center integrals. Since the calculations are dependent on $\frac{1}{r}$, it was assumed that the three and four center integrals were negligibly small compared to the one and two center integrals. Evaluating the remaining one and two center integrals,

$$(\emptyset X|R|X\emptyset) \sim 2(A_1A_2|R|A_1A_2) - 2(A_1B_2|R|A_1B_2)$$
$$+4(l_1l_2|R|l_1l_2) + 16(A_1A_2|R|l_1l_2) + 8(A_1l_2|R|A_1l_2)$$
$$+8(A_15_2'|R|A_15_2'), \quad (18)$$

where A and B are the d_{xy} orbitals on the copper atoms, and l and 5' are the terminal and bridging chlorine p orbitals, as shown in Figure 39.

It should be recognized by the reader that (18) can be made an equation by multiplying each of the integrals by the appropriate wave function coefficient, e.g., the A's in the wave function have $\alpha/(2)^{\frac{1}{2}}$ as a coefficient so that

integrals of the form $(A_1A_2|R|A_1A_2)$ would be multiplied by $\alpha^4/4$. The complete list can be found in table 15.

The values of these integrals are given in table 16, and the coefficients by which each term is to be multiplied are listed in Figure 15. The integrals were evaluated on an IBM 7074 computer by D. M. Silver. The programs were developed by D. Silver and K. Ruedenberg (Ruedenberg, 1969). These gentlemen are both of this laboratory. The calculations are based on the electron electron interactions in the individual atomic orbitals. From these values it can be seen that $\Delta E = E_{triplet} - E_{singlet}$ is less than zero for any choice of coefficients, indicating that the $\phi X - X\phi$ triplet lies lower than the $\phi X + X\phi$ singlet, in accordance with Hund's rule.

One would next like to see if the ϕ^2 or X^2 singlet might lie lower than the $(\phi X - X\phi)$ triplet. The secular determinant is

$$\begin{vmatrix} (\phi X - X\phi|m_1+m_2+R|\phi X - X\phi) - E & 0 \\ 0 & (XX|m_1+m_2+R|XX) - E \end{vmatrix} = 0$$

this yields an energy difference, including normalization,

$$\Delta E = (\phi X|R|\phi X) - (\phi X|R|X\phi) - (XX|R|XX)$$
$$\sim -2(AA|R|AA) - 2(AB|R|AB) - 16(AA|R|11) - 8(A1|R|A1)$$
$$-16(AA|R|55) - 4(11|R|11) \qquad (19)$$

Clearly this ΔE is also negative and larger than the first. On the other hand, if ϕ^2 had been chosen instead of X^2,

the same terms would arise, but 5' would be replaced by 5.

The only remaining calculation which can be made with the zeroth order wave functions is the calculation involving the interaction of the configurations ϕ^2 and X^2, to obtain a more favorable distribution of charge (Roberts, 1962). Furthermore, a singlet-triplet inversion has been reported for this type of interaction (Hansen and Ballhausen, 1965). The secular determinant describing this situation is

$$\begin{vmatrix} (\phi X - X\phi | m_1+m_2+R | \phi X - X\phi) - E & 0 \\ 0 & (\phi^2 - kX^2 | m_1+m_2+R | \phi^2 - kX^2) - E \end{vmatrix} = 0$$

Including normalization, the energy difference is

$$\begin{aligned} \Delta E = {} & (\phi X|R|\phi X) + \left[\frac{2k}{1+k^2} - 1\right](\phi X|R|X\phi) - (XX|R|XX) \\ & \sim \left[\frac{4k}{1+k^2} - 2\right](AA|R|AA) + \left[2 - \frac{4k}{1+k^2}\right](AB|R|AB) \\ & + \left[\frac{8k}{1+k^2} - 4\right](11|R|11) + \left[\frac{32k}{1+k^2} - 16\right](AA|R|11) \\ & + \left[\frac{16k}{1+k^2} - 24\right](A5|R|5A) + \left[\frac{16k}{1+k^2} - 8\right](A1|R|A1), \quad (20). \end{aligned}$$

For similar copper compounds, it is known that the value of the molecular orbital coefficient α should be about 0.9. Using the values of the integrals given in table 16, it can be seen that the singlet cannot be shifted below the triplet for any value of k or β. The energy difference, however, has its minimum value for $k = 1$ and $\beta = 0.6$. This minimum value is 0.0008 eV.

Thus, at this point in the calculation, reasonable values for α and β have been established, but the zeroth order wave functions cannot explain the singlet being lower than the triplet, a result necessary for the validity of our model.

Table 15. Molecular orbital coefficients for $\frac{e^2}{r_{ij}}$ and $\frac{e^2}{r_{i\alpha}}$ integrals

Term	Coefficient
$(A\|m\|A)$, $(AA\|R\|AA)$, $(AB\|R\|AB)$	$\frac{1}{4}\alpha^4$
$(1\|m\|1)$, $(11\|R\|11)$	$\frac{1}{16}(\beta^4-2\alpha^2\beta^4+\alpha^4\beta^2)$
$(AA\|R\|11)$, $(A1\|R\|A1)$	$\frac{1}{8}(\alpha^2\beta^2-\alpha^4\beta^2)$
$(AA\|R\|55)$, $(A5\|R\|A5)$	$\frac{1}{4}(\alpha^2-\alpha^4-\alpha^2\beta^2+\alpha^4\beta^2)$
$(55\|R\|55)$, $(5\|m\|5)$	$\frac{1}{4}(1-2\alpha^2-2\beta^2+4\alpha^2\beta^2-2\alpha^4\beta^2+\alpha^4+\beta^4-2\alpha^2\beta^4+\alpha^4\beta^4)$

In the following four tables the integrals have been calculated using both Slater (Coulson, 1961, P. 40) and Clementi (Clementi and Raimondi, 1963) orbital exponents.

Table 16. Evaluated integrals (in atomic units). A and B refer to copper d_{xy} orbitals

Integral	Value using Slater exponent	Value using Clementi exponent
(AA|R|AA)	0.56962	1.22220
(AB|R|AB)	0.15663	0.15433
(11|R|11)	0.53748	0.53748
(AA|R|11)=(A1|R|1A)	0.00927	0.00032
(A1|R|A1)	0.11668	0.11424
(A5|R|A5)	0.23950	0.23477
(55|R|55)	0.53748	0.53748
(A5|R|5A)	0.00941	0.00027
(1|m|1)	-10.88000	-10.88000
(A|m|A)	-19.91333	-42.72666
(5|m|5)	-10.88000	-10.88000

Table 17. Evaluated integrals. A and B refer to copper $d_{x^2-y^2}$ orbitals

Integral	Slater exponent	Clementi exponent
(AB|R|AB)	0.16000	0.15700
(A1|R|A1)	0.13987	0.13961
(A5|R|A5)	0.23507	0.23304
(A1|R|1A)	0.00257	0.00027

Table 17. (Continued)

Integral	Slater exponent	Clementi exponent
(A5|R|5A)	0.00212	0.00015

Table 18. Evaluated integrals. A and B refer to a linear combination of d_{xz} and d_{yz} on the copper atoms

Integrals	Value using Slater exponent	Value using Clementi exponent
(AB|R|AB)	0.15406	0.15176
(A1|R|A1)	0.17268	0.17034
(A5|R|A5)	0.22880	0.22407
(A1|R|1A)	0.00000	0.00000
(A5|R|5A)	0.00000	0.00000

Table 19. Values of integrals for α=0.9, β=0.6

Integral	Slater exponent	Clementi exponent
(ØX|R|ØX)	0.27412	0.48824
(ØX|R|XØ)	0.15867	0.37466
(XX|R|XX)	0.27506	0.48827

First order corrections to the wave functions

Until this point, we have not considered the spin-orbit

term in the Hamiltonian. If the spin orbit splittings are small compared to previously considered terms, we may write the first order corrected wave functions as

$$\Psi_{corr} = \Psi_o \pm \sum_i \frac{(\Psi i|\lambda L\cdot S|\Psi o)}{\Delta_i} \Psi_i \qquad (21)$$

where Ψ_i are wave functions of excited states with which the ground state is mixed by spin-orbit coupling, and Δ_i is the energy difference between the ground and ith excited states.

Therefore, one must first find the effect of L·S on the zeroth order functions. From this point on, a not so small book could be written about the details of the calculations. It is the author's hope that enough of the work is presented here so that the reader will understand what has been done, yet not so much that no one will want to follow the development.

As shown in Figure 40, the coordinate system has been chosen such that the Z axis is the principal C_2 axis for the system with D_{2h} symmetry. To evaluate the expectation values of the various components of the angular momentum vector with respect to this system of quantization, it is necessary to express the derivatives with respect to the chosen system of quantization in terms of derivatives with respect to coordinate systems centered on the various atoms of the molecule. For example, let L_z be the operator for the Z component of angular momentum about the molecular Z axis, and L_z^1 the Z component of angular momentum about

the Z axis of an atom at a,o,o with respect to the molecular coordinate system. Then $X' = X-a$, $Y' = Y$, and $Z' = Z$, and

$$L_z = \frac{-ih}{2\pi}\left(X\frac{d}{dy} - Y\frac{d}{dx}\right) = \frac{-ih}{2\pi}\left[(X'+a)\frac{d}{dy'} - Y'\frac{d}{d(X'+a)}\right]$$

$$= \frac{ih}{2\pi}\left[X'\frac{d}{dy'} - Y'\frac{d}{dx'}\right] + \frac{iha}{2\pi}\frac{d}{dy} \quad (22)$$

The last term is a linear velocity term with expectation value zero between states of the stationary system under consideration, so $L_z' = L_z$. Similarly, $L_x = L_x'$, $L_y = L_y'$ for an atom at a,o,o.

The L•S operator may be written $\Sigma(L_xS_x + L_yS_y + L_zS_z)$. The Z components will be evaluated first, and stepping operators will be used to get the X and Y components. The Z components are treated as follows:

$$\lambda L_zS_z \left| (\phi X - X\phi)\alpha\alpha\right\rangle = \lambda(L_{z1}S_{z1} + L_{z2}S_{z2}) \left| (\phi_1X_2 - X_1\phi_2)\,\alpha\alpha\right\rangle \quad (23)$$

$$\text{now} \quad S_z\,\alpha\alpha = \tfrac{1}{2}\,\alpha\alpha \;;\; S_z\,\beta\beta = -\tfrac{1}{2}\,\beta\beta \quad (24)$$

$$\text{and } L_z\left|\phi_1X_2\right\rangle = X_2L_{z1}\phi_1 + \phi_1L_{z2}X_x \text{ etc.} \quad (25)$$

We note that

$$L_z\left|\phi\right\rangle = L_z\left|\text{metal}\right\rangle + L_z\left|\text{ligand}\right\rangle \quad (26)$$

Therefore,

$$L_z\left|\phi\right\rangle \text{or } L_z\left|X\right\rangle = L_z\left|d_{xy}\right\rangle + L_z\left|\text{ligand P's}\right\rangle \quad (27)$$

$L_z\left|d_{xy}\right\rangle$ generates d_{x2-y2}, so it seems that L•S coupling mixes the d_{xy} with a d_{x2-y2} orbital. Upon examining the orbital scheme (Figure 1), it is seen that the d_{x2-y2} is

a non-bonded orbital in the absence of π bonding. So, neglecting metal-ligand overlap, the first order corrections go as $\langle d_{x^2-y^2} | \lambda L_z S_z | d_{xy} \rangle$. Thus the $(\phi X - X\phi)\alpha\alpha$ wave functions, corrected for the Z component of spin-orbit coupling is

$$\psi_{\alpha\alpha\,(corr)} = \frac{1}{(2)^{\frac{1}{2}}}(\phi X - X\phi)\,\alpha\alpha \mp \frac{\lambda\alpha}{\Delta_z}\left[(\phi\rho - \rho\phi) - (X\psi - \psi X)\right]\alpha\alpha \qquad (28)$$

where ρ and ψ are the wave functions

$1/(2)^{\frac{1}{2}}(d_{x^2-y^2(A)} + d_{x^2-y^2(B)})$ and $1/(2)^{\frac{1}{2}}(d_{x^2-y^2(A)} - d_{x^2-y^2(B)})$

(A and B again refer to the copper atoms)

respectively, and Δ_Z is the energy level difference between the $(d_{xy})^1(d_{x^2\ y^2})^2$ and the $(d_{xy})^2(d_{x^2-y^2})^1$ states. i.e., Figure 1 shows two electrons in each $d_{x^2-y^2}$ non-bonded orbital, hence, $(d_{x^2-y^2})^2$, and one electron in each d_{xy}, hence $(d_{xy})^1$, considering for the moment only those atomic orbitals rather than the whole molecular orbital. One then assumes that the configuration $(d_{x^2-y^2})^1(d_{xy})^2$ might be a proper excited state, and that transitions of the sort $(d_{x^2-y^2})^1(d_{xy})^2 \rightarrow (d_{x^2-y^2})^2(d_{xy})^1$ lead to the observed optical spectra.

The other corrected wave functions are:

$$\psi_{\beta\beta} = \frac{1}{2^{\frac{1}{2}}}(\phi\chi-\chi\phi)\beta\beta + \frac{\lambda\alpha}{\Delta_z}\left[(\phi\rho-\rho\phi)-(\chi\psi-\psi\chi)\right]\beta\beta \quad (29)$$

$$\psi_{\alpha\beta+\beta\alpha} = \tfrac{1}{2}(\phi\chi-\chi\phi)(\alpha\beta+\beta\alpha) - \frac{\lambda\alpha}{\sqrt{2}\,\Delta_z}\left[(\chi\psi+\psi\chi)-(\phi\rho+\rho\phi)\right](\alpha\beta-\beta\alpha) \quad (30)$$

$$\psi_{\alpha\beta-\beta\alpha} = \frac{1}{\sqrt{2(1+k^2)}}(\phi^2-k\chi^2)(\alpha\beta-\beta\alpha) - \frac{\lambda\alpha}{\sqrt{2}\,\Delta_z}\left[(\chi\rho-\rho\chi)-(\phi\psi-\psi\phi)\right](\alpha\beta+\beta\alpha) \quad (31)$$

The $L_xS_x\left|(\emptyset X-X\emptyset)\alpha\alpha\right\rangle$ operation is evaluated as follows: $L_x = \frac{1}{2}(L^+ + L^-)$ and $S_x = \frac{1}{2}(S^+ + S^-)$, where L^+, L^-, S^+, and S^- are the so called stepping operators, defined by

$$L^+\left|M_L\right\rangle = (L(L+1) - M_L(M_L+1))^{\frac{1}{2}}\left|M_L+1\right\rangle, \quad S^+\beta = \alpha, \quad S^+\alpha = 0$$

$$L^-\left|M_L\right\rangle = (L(L+1) - M_L(M_L-1))^{\frac{1}{2}}\left|M_L-1\right\rangle, \quad S^-\beta = 0, \quad S^-\alpha = \beta \quad (32)$$

Proceeding in an analogous manner as for the Z component, except that stepping operators are now being used instead of the L_z and S_z operators, one finds

$$L_xS_x\left|(\emptyset X - X\emptyset)\alpha\alpha\right\rangle \rightarrow f(d_{xz}, d_{yz}).$$

Therefore one constructs a linear combination of d_{xz} and d_{yz} with which $L_xS_x\left|\emptyset X - X\emptyset\right\rangle$ will mix. Again referring to Figure 1, the d_{xz} and d_{yz} orbitals are non-bonding, and one merely has integrals of the form $\left\langle \text{Metal}(d_{xz}, d_{yz})\right|$ $L_xS_x\left|\text{Metal}(d_{xy})\right\rangle$ to evaluate. Thus, the corrected wave functions are given by:

$$\psi_{\alpha\alpha} = \frac{1}{\sqrt{2}}(\phi\chi-\chi\phi)\alpha\alpha - \frac{\lambda\alpha}{\sqrt{2}\Delta_x}\left[f(d)\,(\alpha\beta-\beta\alpha) + g(d)\,(\alpha\beta+\beta\alpha)\right] \quad (33)$$

$$\psi_{\beta\beta} = \frac{1}{\sqrt{2}}(\phi\chi-\chi\phi)\beta\beta + \frac{\lambda\alpha}{\sqrt{2}\Delta_x}\left[f(d)(\alpha\beta-\beta\alpha) + g(d)(\alpha\beta+\beta\alpha)\right] \quad (34)$$

$$\psi_{\alpha\beta+\beta\alpha} = \tfrac{1}{2}(\phi\chi-\chi\phi)(\alpha\beta+\beta\alpha) - \frac{\lambda\alpha}{2\Delta_x}\left[f'(d)\alpha\alpha + g(d)\beta\beta\right] \quad (35)$$

$$\psi_{\alpha\beta-\beta\alpha} = \frac{1}{\sqrt{2+2k^2}}(\phi^2-k\chi^2)(\alpha\beta-\beta\alpha) - \frac{\lambda\alpha}{2\Delta_x}\left[f'(d)\alpha\alpha + g(d)\beta\beta\right] \quad (36)$$

where f(d) and g(d) refer to the linear combinations of d_{xy}, d_{xz}, and d_{yz} mentioned on the previous page. The $L_yS_y|(\phi\chi - \chi\phi)\alpha\alpha\rangle$ operation is similar, except for a sign change, i.e., $L_y = \frac{1}{2}(L^+ - L^-)$ and $S_y = \frac{1}{2}(S^+ - S^-)$. (Note: the phase factors were consistent throughout all calculations and were as prescribed by Condon and Shortly.).

Except for the sign change, the calculation is exactly like that for L_xS_x. The functions corrected by L_yS_y are:

$$\psi_{\alpha\alpha} = \frac{1}{\sqrt{2}}(\phi\chi-\chi\phi)\alpha\alpha - \frac{\lambda\alpha}{\sqrt{2}\Delta_y}\left[f''(d)(\alpha\beta+\beta\alpha) - g(d)(\alpha\beta-\beta\alpha)\right] \quad (37)$$

$$\psi_{\beta\beta} = \frac{1}{\sqrt{2}}(\phi\chi-\chi\phi)\beta\beta + \frac{\lambda\alpha}{\sqrt{2}\Delta_y}\left[f''(d)(\alpha\beta+\beta\alpha) - g(d)(\alpha\beta-\beta\alpha)\right] \quad (38)$$

$$\psi_{\alpha\beta+\beta\alpha} = \tfrac{1}{2}(\phi\chi-\chi\phi)(\alpha\beta+\beta\alpha) - \frac{\lambda\alpha}{2\Delta_y}\left[f''(d)\alpha\alpha - g'(d)\beta\beta\right] \quad (39)$$

$$\psi_{\alpha\beta+\beta\alpha} = \frac{1}{\sqrt{2+2k^2}} (\phi^2 - k\chi^2)(\alpha\beta-\beta\alpha) - \frac{\lambda\alpha}{2\Delta_y}\left[\overline{f}''(d)\,\alpha\alpha - \overline{g}''(d)\,\beta\beta\right] \qquad (40)$$

It is now of interest to see if the corrected wave functions can be used to arrange a singlet lying lower than the triplet. The problem to be solved is

$$\begin{vmatrix} \langle\psi_1|R|\psi_1\rangle - E & \langle\psi_1|R|\psi_2\rangle \\ \langle\psi_2|R|\psi_1\rangle & \langle\psi_2|R|\psi_2\rangle - E \end{vmatrix} = 0$$

where ψ = ψ triplet, corrected for $\overline{L}\cdot\overline{S}$

ψ = ψ singlet, corrected for $\overline{L}\cdot\overline{S}$

$R = \frac{e^2}{r_{ij}}$

Because of the orthogonality of the spin functions and/or the symmetries of the space functions,

$$\langle\psi_1|R|\psi_2\rangle = \langle\psi_2|R|\psi_1\rangle = 0$$

Therefore $\Delta E = E_{triplet} - E_{singlet}$.

$$= \langle\psi_2|R|\psi_2\rangle - \langle\psi_1|R|\psi_1\rangle \qquad (41)$$

Substituting the values from tables 15, 16, 17 and 18, one obtains, using the corrected wave functions:

$$\Delta E = \langle\phi X|R|\phi X\rangle + \left(\frac{2k}{1+k^2} - 1\right)\langle\phi X|R|X\phi\rangle - \langle X^2|R|X^2\rangle$$

$$+ \frac{\lambda^2\alpha^2}{\Delta_z^2}\left[\langle f(d_{xy}, d_{x^2-y^2})|R|f(d_{xy}, d_{x^2-y^2})\rangle\right]$$

$$+ \frac{\lambda^2\alpha^2}{\Delta_x^2}\left[\left\langle f(d_{xy},d_{xz},d_{yz})|R|f(d_{xy},d_{xz},d_{yz})\right\rangle\right]$$

$$+ \frac{\lambda^2\alpha^2}{\Delta_y^2}\left[\left\langle f(d_{xy},d_{xz},d_{yz})|R|f(d_{xy},d_{xz},d_{yz})\right\rangle\right] \qquad (42)$$

Using the evaluated integrals, the free ion value of (-830 cm^{-1} for Cu), and the experimental energy level difference of $\Delta E = .005$eV one obtains:

$k = 1.50$ or 0.66

The same values are obtained for either the Slater or Clementi integrals.

The overall energy level diagram for the system is given in Figure 41.

Calculation of the g values

The wave functions for the triplet are

$$\psi_1 = \frac{1}{(2)^{\frac{1}{2}}}(\emptyset X - X\emptyset)\,\alpha\alpha$$

$$\psi_2 = \frac{1}{2}(\emptyset X - X\emptyset)\,(\alpha\beta + \beta\alpha)$$

$$\psi_3 = \frac{1}{(2)^{\frac{1}{2}}}(\emptyset X - X\emptyset)\,\beta\beta$$

The wave functions corrected for L•S mixing have been given in the last section. In order to solve for the g values, which are proportional to the splitting between the triplet levels when a magnetic field is applied, the Zeeman operator, L +2S must be applied to the corrected wave

functions component wise, i.e., the problem to be solved is

$$\begin{vmatrix} (\psi'_{1i}|\Xi|\psi'_{1i}) - \varepsilon & (\psi'_{1i}|\Xi|\psi'_{2i}) & (\psi'_{1i}|\Xi|\psi'_{3i}) \\ (\psi'_{2i}|\Xi|\psi'_{1i}) & (\psi'_{2i}|\Xi|\psi'_{2i})-\varepsilon & (\psi'_{2i}|\Xi|\psi'_{3i}) \\ (\psi'_{3i}|\Xi|\psi'_{1i}) & (\psi'_{3i}|\Xi|\psi'_{2i}) & (\psi'_{3i}|\Xi|\psi'_{3i})-\varepsilon \end{vmatrix} = 0$$

$$\Xi = \beta H_i (L_i + 2S_i)$$

where the primed ψ's are the above wave functions corrected for $\overline{L}\cdot\overline{S}$ mixing and i = X, Y, or Z.

The mechanism of operating with L and S is exactly the same as in the last section, except that one now takes sums instead of products. Therefore only the minimum amount required for comprehension will be presented here.

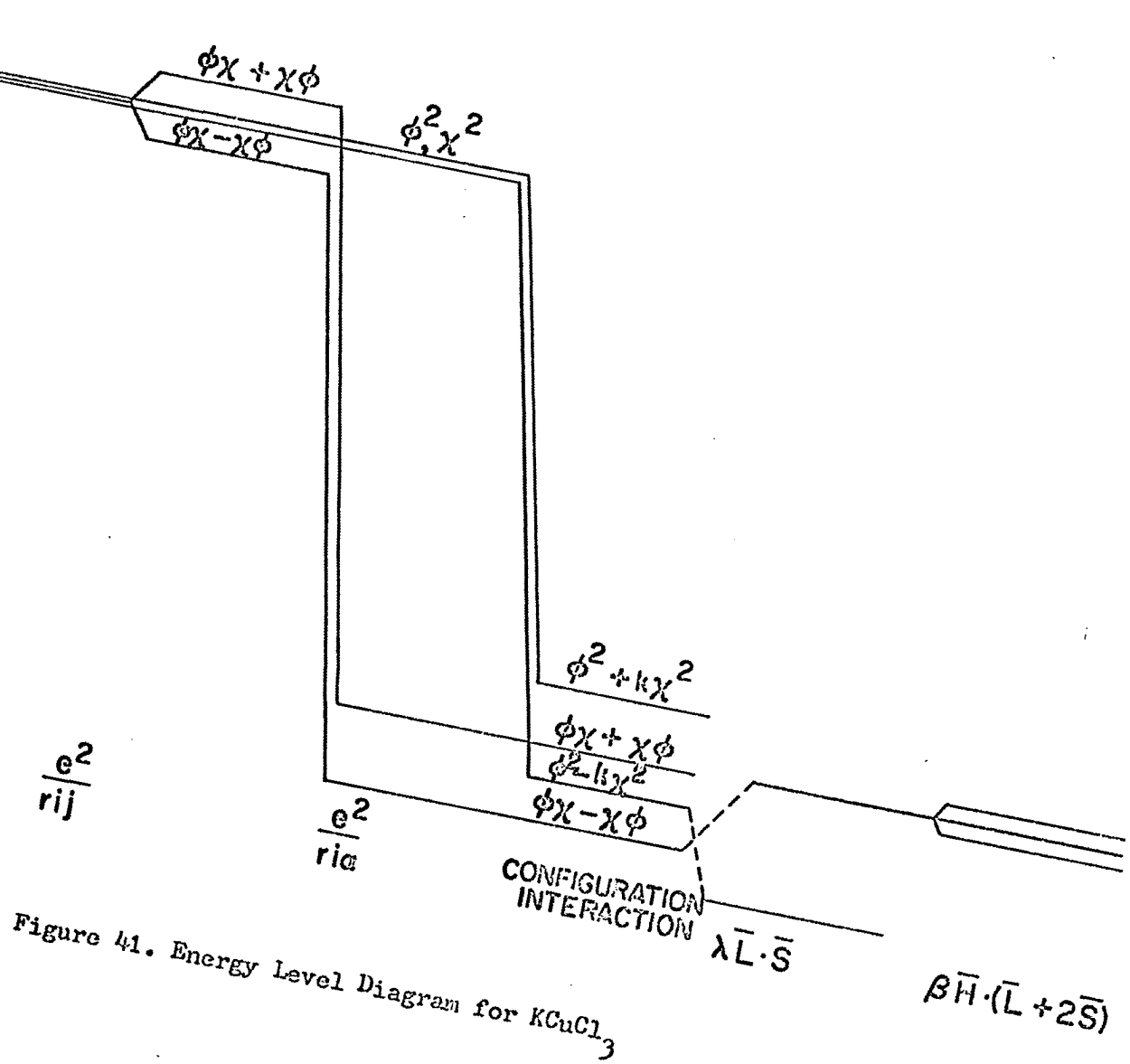

Figure 41. Energy Level Diagram for $KCuCl_3$

Calculation of g_z

For the z component, the secular determinant becomes,

$$\begin{vmatrix} (\psi'_{1z}|\beta H_z(L_z+2S_z)|\psi'_{1z})-E & 0 & 0 \\ 0 & (\psi'_{2z}|\beta H_z(L_z+2S_z)|\psi'_{2z})-E & 0 \\ 0 & 0 & (\psi'_{3z}|\beta H_z(L_z+2S_z)|\psi'_{3z})-E \end{vmatrix} = 0$$

Therefore, for $\psi'_{iz} = \Psi_i$ and $\beta H_z(L_z+2S_z) = T$

$$\Delta E = g_z\beta H_z = (\Psi_1|T|\Psi_1) - (\Psi_2|T|\Psi_2) = (\Psi_2|T|\Psi_2) - (\Psi_3|T|\Psi_3)$$

$$\text{or} \quad = \tfrac{1}{2}(\Psi_1|T|\Psi_1) - \tfrac{1}{2}(\Psi_3|T|\Psi_3)$$

Computationally, the last equation is easiest to solve, so taking that, one obtains:

$$g_z\beta H_z = \frac{1}{2}\left\{ 4 - \frac{8\lambda\alpha^2}{\Delta_z} \right\}\beta H_z \qquad (44)$$

$$= 2.27 \text{ for } \lambda = -830 \text{ cm}^{-1}, \ \alpha = 0.9, \ \Delta_z = 10{,}000 \text{ cm}^{-1}.$$

Compare this with the experimental $g_z = 2.215$.

If λ is reduced by 19% to -675 cm^{-1} then $g = 2.22$, in good agreement with experiment. Such reduction, due to charge transfer shielding, has been reported by Dunn (1959) and by Marshall and Stuart (1961).

Calculation of g_x

For the x component, the secular determinant becomes,

$$\begin{vmatrix} -E & A & 0 \\ A & -E & B \\ 0 & B & -E \end{vmatrix} = 0$$

which has solutions, $E = \pm(A^2+B^2)^{\frac{1}{2}}, 0$ (Gray, 1962).

Therefore $g_x = (A^2+B^2)^{\frac{1}{2}}$ where A and B are the x components,

$$A = (\Psi_2|T|\Psi_1) = (\Psi_1|T|\Psi_2)$$

$$B = (\Psi_2|T|\Psi_3) = (\Psi_3|T|\Psi_2)$$

and $$g_x\beta H_x = \left\{\left[\left(\frac{2}{\sqrt{2}} + \frac{8\lambda^2\alpha^2}{\sqrt{2}\,\Delta_x}\right) + \left(\frac{-\lambda\alpha}{\Delta_x}\right)\right]^2 + \left[\frac{2}{\sqrt{2}} + \frac{8\lambda^2\alpha^2}{\sqrt{2}\,\Delta_x}\right]^2\right\}^{\frac{1}{2}} \beta H_x$$

$$\therefore \quad g_x = 2.08$$

Compare this with the experimental $g_x = 2.057$.

Calculation of g_y

The secular determinant for the calculation of g_y has the same form as for the calculation of g_x. One will see by looking at the corrected wave functions, however, that there is a sign change in the $\alpha\alpha$ and $\beta\beta$ functions for the y component. Taking this into account,

$$g_y\beta H_y = \left\{\left[\frac{2}{\sqrt{2}} + \frac{8\lambda^2\alpha^2}{\sqrt{2}\,\Delta_y}\right]^2 + \left[\left(\frac{2}{\sqrt{2}} + \frac{8\lambda^2\alpha^2}{\sqrt{2}\,\Delta_y}\right) + \left(\frac{-\lambda\alpha}{\Delta_y}\right)\right]^2\right\}^{\frac{1}{2}} \beta H_y$$

Therefore $g_y = 2.08$. Compare this with the experimental $g_y = 2.124$.

(N. B.: For the last two calculations,

$$\alpha = 0.9$$

$$\lambda = -830 \text{ cm}^{-1}$$

$$\Delta_x = \Delta_y = 12{,}700 \text{ cm})$$

CONCLUSIONS

As the calculations section has clearly shown, a model has been established which successfully explains the susceptibility results down to 17°K and the g values insofar as the experimental energy level differences and the spin orbit coupling parameter are known. The $KCuCl_3$ system has been an excellent testing ground for determining when cooperative and when non-interacting descriptions are appropriate. In this case, the mathematical treatment indicates that for interdimer bonds being about 1 Å longer than the "normal" Cu - Cl intradimer bonds, a depopulation from the triplet to the singlet explains the observations, while antiferromagnetism, as described by the Ising model, does not. Furthermore, an "ordering" temperature, at which this description becomes inappropriate, is obviously indicated.

At the outset of this work, it was mentioned that the validity of the Willet - Rundle molecular orbital was to be investigated. At the end of this work, one may say that the scheme is valid down to 17°K in that it describes the energy levels of the system by the energy levels of a single dimer, but it does not go far enough, as the complete breakdown of the B^*_{1g} and B^*_{2u} levels (Figure 41) indicates.

Four parameters have been adjusted in this work, but a separate calculation was used to establish each parameter, thus adding credence to the overall treatment.

A certain amount of further work is required to concretize the developments presented here. The first of these is neutron diffraction of the compound below 17°K to see if ordering does occur. Flippen and Friedberg (1963) have reported that $Cu(HCO_2)_2 \cdot 4H_2O$ powder and single crystals exhibits a sharp maximum in $\frac{1}{\chi_m}$ vs. T at 16.8°K with what appears to be low temperature ferromagnetism occurring below that temperature. The second is an independent evaluation of the parameters via a spin hamiltonian analysis. ESR data has been used to evaluate molecular orbital mixing coefficients (Chen and Das, 1966). Both these investigations are in progress at the time of writing. It would also be of interest to monitor the crystal structure of the compound in the range 15 to 35°K when this technique becomes available.

BIBLIOGRAPHY

Aiyama, Y., 1966, Phys. Jap., 21, 1684.

Ballhausen, C. J., 1962, "Introduction to Ligand Field Theory," McGraw-Hill Book Co., New York, New York.

Barraclough, C.G. and Ng, C. F., 1964, Trans. Far. Soc., 60, 836.

Bleaney, B. I. and Bleaney, B., 1957, "Electricity and Magnetism," Oxford University Press, Oxford, England.

Carlin, R. L., 1966, J. Chem. Ed., 43, 521.

Chen, I. and Das, T. P., 1966, J. Chem. Phys., 45, 3526.

Clement, J. R., 1955, Helium Vapor Pressure Tables, Naval Research Laboratory.

Clementi, E. and Raimondi, D. L., 1963, J. Chem. Phys., 38, 2686.

Cotton, F. A., 1964, "Chemical Applications of Group Theory," J. Wiley and Sons, Inc., New York, New York.

Cotton-Feytis, E., 1945, Ann. Chim. (Paris), 4, 9.

Coulson, C. A., 1961, "Valance," Oxford University Press, Oxford, England.

Czanderna, A. W., 1966, J. Chem. Phys., 45, 3159.

Dallolio, A., Dascola, G. and Varracca, V., 1966, Nuovo Cimento, 43, 192.

Dorain, P. B., 1962, "Symmetry in Inorganic Chemistry," Addison-Wesley Publishing Co., New York, New York.

Dunn, T. M., 1959, J. Chem. Soc., 623.

Ewald, A. H., Martin, R. L., Ross, I. G. and White, A. H., 1964, Proc. Roy. Soc., A280, 235.

Figgis, B. N. and Martin, R. L., 1956, J. Chem. Soc., 3837.

Fisher, M. E., 1966, J. Math. Phys., 7, 1776.

Flippen, A. R. and Friedberg, S. A., 1963, J. Chem. Phys., 38, 2652.

Fowler, R. and Guggenheim, E. A., 1952, "Statistical Thermodynamics," Cambridge University Press, Cambridge, England.

Gerstein, B. C. and Spedding, F. H., 1960, U. S. Atomic Energy Commission Report, IS-331, (Iowa State University of Science and Technology, Ames, Iowa, Institute for Atomic Research).

Gray, H. B., 1962, "Electrons and Chemical Bonding," W. A. Benjamin, Inc., New York, New York.

Greiner, J. D., Smith, J. F., Corbett, J. D. and Jelinek, F. J., 1966, J. Inorg. Nuc., 28, 971.

Griffiths, R. B., 1961, U. S. Atomic Energy Commission Report, AFOSR-1934, (Air Force Office of Scientific Research, Washington, D. C.).

Groger, M., 1899, Z. Anorg. Chem., 19, 328.

Grover, F. W., 1946, "Inductance Calculations," D. Van Nostrand Co. Inc., New York, New York.

Hansen, A. E. and Ballhausen, C. J., 1965, Trans. Far. Soc., 61, 631.

Hartshorn, L. M., 1925, J. Sci. Inst., 2, 145.

Helmholz, H., 1964, J. Am. Chem. Soc., 69, 886.

Hesterman, V. H., 1958, "The Effects of Deformation on Superconducting Metals." Unpublished M. S. thesis. Iowa State University of Science and Technology, Ames, Iowa.

Hoare, F. E., Jackson, L. C. and Kurti, N., 1961, "Experimental Cryophysics," Butterworth and Co., Ltd., London, England.

Hutchinson, C. A. and Mangrum, B. W., 1961, J. Chem. Phys., 34, 908.

Jennings, L. D., 1960, Rev. Sci. Instr., 31, 1269.

Joenk, R. J. and Bozorth, R. M., 1965, J. App. Phys., 36, 1167.

Kato, M., Jonassen, H. B. and Fanning, J. C., 1964, Trans.

Far. Soc., 60, 99.

Keen, B. E., Landau, D. P. and Wolf, W. P., 1966, Phys. Letters, 23, 202.

Kotani, M., 1949, J. Phys. Soc., Japan, 4, 293.

Haass, G. J., Gerstein, B. C. and Willett, R. D., 1967, J. Chem. Phys., 46, 401.

Marshall, W. and Stuart, R., 1961, Phys. Rev., L23, 2048.

Mermin, N. D. and Wagner, H., 1966, Phys. Rev. Let., 17, 1133.

Meyerhoffer, W. Z., 1889, Physik. Chem., 3, 185.

Newell, G. E. and Montroll, E. W., 1953, Rev. Mod. Phys., 25, 252.

Owen, J., 1955, Proc. Roy. Soc., A227, 183.

Pake, G. E., 1962, "Paramagnetic Resonance," W. A. Benjamin and Sons, Inc., New York, New York.

Pryce, M. H. L., 1950, Proc. Phys. Soc., London, A63, 25.

Rioux, F. J., 1967, "Thermal and Magnetic Studies of Ligand Field Levels in Cesium Copper Chloride - $CsCuCl_3$." Unpublished M. S. thesis. Library, Iowa State University of Science and Technology, Ames, Iowa.

Roberts, J. D., 1962, "Molecular Orbital Calculations," W. A. Benjamin and Sons, Inc., New York, New York.

Ruedenberg, K. and Silver, D., 1968, J. Chem. Phys., 49, 4301.

Rundle, R. E., 1957, J. Am. Chem. Soc., 79, 3372.

Schleuter, A. W., Jacobson, R. A. and Rundle, R. E., 1966, Inorg. Chem., 5, 277.

Shulman, R. G. and Rahn, R. O., 1966, J. Chem. Phys., 45, 2940.

Schlichter, C. P., 1963, "Principles of Magnetic Resonance," Harper and Row, New York, New York.

Slater, J. C., 1965, "Quantum Theory of Molecules and Solids," Mc-Graw- Hill Book Co., New York, New York.

Stevens, K. W., 1953, Proc. Roy. Soc., A219, 542.

Umebayashi, H., Shirane, G., Frazer, B. C. and Cox, D. E., 1967, J. Appl. Phys., 38, 1461.

Van Vleck, J. H., 1940, J. Chem. Phys., 9, 85.

Van Vleck, J. H., 1932, "Theory of Electric and Magnetic Susceptibilities," Oxford University Press, London, England.

Vossos, P. H., Fitzwater, D. R. and Rundle, R. E., 1963, Acta-Crysta., 16, 1037.

Vossos, P. H., Jennings, L. D. and Rundle, R. E., 1960, J. Chem. Phys., 32, 1590.

Wells, A. F., 1947, J. Chem. Soc., 1690.

Wells, A. F., 1962, "Structural Inorganic Chemistry," Oxford University Press, Oxford, England.

Willett, R. D., 1962, "The Crystal Structures and Magnetic Properties of Some Red Cupric Chloride Complexes." Unpublished Ph. D. thesis. Library, Iowa State University of Science and Technology, Ames, Iowa.

Willett, R. D., Dwiggins, C., Kruh, R. F. and Rundle, R. E., 1963, J. Chem. Phys., 38, 2429.

ACKNOWLEDGEMENTS

The author is indebted to many people for their help in this work.

First of all, I am grateful to Professor Gerstein for suggesting the project and for all his help along the way.

My thanks must also go to the following: To F. Birse, for his help with the theoretical understanding of the problem; to G. Pearson, for help with the ESR spectra; to D. Silver and K. Ruedenberg, for the evaluation of the integrals; to J. Ugro, for the single crystal x-ray work; to A. Miller, for writing the program used to calculate the configuration of the mutual inductance coils; to R. Willett, for elucidating the structure of $KCuCl_3$ and for supplying some of the larger single crystals; to S. Liu, for the formula for the spin 1 Ising model.

Finally, my deepest love and appreciation to my wife, Monica, who put up with the rigors of being a graduate school wife uncomplainingly. Without her constant help and encouragement, this work would not have been possible.

APPENDIX

$f(d) = \phi a + a\phi$

$f'(d) = \phi a - a\phi$

$f''(d) = \phi b - b\phi$

$g(d) = Xc - cX$

$g'(d) = Xd + dX$

$g''(d) = Xd - dX$

where

$c = (d_{xz}-d_{yz})_a + (d_{xz}-d_{yz})_b$

$b = (d_{xz}+d_{yz})_a + (d_{xz}+d_{yz})_b$

$c = (d_{xz}-d_{yz})_a - (d_{xz}-d_{yz})_b$

$d = (d_{xz}+d_{yz})_a - (d_{xz}+d_{yz})_b$